Experimental and Modelling Analyses of Saltwater Upconing

submitted by

Danica Jakovović

As a requirement in full for the degree of

Doctor of Philosophy

in the

School of the Environment

Flinders University of South Australia

November 2013

Table of contents

List of Figures

List of Tables

Summary

Saltwater upconing is a process that occurs when salty groundwater that underlies fresh groundwater rises towards a pumping well. It is an important problem in many coastal aquifers around the world, leading to the deterioration in water quality of freshwater wells. Once a well is intruded by saltwater, it may require the well to be decommissioned, and hence, controlling bore salinisation through upconing is essential. In this study, the mechanisms of saltwater upconing are assessed to improve the current body of knowledge of the associated density-dependent flow and transport processes.

Saltwater upconing is particularly difficult to measure under field situations, and there are no previous examples of well characterised field-scale saltwater upconing plumes. Prior to the current research, there were also no published observations of upconing under controlled laboratory experimental conditions, notwithstanding previous studies of lateral saltwater intrusion in which incidental vertical movements in saltwater plumes were observed. Laboratory experiments and numerical modelling analyses of saltwater upconing processes were undertaken to provide insight and understanding of the mechanisms responsible for the salinisation of freshwater wells. The research focuses mainly on laboratory-scale upconing, through which saltwater rise under a pumping well and the related impacts in terms of well salinity and plume rise and extent are examined.

Firstly, saltwater upconing observations from four controlled sand-tank experiments were quantified and compared to an existing analytical solution of transient upconing. These results were subsequently extended using a numerical modelling analysis of the laboratory experiments to better understand the flow and transport processes occurring in the sand tank. An important outcome of this work is the numerical reproducibility of the experimentally observed temporal development of saltwater plumes under a pumping bore, albeit for three of the four experiments. The “double peak” upconing observed in one of the laboratory experiments was not reproduced by this model. Numerical modelling results were compared with an existing sharp-interface analytical solution, which

corresponded well with the numerical modelling results for early stages of the four upconing experiments.

Secondly, additional laboratory experimentation and numerical modelling were undertaken to investigate double-peaked upconing that remained unresolved. Laboratory experiments successfully reproduced the double-peaked plume demonstrating that this phenomenon was not an experimental nuance in previous experiments. The modelling undertaken in this analysis demonstrated that sorption is an important consideration when using Rhodmaine WT as a visual aid in sand-tank experiments, especially under slow flow, density-dependent conditions.

The final component of the study extended the laboratory-scale investigation to scales that apply to real-world settings. The aim was to define and characterize the "saltwater upconing zone of influence", which is the extent of saltwater upconing impact, in terms of saltwater rise attributed to pumping, in a largely hypothetical, three-dimensional coastal setting involving a sloping regional freshwater-seawater interface. Both radial and three-dimensional numerical modelling of saltwater upconing at the field scale were undertaken. The results indicate that the sharp-interface approximations of SUZI, for both radial and three-dimensional cases, are larger compared to the numerical model predictions. It was also found that the lateral flow towards the coast significantly influences both the SUZI and the salinity of the extracted groundwater. This part of the study demonstrated that the three-dimensional modelling that includes inclined interfaces and lateral flow towards the coast is essential in studying SUZI in typical coastal areas. That is, radial modelling, which does not capture the lateral flow effects, over-estimates the SUZI extent as well as the pumped water salinity.

Declaration of Originality

I certify that this thesis does not incorporate, without acknowledgement, any material previously submitted for a degree or diploma in any other university; and that to the best of my knowledge and belief it does not contain any material previously published or written by another person except where due reference is made in the text.

Danica Jakovović

Acknowledgements

My sincere gratitude and appreciation goes to my supervisors, Assoc. Prof. Adrian Werner, Dr Vincent Post and Prof. Craig Simmons, for their guidance and support through the last four years. In particular, I would like to tank Adrian for his invaluable guidance, numerous ideas, countless reviews, and passionate encouragement for learning, Vincent for his enormous support, patience, inspiration and passionate love of science, and Craig for his support and guidance at initial stages of my PhD.

PhD scholarship by AJ & IM Nylon and conferences funding by the National Centre for Groundwater Research and Training (NCGRT) are sincerely acknowledged.

I gratefully acknowledge help with the laboratory experimentation by Brenton Perkins, Oliver Mannicke, Etienne Lasage, Dirk Eliander, Simon Jacobs and Megan Sebben.

It has been a great experience to work and interact with all the NCGRT Programs 2, 3 and 4 fellow colleagues at Flinders University.

Many thanks to Dr Chunhui Lu, Leanne Morgan, Dr Perry de Louw, Dr Maria Pool and Eugenia Hirthe for many scientific discussions, especially towards the end of my PhD.

My fellow office-226 mates, Carlos Miraldo, Dr Maria Pool, Eugenia Hirthe, Miguel Cambron, Dr Perry de Louw, Charlotte Schmitt, Le Dung Dang, Dr Yueqing Xie, Ty Watson and Anna Seidel: times shared with you are an invaluable part of my PhD experience. Etienne, Daan, Matt and Megs: you are a part of this invaluable experience too.

Goran, your continued encouragement and passion for learning have been a major driving force throughout my PhD. Thank you.

Very special and huge thanks to my family. Your support has been invaluable to me in completing this thesis.

Chapter 1

Background and objectives

In coastal regions, groundwater is often the major source of freshwater, and hence a proper understanding of the processes leading to salinisation of wells is essential. There are numerous processes influencing salt movements in coastal systems, occurring across a wide range of scales, including buoyancy effects due to freshwater-saltwater density contrasts, recharge and regional flow dynamics, and pumping impacts. In the near vicinity of pumping wells, saltwater upconing may occur. Saltwater upconing is the upward vertical transport of salty groundwater towards a pumping well in an aquifer where freshwater is underlain by saltwater. It may lead to considerable deterioration in the quality of extracted water, and is therefore an important problem in many coastal aquifers around the world. Once a freshwater bore is intruded by saltwater, the pumping well is often abandoned (Zhou et al., 2005; Narayan et al., 2006).

Bore salinisation due to saltwater upconing was probably first explored in the 1910s. Pennink (1915) used a sandbox to explore patterns of saltwater movement below a drain and observed brackish and saltwater rise to the bottom of the well. He also examined the influence of lateral flows on up-coning behaviour, and found that these tend to push the saline water downstream of the well. The sand-tank set-up that Pennink (1915) adopted, led to saltwater entering the well from the ocean side, i.e. rather than from beneath, as occurs in the absence of lateral flow (e.g. Diersch et al, 1984; Reilly and Goodman, 1987; Zhou et al., 2005). Dagan and Bear (1968) were among the first to obtain a non-steady solution for saltwater upconing. They adopted the method of small perturbations to obtain solutions for sharp-interface rise below a well, in both two-dimensional cross section and in radial coordinates, in an infinite aquifer. They compared their analytical solution to laboratory results in the form of interface movements inferred from sand-box salinity measurements. The

solution was found to be valid for interface rise approximately up to one-third the distance between the bottom of the well and the initial interface position.

The sharp-interface approximation of the freshwater-saltwater mixing zone adopted by Dagan and Bear (1968) has been applied by others in developing subsequent analytical solutions (e.g. Haubold, 1975; Motz, 1992; Zhang et al., 1997; Bower et al., 1999). In these cases, freshwater and saltwater are considered as immiscible fluids separated by a sharp boundary, and head losses and fluxes in the saltwater zone are neglected. While the sharp-interface assumption allows for the development of rapid, first-order methods of analysis, this approach neglects dispersive transport, which was shown by Reilly and Goodman (1987) to be important for the evaluation of well salinities, and in studying upconing processes more generally.

Many studies have implemented the sharp-interface approach, using both analytical and numerical solutions (e.g. Chandler and McWhorter, 1975; Wirojanagud and Charbeneau, 1985; Aharmouch and Larabi, 2001). Based on the sharp-interface approach, it has been shown that, theoretically at least, the interface can be maintained in a position below the well (i.e. a stable saltwater plume can develop below the well) if freshwater extraction is kept below a certain critical pumping rate (e.g. Bear, 1979; Motz, 1992; Zhang et al., 1997). That is, the critical pumping rate can be defined as the maximum permissible discharge for which the interface does not encounter the well. However, the occurrence of stable saltwater plumes below pumping wells has not been demonstrated in real-world settings or under controlled laboratory conditions, and rather, stable upconing plumes have been produced under only idealised (e.g. theoretical, sharp-interface) conditions.

Given that only 2% of seawater mixed with fresh groundwater renders a coastal pumping well unusable for most applications, the behaviour of the transition zone is an essential element of assessing upconing and its potential impacts on groundwater extraction in practical coastal aquifer problems. Previous studies of transition zone behaviour during upconing identified some important observations. For example, the transition zone widens as pumping draws the interface upwards from its initial position (Reilly and Goodman, 1987). Further,

it has been shown in lateral seawater intrusion studies that the transition zone is controlled by mechanical dispersion, molecular diffusion, advection, density effects and geological controls (Abarca and Clement, 2009; Lu et al., 2009), and these can affect the salinity of the pumped water.

Diersch et al. (1984) were among the first to numerically model variable-density, dispersive flow and transport processes associated with saltwater upconing. They studied the sensitivity of dispersivity and found that the well salinity is strongly influenced by dispersion (i.e. higher dispersion leads to earlier breakthroughs of low salinity water and a longer transition to the breakthrough of seawater into the pumping well). Reilly and Goodman (1987) simulated a field situation of saltwater upconing using a numerical model of density-dependent groundwater flow and dispersive solute transport. They compared sharp-interface and dispersive transport approaches and concluded that the dispersive transport approach is needed to reproduce upconing situations involving wide transition zones (e.g. under cyclic pumping). Konz et al. (2009) produced saltwater intrusion experimental results for benchmarking variable-density numerical codes. Saltwater intrusion was observed occurring both laterally and vertically (i.e. saltwater upconing), albeit the focus of the study was lateral seawater intrusion. Highly-dispersive upconing was observed in both laboratory experiments and modelling results, i.e. only the 10% isochlor reached the well. The Konz et al. (2009) experiments demonstrated that dispersion may be an important phenomenon when considering bore salinisation processes; further work is needed to explore dispersive processes for a broader range of saltwater upconing conditions.

Saltwater upconing is particularly difficult to measure under field situations, and there are no previous examples of well characterised field-scale saltwater upconing plumes. Prior to the commencement of this thesis, the only examples of published laboratory experimentation of saltwater upconing appeared to be the works of Dagan and Bear (1968) and Oswald (1998). Oswald (1998) produced saltwater upconing in a three-dimensional sand box and salinity plumes were delineated using geophysical interpretations (i.e. there were no direct visual observations of saltwater upconing). Dagan and Bear (1968) provided only a summarised account of their laboratory results (i.e. the shapes of

salt plumes were not given and experimental photography was not published), and therefore the salt plume behaviour leading to bore salinisation was not observed directly. Direct observations of saltwater upconing are required to complement previous modelling analyses and to extend the laboratory experimentation of Dagan and Bear (1968) and Oswald (1998) for a broader range of saltwater upconing conditions.

The current research project commences with analyses of four saltwater upconing laboratory experiments undertaken as part of a previous undergraduate research project, which produced experimental photography and a set of laboratory observations. The saltwater upconing results, including water and salt mass balances, boundary condition observations, and saltwater upconing trends are critically evaluated and compared to the analytical solution of Dagan and Bear (1968) for transient, sharp-interface upconing. The results of the analyses of these four laboratory experiments provide the starting point for the remainder of the thesis, which examines saltwater upconing in more detail, including further laboratory experimentation, a closer examination of the transport processes observed under controlled laboratory conditions, and an extension to field-scale upconing problems.

This thesis consists of seven chapters including the current chapter. Chapter 1 provides a basic background to this research and summarises briefly each chapter. Chapters 2, 3, 4 and 5 are based on journal publications, and references to the papers are specified at the start of each chapter. Chapter 6 is not directly related to chapters 2, 3, 4 and 5, and can be read independently. Chapter 7 summarises the main conclusions of this research.

The first stage of this thesis (Chapter 2) involved the investigation of saltwater upconing imagery and experimental data to produce a well-characterised account of laboratory measurements of saltwater upconing, thereby extending the work of Dagan and Bear (1968) and Oswald (1998). This part of the study provided the first published time-series observations of saltwater upconing under controlled laboratory experimental conditions. Following this, a numerical modelling analysis of the laboratory experiments was undertaken (Chapter 3) to better understand the flow and transport processes occurring in the sand tank. An

important outcome of this work is the numerical reproducibility of the experimentally observed temporal development of saltwater plumes under a pumping bore, albeit for three of the four experiments. The "double peak" upconing observed in one of the laboratory experiments was not reproduced by this model. This led to additional laboratory experimentation and numerical modelling (Chapter 4) to investigate tracer adsorption effects in sand-tank experiments of saltwater upconing. Laboratory experiments successfully reproduced the double-peaked plume demonstrating that this phenomenon was not an experimental nuance in previous experiments. The modelling undertaken in this analysis demonstrated that sorption is an important consideration when using Rhodmaine WT as a visual aid in sand-tank experiments, especially under slow flow, density-dependent conditions. The previous three chapters led to a discussion on the relevance of the upconing criticality conditions to the current work (Chapter 5). That is, a short analysis was undertaken to assess whether the upconing criticality conditions hold for the saltwater upconing laboratory experiments that were carried out. This chapter aimed rather at opening questions on applicability of the stable plume theory to dispersive upconing. The final component of this study (Chapter 6) extended the laboratory-scale investigation to scales that apply to real-world settings. The aim was to define and characterise the "saltwater upconing zone of influence", which is the extent of saltwater upconing impact, in terms of saltwater rise attributed to pumping. This concept is explored and demonstrated through three-dimensional numerical modelling, and as such is the first attempt to quantify saltwater upconing zone of influence in coastal areas and hence under the impact of lateral flow towards the coast. Chapter 7 provides the main conclusions of this thesis.

Chapter 2

Analysis of laboratory experiments of saltwater upconing

This chapter is based on the following paper:

Werner A.D., Jakovovic D., Simmons C.T., 2009. Experimental observations of saltwater up-coning. Journal of Hydrology 373, 230-241.

Note: The laboratory experiments of saltwater upconing analysed here were carried out as part of a previous undergraduate research project. This research commenced with the quantification of the observations from those experiments. Therefore, only parts of the publication referenced above are reproduced here. For the full content of this paper see the publication referenced above.

2.1 Experiments

A set of saltwater upconing experiments was conducted under controlled conditions in a laboratory sand tank. These experiments are referred to as Experiment 1, Experiment 2, Experiment 3 and Experiment 4, throughout this thesis. Experimental results are compared to the analytical solution of Dagan and Bear (1968) to assess the agreement between experimental observations and sharp-interface mathematical predictions of upconing behaviour.

Four different combinations of pumping rate (Q) and freshwater–saltwater density difference ($\Delta\rho$) were tested in upconing experiments (high Q-low $\Delta\rho$, high Q-medium $\Delta\rho$, medium Q-medium $\Delta\rho$, low Q-high $\Delta\rho$), with the aim of examining the effects of buoyancy (i.e. tending to stabilise the salt plume) and advection (i.e. tending to de-stabilise the salt plume) on upconing behaviour.

The geometric variables of the experiments are illustrated in Figure 2.1, and experimental parameters are listed in Table 2.1. In Figure 2.1, a (L) is the initial

vertical thickness of freshwater, D (L) is the initial depth of saltwater, d (L) is the height of the bottom of the well above the initial interface, Q (L^3T^{-1}) is the pumping rate, $Z(t)$ (L) is the time-dependent height of the interface apex above the initial interface, and $W(t)$ (L) is the time-dependent salt plume width at mid-height between the initial interface and the interface apex (i.e. at a height of $Z(t)/2$).

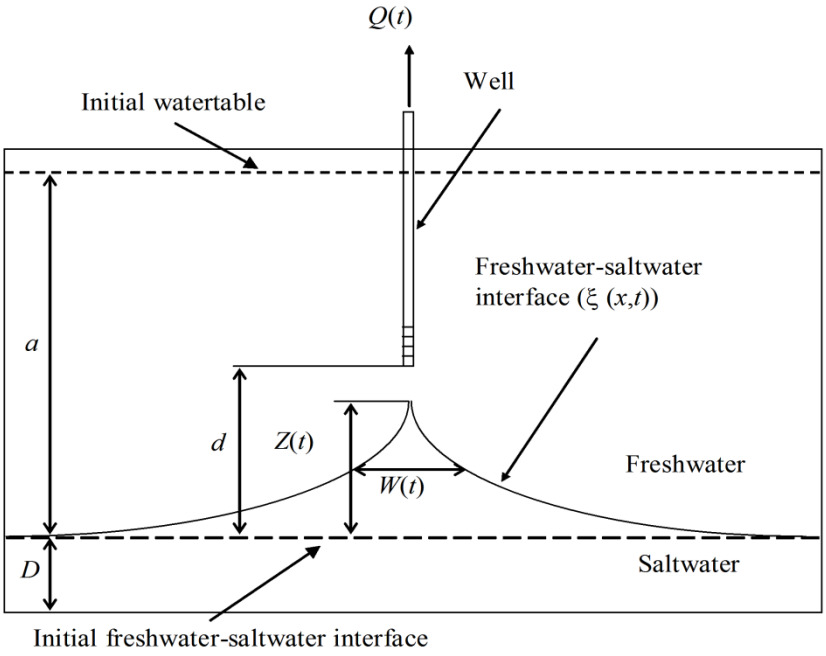

Figure 2.1. Schematic of sand-tank experiments, showing various geometric variables.

Table 2.1. Parameters used in upconing experiments.

Parameters	Exp. 1	Exp. 2	Exp. 3	Exp. 4
Pumping rate, Q (m^3/s)	3.8×10^{-6}	3.9×10^{-6}	2.2×10^{-6}	5.3×10^{-7}
Saltwater density, ρ_s (kg/m^3)	1011	1025	1025	1096
Bore-to-initial interface, d (m)	0.43	0.40	0.41	0.38
Initial watertable-to-interface, a (m)	0.97	0.95	0.96	0.93
Initial depth of saltwater, D (m)	0.13	0.15	0.14	0.17

2.2 Theory and analysis of experimental design

In this study, the analytical solution of Dagan and Bear (1968) for interface rise under groundwater discharge to a drain, i.e. analogous to our laboratory setting of a two-dimensional cross section, was used to compare against the results of upconing experiments. Dagan and Bear (1968) used the method of small perturbations and assumed a homogeneous incompressible aquifer containing two immiscible fluids in developing an equation for the temporal progression of upconing in terms of the freshwater–saltwater interface position $\xi(x,t)$, given for the isotropic case as:

$$\xi(x,t) = \frac{\alpha_1 q}{\pi}\int_0^{\infty}\frac{1}{\lambda}\frac{\cosh[\lambda(a-d)]}{\sinh(\lambda a)} \times \left\{1 - \exp\left(\frac{-\lambda}{\beta_1\coth(\lambda a)+\beta_2\coth\lambda b}\right)t\right\}\cos(\lambda x)d\lambda \qquad (2.1)$$

where x is the horizontal dimension (L) (origin at the well/drain), $\alpha_i = \frac{\mu_i}{k(\gamma_2-\gamma_1)}$ (TL^{-1}) (i = 1 refers to freshwater and i = 2 refers to saltwater), μ is dynamic viscosity ($ML^{-1}T^{-1}$), k is permeability (L^2), γ is specific weight ($ML^{-2}T^{-2}$), λ is the integration variable, $\beta_i = n\alpha_i$ (TL-1), n is porosity (dimensionless), q is the rate of groundwater extraction per drain length (L^2T^{-1}) and other variables are as defined for Figure 2.1 and Table 2.1. Equation (2.1) is valid for only finite deviations from the initial interface position due to the method of solution (i.e. small perturbations). Dagan and Bear (1968) tested the range of applicability of Equation (2.1) by comparing to laboratory experiments, and they found that Equation (2.1) was a reasonable predictor of experimental results for the range $Z(t) < d/3$. Bear (1979) suggests that Equation (2.1) may be valid for interface rise up to $d/2$; although they recommend using $d/4$ to $d/3$ as the upper limit of applicability ($d/3$ is adopted in this study).

Dagan and Bear (1968) used a dimensionless formulation involving three scaling ratios for the horizontal dimension (x), vertical interface rise (ξ) and time (t) – denoted here as A (L^{-1}), B (L^{-1}) and C (T^{-1}), respectively, and defined for the anisotropic case (see Dagan and Bear (1968) for derivation of anisotropic upconing equations) as:

$$A = \frac{1}{d}\left(\frac{k_z}{k_x}\right)^{1/2}, B = \frac{(k_x k_z)^{\frac{1}{2}}(\gamma_2-\gamma_1)}{\mu_1 q}, C = \frac{k_z(\gamma_2-\gamma_1)}{n(\mu_1+\mu_2)d} \qquad (2.2)$$

where k_x and k_z refer to the components of permeability in the horizontal and vertical directions, and subscripts 1 and 2 denote freshwater and saltwater as defined previously. In the current study, we use the Dagan and Bear (1968) scaling ratios to analyse the experimental design, by comparing the experimental variables to those of real-world settings. Bear and Dagan (1964) and Bear (1979) distinguish critical and sub-critical upconing situations, whereby a sharp freshwater–saltwater interface will eventually enter the well if the interface is within a critical vertical distance b_{cr} (=0.097$q\delta/K_1$, where $\delta = \gamma_1/(\gamma_2-\gamma_1)$ and K_1 is the freshwater hydraulic conductivity; Bear, 1979) of the pumping well. Bear (1979) illustrates that the shape of the freshwater–saltwater interface (i.e. near the apex of the upconing plume) is convex for the sub-critical case and is concave for the critical situation. More recently, Bower et al. (1999) adopted a ‘‘critical interface rise ratio” (=(d-b_{cr})/d) and identified the large variability in this parameter in published studies, ranging from 0.25 to 0.9 (i.e. giving b_{cr} ranging from 0.04 m to 0.3 m for the current experimental set-up). It should be noted that critical rise concepts are not the focus of this analysis, but rather the aim is to examine salt plume processes occurring near a pumping well.

While upconing experiments were not meant to represent down-scaled versions of any real-world settings, an assessment of the relativity between the experimental parameters and those of real-world situations was necessary to interpret the observed upconing behaviour in terms of practical applications. A host of real-world situations (e.g. Schmorak and Mercado, 1969; Reilly and Goodman, 1987; Aliewi et al., 2001; Zhang et al., 2004; Werner and Gallagher, 2006; Narayan et al., 2006) was used to generate typical ranges of coastal aquifer parameters and of the relevant upconing variables (i.e. variables are shown in Figure 2.1 and as used in *A*, *B* and *C*). The following parameter ranges were adopted as representative of typical coastal aquifer settings: d (5–100 m), k_x (1.2×10^{-11}–1.8×10^{-10} m^2), k_z/k_x (0.05–1.5), γ_2-γ_1 (120–250 kg/m^2/s^2), μ_1 (1×10^{-3}–1.12×10^{-3} kg/m/s), μ_2 (1×10^{-3}–1.2×10^{-3} kg/m/s), q (7×10^{-6}–1.3×10^{-4} m^2/s), n (0.15–0.45). Table 2.2 provides values of *A*, *B*, *C* and b_{cr} for upconing experiments and for typical real-world parameter ranges.

Table 2.2. Comparison of scaling ratios and critical depths (b_{cr}): typical real-world settings versus laboratory experiments.

	Real-world ranges	Exp. 1	Exp. 2	Exp. 3	Exp. 4
A (1/m)	0.002 to 0.2	2.4	2.5	2.4	2.6
B (1/m)	0.002 to 8	0.30	0.62	1.1	17
C (1/s)	$7x10^{-10}$ to $5x10^{-5}$	$6.2x10^{-5}$	$1.4x10^{-4}$	$1.4x10^{-4}$	$5.4x10^{-4}$
b_{cr} (m)	0.01 to 9	0.32	0.16	0.086	0.0057

The Table 2.2 values indicate that scaling parameters A and C for laboratory experiments were high compared to the range of values obtained from real-world settings, due to the small value of d and the relatively high k_z value. Nevertheless, d was not within the critical depth b_{cr}. Therefore, according to the definitions of Bear (1979) and Bear and Dagan (1964), initial upconing plumes were expected to have a convex shape (near the plume apex) and stable plumes were expected to develop. However, upconing proceeded until the interface intercepted the well in the experiments of this study, and therefore the steady-state conditions of criticality that others have reported (e.g. Bower et al., 1999) do not appear to be transferable to the current analysis. Therefore, b_{cr} is considered only as a measure of the likely depth of transformation from convex to concave interface shape in the remainder of this study, and comments relating to the expected persistence of stationary upconing plumes are intentionally avoided. The scaling parameter B obtained for the laboratory experiments presents as a mixed convection ratio (e.g. Massmann et al., 2006). The experimental and real-world ranges of B are relatively well matched, indicating that typical free convection-to-forced convection ratios have been captured in the experimental design. In general, the results of Table 2.2 indicate that experiments are reasonable analogues of field settings in which the bottom of the bore is relatively close to the initial interface, K is reasonably high and pumping duration is short.

2.3 Quantifying experimental results

Solute transport behaviour in experiments was quantified in the form of time-series of experimental variables (e.g. see Figure 2.1), such as: $Z(t)$ (the rise of the

apex of the upconing plume), $W(t)$ (plume width at mid-height), normalised electrical conductivity (NEC) of pumped water, and hydraulic heads at the side boundaries. NEC represented the EC of the water normalised to the saltwater EC, and allowed for a comparison of the relative buoyancy effects between experiments. Observations of $Z(t)$ and $W(t)$ were compared to Dagan and Bear (1968) predictions, while the side boundary heads were monitored to observe the departure from the initial head condition and to provide insight into the hydraulic functioning of the sand tank (note that side boundary conditions were head-dependent flux conditions, and therefore pumping caused drawdown at the boundary). $Z(t)$ and $W(t)$ values were determined using the assumption that a relative salinity of 50% (visually judged as the middle of the dispersion zone) was an appropriate surrogate for the position of the freshwater–saltwater interface; a similar assumption to that of Dagan and Bear (1968).

Experimental $Z(t)$ trends were compared to the analytical solution for $Z(t) < d/3$, i.e. the suggested range of applicability of Equation (2.1), as shown in Figure 2.2. The times for experimental $Z(t)$ to reach $d/3$ were 75 min, 57 min, 190 min and 1950 min for Experiments 1, 2, 3 and 4, respectively. In the first two experiments, rates of interface rise (for all $Z(t)$) were somewhat similar and were closely matched with Equation (2.1) predictions. The experimental results and the analytical solution both show that the marginally higher rate of pumping and slightly smaller value of d in Experiment 2 (compared to Experiment 1) produced more rapid rates of upconing, despite increased saltwater density (experimental parameters are given in Table 2.1).

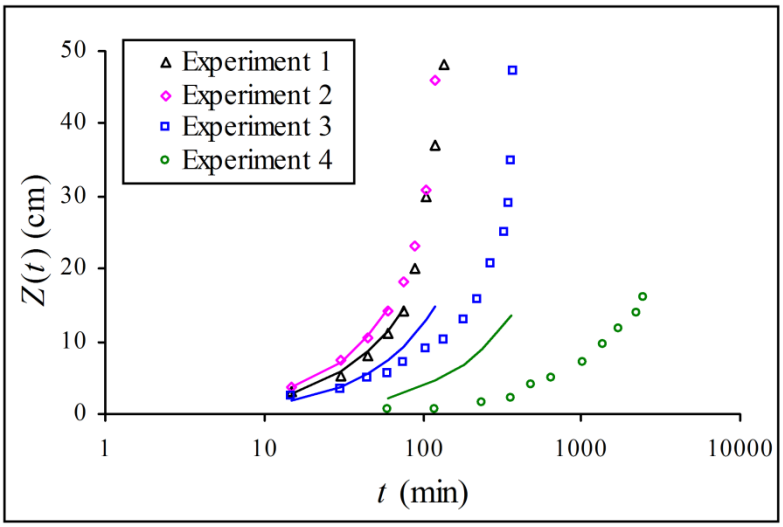

Figure 2.2. Experimental results (points) and theoretical predictions (lines) of $Z(t)$.

The reduced q used in Experiment 3 (i.e. q in Experiment 3 was 56% of q in Experiment 2) produced considerably slower rates of upconing, with the plume reaching the bore after about 6.3 h, compared to about 2 h for Experiment 2. Relative to the experimental observations, Equation (2.1) over-estimated the rate of rise in Experiment 3 and even more so in Experiment 4. Dagan and Bear (1968) tested Equation (2.1) against laboratory experiments using a single freshwater–saltwater density difference of 0.03 g/cm^3, and therefore the current experiments extend their work by testing a range of δ values. We found that Equation (2.1) failed to predict some of the laboratory results, although it is important to note that the limited number of experiments, uncertainties in boundary conditions, and the somewhat approximate nature of the analytical solution preclude our ability to make conclusive statements about the general applicability of Equation (2.1). In any case, the field-scale and experimental values of A, B, C and b_{cr} (Table 2.2) indicate that Experiment 1 is the closest representation to typical real-world situations, and given the close match obtained for that case, Equation (2.1) likely applies to most practical applications.

Experimental values of $W(t)$ were obtained from visual interpretation of the upconing images. The analytical solution of Dagan and Bear (1968) predicts that, for the parameters of the experiments and for the range $Z(t) < d/3$, $W(t)$ is essentially constant in time. Theoretical $W(t)$ values of 58 cm, 53 cm, 52 cm and

54 cm were calculated for Experiments 1, 2, 3 and 4, respectively. Experimental values of $W(t)$ from the first three experiments are given in Figure 2.3; note that $W(t)$ was not easily ascertained for Experiment 4 and is therefore omitted. In general terms, there was a reasonable correlation between $W(t)$ values from the analytical and the experimental results for very early times (i.e. for $Z(t) < d/3$; times when $Z(t) = d/3$ are given above), but there was a decreasing trend in $W(t)$ when the interface was below the bottom of the bore, i.e. when narrow salt spikes were forming and rising, in all experiments. It is difficult to draw conclusions from the comparison between Equation (2.1) predictions and the experimental results because Equation (2.1) is valid only for a small proportion of the experimental duration. $W(t)$ increased in Experiments 1 and 2 after 150 min and 120 min, respectively, corresponding to times when interfaces reached the bore and subsequently widened. It is possible that an asymptotic value for $W(t)$ exists under the experimental conditions (i.e. subsequent to the interface reaching the bore), given that $W(t)$ appeared to somewhat stabilise in the first three experiments (Figure 2.3). These observations of plume geometry during ‘‘critical” periods of the experiment represent the first such discussion on this phase of saltwater upconing. We hypothesise that $W(t)$ will be correlated to the rate of saltwater entering the well (relative to the rate of freshwater discharge) and therefore to the salinity of pumped water, during the period when $Z(t) = d$. This correlation was briefly explored and is discussed below. Clearly, the period when $Z(t) = d$ is an important and poorly understood phase of upconing that requires more attention.

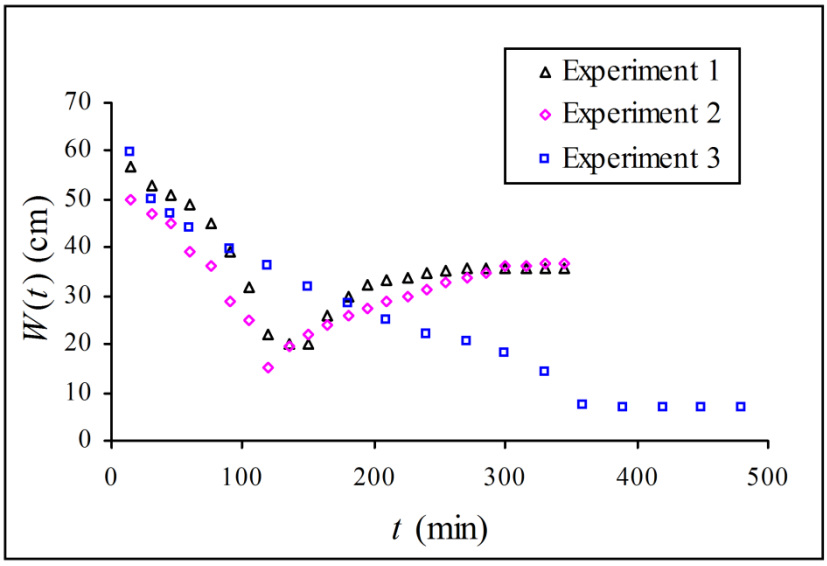

Figure 2.3. $W(t)$ from Experiments 1, 2 and 3.

Trends in NEC are illustrated in Figure 2.4. Experiments 1 and 2 produced NEC curves that are similar in shape (Figure 2.4a), with Experiment 1 NEC slightly exceeding that of Experiment 2 likely due to buoyancy effects, although differences were small. The NEC curves from Experiments 1 and 2 started to stabilise (in a similar fashion to $W(t)$ trends), indicating that a steady-state NEC probably exists. It is not possible to interpret asymptotic NEC values from Experiments 3 and 4 (Figure 2.4b), which were probably terminated prior to the development of steady-state conditions. Only a few studies have focused on the behaviour of salt plumes after the interface has intercepted the production bore (e.g. Reilly and Goodman, 1987), possibly because it is the objective of most management strategies to avoid this condition. However, it is interesting to note that in Experiment 3, NEC was relatively low (Figure 2.4b) as was the bore water EC (<1000 μS/cm), despite visual confirmation that the salt plume had reached the well. The dilution caused by mixing in and around the well produced groundwater that would be useable (from a salinity perspective) in most real-world situations. While the two-dimensional nature of the experiments does not allow for direct inferences to real-world settings in terms of bore salinity trends and the associated relationships to physical parameters, the situation of a bore in contact with the freshwater– saltwater interface and continuing groundwater abstraction, is clearly possible under certain conditions, and may be a common situation in real systems. Therefore, further research into this condition and the

related salt plume behaviour and well salinity dynamics, adding to the preliminary analyses of Reilly and Goodman (1987), is warranted.

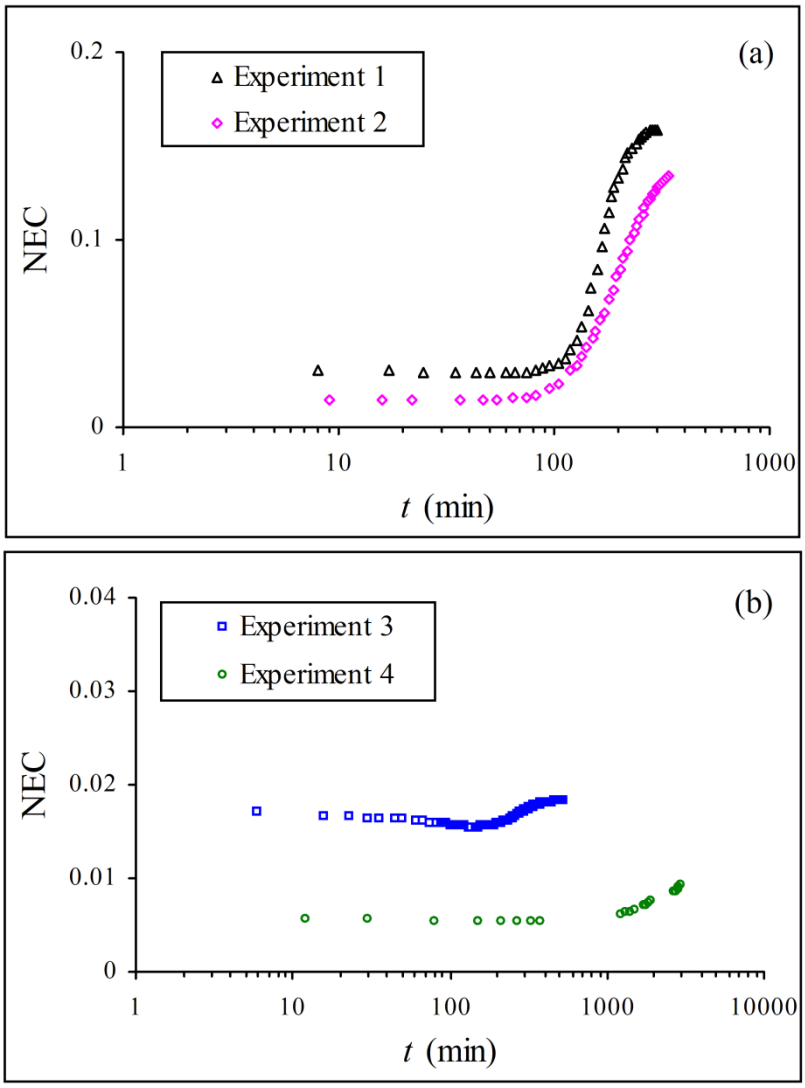

Figure 2.4. Bore water NEC curves for: (a) Experiments 1 and 2, and (b) Experiments 3 and 4.

The correlation between bore EC and the rise of the freshwater–saltwater interface (i.e. Figures 2.2 and 2.4) is an important consideration for the management of coastal bores overlying saline groundwater, because bore EC is usually the only measure of impending salinisation from upconing. This correlation was assessed in simple terms for each experiment by comparing $Z(t)$ to NEC at key points in the experiments, namely at: $Z(t) = 0$ (initial conditions), $Z(t) = d/3$, $Z(t) = d$, and at the end of each experiment; the results are summarised in Table 2.3. The correlation between $Z(t)$ and $W(t)$ was considered

in a similar fashion, and the corresponding $W(t)$ values are presented in Table 2.4. The experimental results indicate that by the time the interface (i.e. represented by the 50% relative salinity) had visibly intercepted the bore (i.e. $Z(t) = d$), the bore NEC increased by up to 80% of the original fresh bore water salinity. This NEC change was subtle relative to the saltwater salinity. In the case of the medium-to-low flow experiments (Experiments 3 and 4), interface-bore interception (i.e. $Z(t) = d$) produced fairly minor increases in bore NEC. In most cases, the bore NEC continued to rise during the subsequent period (i.e. while $Z(t) = d$), and this was linked to widening of the salt plume (i.e. as shown in Figure 2.3). This is highlighted by the results in Table 2.4, which clearly demonstrate that increasing $W(t)$ was associated with increasing NEC once the salt plume was in contact with the bore. Specifically, significant bore NEC increases occurred in Experiments 1 and 2 where an appreciable salt plume widening was observed, whereas no salt plume widening (i.e. while $Z(t) = d$) and almost negligible NEC increase occurred in Experiment 3. Experiment 4 produced an upconing pattern that was unique, and plume widening measurements were not comparable to the other experiments, and hence it was difficult to interpret bore NEC changes. Further, the 50% salinity did not quite reach the bore by the end of the experiment (hence the ‘‘No result” in Table 2.3). It is challenging to draw implications from these observations for the management of field-scale upconing, although the experimental findings indicate that the management of upconing in real situations may need to consider the behaviour of salt plumes under conditions where bore-interface interception has already occurred. This may be important in the design of management actions, as bore-interface interaction may be a widespread phenomenon given that bore EC changes were sometimes relatively small when this occurred in the laboratory.

Table 2.3. NEC at $Z(t) = 0$, $Z(t) = d/3$ and $Z(t) = d$.

$Z(t)$	NEC			
	Exp. 1	Exp. 2	Exp. 3	Exp. 4
Initial	0.03	0.02	0.02	0.006
$d/3$	0.03	0.02	0.02	0.006
d (Interface reaches bore)	0.05	0.03	0.02	No result
End of Experiment	0.16	0.13	0.02	0.009

Table 2.4. $W(t)$ at $Z(t) = 0$, $Z(t) = d/3$ and $Z(t) = d$.

$Z(t)$	$W(t)$ (cm)		
	Exp. 1	Exp. 2	Exp. 3
Initial	0	0	0
$d/3$	45	40	27
d (Interface reaches bore)	20	15	7
End of Experiment	36	37	7

The majority of the laboratory analysis focused on transport behaviour; however the hydraulic functioning of the tank was also a consideration. The initial watertable positions (defined by manometer measurements) in all experiments were set to 110 cm from the bottom of the tank. Hydraulic heads were monitored at two different depths at the boundary throughout each experiment to assist in quantifying sand tank hydraulics under pumping; a necessary aspect of the study due to the head-dependent flux boundary conditions imposed at the side boundaries. Boundary hydraulic heads at different depths were virtually the same, and the heads on both sides of the tank were in agreement in all experiments. The pumping-induced drawdown at the boundary in each of the experiments is given in Figure 2.5. It was anticipated that drawdown would asymptote to a steady-state value, and this was indeed observed in the slower pumping experiments (3 and 4), whereas drawdown appeared to continue to gradually increase in the higher pumping experiments (1 and 2). The drawdown is larger for the cases of higher pumping, as anticipated, although the difference in drawdowns between Experiments 1 and 2 was expected to be smaller than that observed because the associated pumping rates were almost the same. The

influence of buoyancy effects on the behaviour of the side boundaries appears to be complex in some cases, and numerical modelling is required to properly elucidate the relative contributions of the saltwater forcing heads in the overall hydraulic functioning of the sand tank boundaries. The assumption here is that the side boundaries are sufficiently distant from the well such that they have only minor influence over upconing near the well.

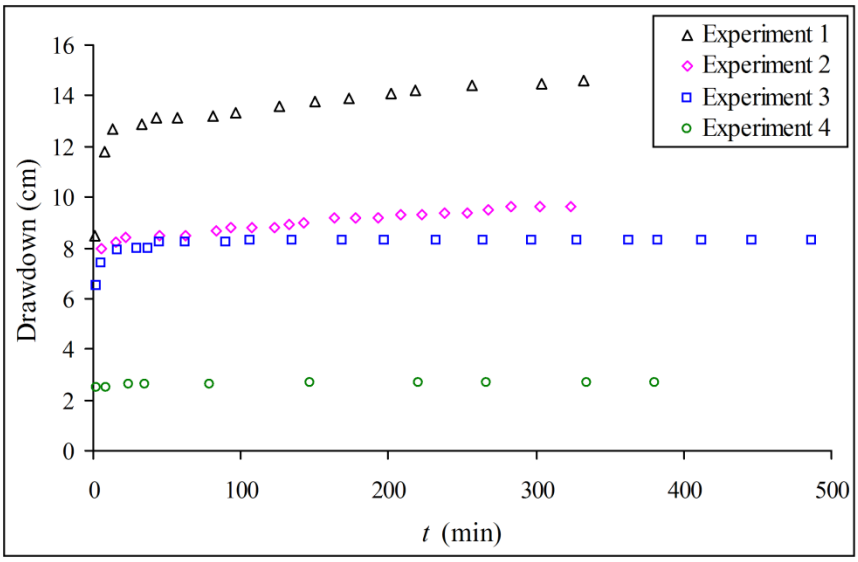

Figure 2.5. Watertable drawdown at the side boundaries.

2.4 Summary

Four saltwater upconing experiments were conducted under controlled conditions in a laboratory sand tank. Upconing was analysed in terms of apex rise, plume width and bore salinity. Experiments were designed to evaluate upconing under different mixed convection ratios, manifested by changing the freshwater-saltwater density difference and the rate of groundwater extraction. Saltwater is shown to intercept the well in all cases. The visualisations of upconing arising from the experiments are the first such images to be presented in the literature. Patterns of upconing were in agreement with the analytical solution of Dagan and Bear (1968) up to a certain density-pumping condition, but beyond that there was a departure from theoretical sharp-interface upconing behaviour in terms of rates and upconing shapes.

The most rapid and significant upconing occurred under high pumping and low density difference. The influence of density was shown to be minor relative to combined influence of the rate of pumping and the distance from the bore to the initial interface, in certain situations. Dispersion effects were apparent during early times, and were especially important during “critical phase” upconing, involving the rise of an initially dilute salt spike. In the experiments where the plume was in direct and prolonged contact with the bore, the plume width and salinity increased until the bore water salinity approached asymptotic values. Eventually, the saltwater plume became non-dispersive.

A departure from the classical upconing shape was obtained for the situation of highest saltwater density and lowest pumping, in which upsoning occurred as an almost horizontal interface for the majority of the experiment, eventually producing a double-peak shape as the interface neared the well.

Chapter 3

Numerical modelling of saltwater upconing: comparison with experimental laboratory observations

This chapter is based on the following paper:

Jakovovic D., Werner A.D., Simmons C.T., 2011. Numerical modelling of saltwater up-coning: comparison with experimental laboratory observations. Journal of Hydrology 402, 261-273.

Abstract

In this study, previous interpretations of the density-dependent flow and transport processes induced by pumping freshwater above denser saltwater in four laboratory sand-tank experiments are extended using numerical modelling. The numerical model captured the transition in dispersiveness of upconing plumes observed in the laboratory (i.e. highly dispersive at early times tending to sharp interfaces after saltwater reaches the well). This demonstrates the applicability of the velocity-dependent dispersion of the modelling code. In all four experiments, head-dependent flux boundary conditions were used to simulate the sand-tank side boundary conditions. The experimentally derived boundary conductance values indicate non-linear variations in the resistance to flow through side inflow ports between the different experiments. Nonetheless, linear boundary head-inflow relationships adequately reproduced laboratory upconing. The numerical model was able to reproduce the laboratory results within a reasonable level of accuracy and with minimal calibration of model parameters for three of the four experiments. This serves to validate those particular laboratory observations. The "double peak" upconing observed late in the fourth laboratory experiment was not reproduced by the model. Further

analysis considering adsorption of the Rhodamine tracer is suggested to explore the cause of this effect. Numerical modelling results were compared to an existing sharp-interface analytical solution, which corresponded well with the numerical modelling results for early stages of the four upconing experiments, despite the dominant influence of dispersion at early times.

3.1 Introduction

Saltwater upconing is the vertical upward movement of saltwater towards a pumping well and is a problem in groundwater exploitation for many coastal aquifers around the world (FAO, 1997). Previous studies suggest that contamination from upconing generally requires the pumping well to be shut down due to water quality degradation (Zhou et al., 2005; Narayan et al., 2006). To date, saltwater upconing research has been based predominantly on theoretical analyses because of the challenges of undertaking field-based measurements of salt transport dynamics occurring below pumping wells.

The most widely used analytical solution to transient saltwater upconing was developed by Dagan and Bear (1968). They obtained a non-steady solution for interface rise below a well in an infinite aquifer by using the method of small perturbations. Dagan and Bear (1968) compared their analytical solution to laboratory results in the form of interface movements inferred from sand-box salinity measurements. The solution was found to be valid for interface rise approximately up to one-third the distance between the bottom of the well and the initial interface position. In adopting the sharp-interface approximation, Dagan and Bear (1968) neglected dispersive transport processes and were therefore unable to reconcile observed salinity trends of the pumping well with their theoretical analysis.

Diersch et al. (1984) were among the first to numerically model variable density and dispersion effects for saltwater upconing below pumping wells. They studied the sensitivity of dispersivity and found that the well salinity is strongly influenced by dispersion (i.e. dispersion governs the transitive phase of the salinity breakthrough curve). This was further discussed and reconfirmed by Holzbecher (1998) who remodelled the Diersch et al. (1984) numerical experiments. In addition, Holzbecher (1998) concluded that at the start of pumping the salt transport is mainly governed by the longitudinal dispersivity. Both of these studies were based on numerical analyses only. Reilly and Goodman (1987) simulated a field situation of saltwater upconing using a numerical model of density-dependent groundwater flow and dispersive solute transport. They compared sharp-interface and dispersive transport approaches

and concluded that the dispersive transport approach is needed to reproduce certain upconing conditions (e.g. under cyclic pumping) involving wide transition zones. Johanssen et al. (2002) used a numerical model to simulate the laboratory results of Oswald (1998), who produced saltwater upconing in a 3D sand box. Johanssen et al. (2002) were able to reproduce experimental results following calibration of model parameters such as permeability, porosity and transverse dispersivity. They concluded that it was not possible to obtain an accurate match of the experiments without calibrating the input parameters, albeit primarily within the bounds of measurement errors in the parameter values. Konz et al. (2009) produced saltwater intrusion experimental results for benchmarking variable-density numerical codes. Saltwater intrusion was observed occurring both laterally and vertically (i.e. saltwater upconing), albeit the focus of the study was lateral seawater intrusion. Highly dispersive upconing was observed in both laboratory experiments and modelling results, i.e. only the 10% isochlor reached the well. The Konz et al. (2009) experiments demonstrated that dispersion is an important phenomenon in controlling bore salinisation; further work is needed to explore dispersive processes for a broader range of saltwater upconing conditions.

Recently, Werner et al. (2009) performed a series of saltwater upconing experiments that captured the behaviour of dense saline plumes near a pumping well and provided the associated breakthrough curves of the well. They showed that dispersive transport processes were important during the early phase of upconing (i.e. during initial salt-plume rise). The dispersed interface produced gradual increases in pumped water salinity rather than the abrupt salinity changes expected under the conditions of a sharp interface. However, Werner et al. (2009) also observed that the interface eventually became sharp (i.e. non-dispersive). The transitional dispersiveness observed in their experiments may be the consequence of longitudinal dispersion controlling early-time behaviour, which involved upward saltwater transport, and the smaller transverse dispersion controlling late-time transport under stable conditions of the interface being in contact with the well. The transition from dispersive to non-dispersive saltwater upconing observed by Werner et al. (2009) requires further analysis to assess both the validity of laboratory observations and the controls on upconing

processes, and to test whether the dispersive transition observed in the experiments is reproducible in numerical model simulation, and is therefore predictable. Werner et al. (2009) also reported that boundary conditions might have had some effect on upconing at the tank edges, since asymmetry in the interface was observed, as was an early-time wave-like rise of the interface at the start of the experiments. They recommended modelling of the laboratory experiments to provide further insight into the observed flow and transport processes and boundary condition effects.

In this study, the laboratory experiments of Werner et al. (2009) are analysed using a density-dependent flow and transport model to explore the temporal development of experimental saltwater plumes beyond the simple analysis previously undertaken. The aim is to assess whether the laboratory observations are reliable and are not adversely influenced by experimental nuances. The numerical analysis of the laboratory experiments serves to provide further insight into the physical processes of saltwater upconing, which cannot be perceived from physical experiments alone (e.g. numerical modelling allows for evaluation of velocity fields). In addition, the numerical model is used to test whether various observed phenomena (e.g. transitions from dispersive to non-dispersive interfaces, drawdown at the sand-tank edges) as observed by Werner at al. (2009) are reproducible using a common numerical modelling approach. This study builds on similar numerical modelling analyses of sand tank experimentation by Johannsen et al. (2002) and Oswald and Kinzelbach (2004) by considering new (albeit constrained) upconing scenarios and by comparing modelling results to direct visualisations of upconing, thereby eliminating the need for geophysical interpretations of salinity plumes. Also, the arrangement of the laboratory experiments of Werner et al. (2009) allows for a comparison of numerical modelling results with Dagan and Bear's (1968) sharp-interface analytical solution of saltwater upconing to evaluate the validity of the analytical solution relative to the numerical model for the experimental conditions.

3.2 Methods

3.2.1 Conceptual model

Werner et al. (2009) undertook only a simple analysis of the observed flow and transport processes pertaining to their four laboratory experiments of saltwater upconing. They varied the discharge rate and saltwater-freshwater density differences, and this had a significant influence on the upconing shape and extent (see Table 3.1 for density difference and pumping rate variations in the four laboratory experiments). A simplified diagram of the experimental set-up is illustrated in Figure 3.1.

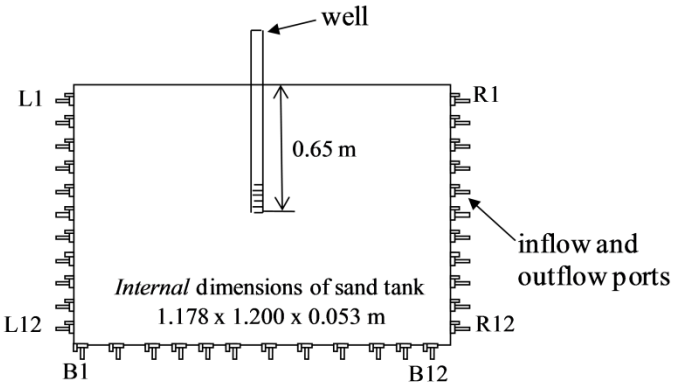

Figure 3.1. A schematic of the experimental set-up of Werner et al. (2009).

The sand tank of Werner et al. (2009) contained a relatively homogeneous porous medium (i.e. medium sand with a representative grain-size distribution (d_{50}) of 0.46 mm). Inflow/outflow taps positioned at 10 cm intervals on the sides of the sand tank were used to supply freshwater (i.e. via taps L3, L5, L7, L9, R3, R5, R7 and R9) and saltwater (i.e. via taps L12 and R12) (see Figure 3.1). Water extraction occurred through a well embedded to a depth of 0.65 m from the top of the sand tank.

A conceptual model for the sand-tank simulation is shown in Figure 3.2, corresponding with the laboratory experimental set-up. In Figure 3.2, *b* (m) is the initial thickness of the saltwater layer, *a* (m) is the initial thickness of the freshwater layer, *D* (m) is the distance from the top of the sand tank to the

bottom of the well, and l_w (m) is the length of the slotted section of the well. C_0 and C_S represent relative concentrations of freshwater and saltwater, respectively. The model dimensions were length A = 1.178 m and height B = 1.175 m and a two-dimensional representation was considered. Freshwater entered the model via eight single nodes (four on each side of the model), labelled as q_{F1} and q_{F2} groups in Figure 3.2, and saltwater entered the model via two single nodes (one on each side of the model) labelled q_{S1} and q_{S2} in Figure 2.2. Note that q refers to flow rates in the two dimensional domain [L^2T^{-1}], as obtained through scaling from experimental Q [L^3T^{-1}] values. Inflow nodes were located at 5 cm (saltwater inflow port), 35 cm, 55 cm, 75 cm and 95 cm (freshwater inflow ports) above the base of the sand tank.

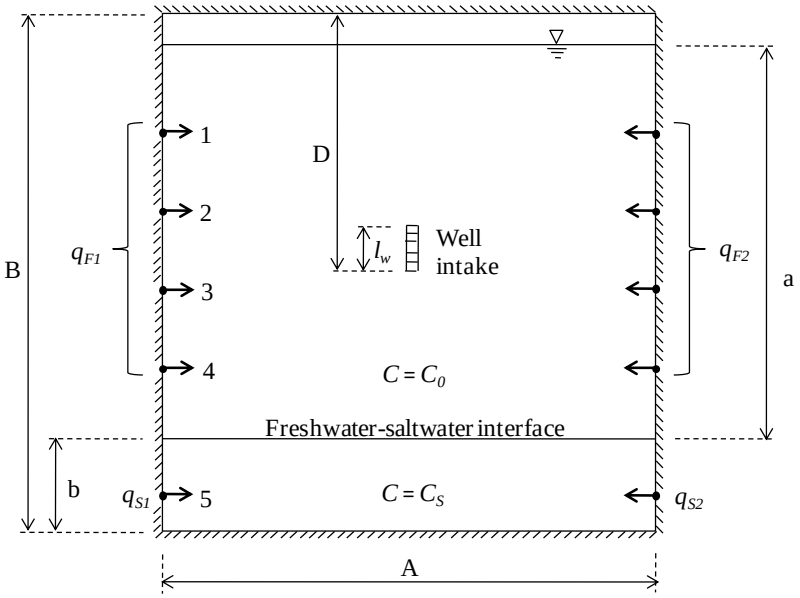

Figure 3.2. Conceptual model of the simulated experiments.

3.2.2 Numerical model development

The laboratory experiments of Werner et al. (2009) were investigated through numerical modelling using the finite-element FEFLOW code, which simulates variably saturated, density-dependent flow and solute transport processes. FEFLOW has successfully reproduced such benchmark problems as the Elder problem (Diersch and Kolditz, 2002) and the Henry problem (Diersch, 2005). Information on the mathematical formulation of FEFLOW is given in the user manual (Diersch, 2005) and is not repeated here.

The model was used to predict breakthrough curves and the temporal rise of upconing for comparison with the experimental results. The model domain is the full two-dimensional representation of the sand-tank (i.e. not a symmetric half domain). For three of the four simulations, the model domain was discretized to form a uniform mesh containing 100,806 nodes and 100,172 quadrilateral elements with $\Delta x = \Delta z = 0.00372$ m. Grid convergence was tested to evaluate the adequacy of the spatial discretization. Breakthrough curves and the movement of the 50% relative salinity contour were simulated using 100,172, 249,999 and 499,848 elements. The different levels of discretization all produced results that were in close agreement (results not shown), and so the grid of 100,172 elements was used because it allowed for the shortest run-times. For the fourth simulation, with highest density and lowest pumping rate, the model domain contained 201,152 nodes and 200,256 quadrilateral elements with $\Delta x = \Delta z = 0.00263$ m. Due to the large buoyancy effect and low advection, the fourth simulation required finer discretization to achieve grid convergence.

All simulations used the forward Adams-Bashforth/backward trapezoidal predictor-corrector scheme with automatic time-step control and no upwind (Galerkin-FEM) method. Such numerical conditions provide minimum numerical dispersion (Diersch, 2005). The initial time-step length was set to 10^{-6} days, increasing up to 0.002 days towards the end of simulations. There was no limit set for the maximum time-step length, since FEFLOW prevents time steps becoming too large by an error-checking algorithm. In this case, error tolerance was set to maximum error norm, which is FEFLOW's strongest error measure (Diersch, 2005).

The bottom and the top of the model were set to no-flow boundaries. Specified head boundary (SHB) conditions represented the side boundaries in preliminary modelling attempts. Two cases of SHB were considered; SHB applied continuously along the side boundaries and SHB applied only at the individual nodes, representing the inflow ports of the sand tank. However, drawdown was observed at the side boundaries during laboratory experiments, and so a head-

dependent flux boundary condition was adopted (i.e. a "general head boundary" or GHB) to accommodate the transient development of boundary drawdown. The GHB was applied using the following equation (Harbaugh et al., 2000):

$$Q = M(H_b - H_m) \tag{3.1}$$

Here, Q is the flux into or out of a boundary node (L^3T^{-1}), H_b is the externally applied boundary head (L), H_m is the internal head at the boundary as computed by the model (L), and M is the boundary conductance (L^2T^{-1}). M represents the resistance to inflow between the constant head reservoirs and the porous medium boundary of the Werner et al. (2009) laboratory experiments.

Q, H_b and H_m were measured in the laboratory (H_m was taken as the late-time boundary head in the sand-tank), allowing M to be calculated from late-time experimental observations using equation (2.1). M values were calculated for each experiment because Q and H_m differed between experiments, i.e. different Q values were tested between experiments and H_m changed accordingly. H_b was set in experiments to be equal for both freshwater and saltwater, and for all four experiments H_b = 1.15 m (i.e. the freshwater head measured from the base of the sand tank). M values for both freshwater and saltwater ports are given in Table 2.1, which also lists other factors that differ between the four experiments. There is a trend of decreasing M values with decreasing Q, indicating that the resistance to flow through side inflow ports was higher for smaller pumping rates. M values may also be influenced by grain compaction near inflow ports and/or well-screen clogging. It was not possible to diagnose the cause of boundary conductance differences between experiments. Nonetheless, the application of GHB conditions facilitated assessment of the side boundary conditions that would otherwise have been precluded by adopting SHB conditions. This proved to be an important aspect of the modelling analysis, because GHB boundary conditions allowed inter-experimental differences to be captured in the modelling framework, without the need for model calibration. Extremely low saltwater port M values were obtained for the low-pumping experiments, i.e. saltwater inflow was a smaller proportion of the pumping rate in low pumping experiments. Saltwater inflows were lower than freshwater inflows (i.e. based on the average flow through a single port) in all experiments. It is difficult to attribute these observations to a physical cause without further

laboratory experimentation, but it appears that *M* may be non-linear across the spectrum of high and low flow rates, whereby *M* is disproportionally lower at lower values of *Q*. An assessment of experimental controls of the *M*-*Q* relationship is the subject of ongoing analysis.

Table 3.1. Experimental values of conductance (*M*), pumping rate (*q*) and density (ρ).

	Experiments			
	1	**2**	**3**	**4**
Freshwater ports *M* (m^2d^{-1})	0.179	0.245	0.165	0.065
Saltwater ports *M* (m^2d^{-1})	0.107	0.140	0.017	0.019
Saltwater density, ρ_S (kgm^{-3})	1011	1025	1025	1096
Freshwater density ρ_f (kgm^{-3})	998	998	998	998
Pumping rate, *q* (m^2d^{-1})	5.89	6.04	3.34	0.82

The extraction well was simulated in the model using a zone of high-*K* cells, representing the slotted section of the well. The high-*K* zone was 50 mm high and 14 mm wide, and *K* was set arbitrarily to 450 m/d. Extraction was via a single-node point source, placed midway in the high-*K* zone. Various other well representations were tested (i.e. single-node point source placed at the top and bottom of the high-*K* zone), producing only small variations in well salinities.

The unsaturated zone was modelled using van Genuchten (1980) functions. van Genuchten (1980) parameters were obtained experimentally for the purposes of populating the FEFLOW parameter requirements. The van Genuchten (1980) parameters were calculated from water retention curves using the method of Wraith and Or (1998). The results are provided in Table 3.2, which also lists other physical attributes and model parameters. The van Genuchten (1980) parameters obtained experimentally provided reasonable agreement to laboratory observations in terms of drawdown at the side boundaries. However, a sensitivity analysis showed that drawdown predictions were relatively

insensitive to variations in the unsaturated zone parameters, likely due to the narrow unsaturated zone relative to the saturated thickness.

Table 3.2. Model input parameters.

Parameter	**Value**
Model height, z (m)	1.175
Model width, x (m)	1.178
Hydraulic conductivity, K (md^{-1})	140
Porosity, n (-)	0.38
Longitudinal dispersivity, β_L (m)	0.002
Transverse dispersivity, β_T (m)	$=\beta_L/20 = 0.0001$
Molecular diffusivity, D_f (m^2s^{-1})	10^{-9}
Sand maximum saturation, S_s (-)	1
Sand residual saturation, S_r (-)	0.14
van Genuchten (1980) curve-fitting parameter, α (m^{-1})	55
van Genuchten (1980) pore size distribution index, N (-)	2.4

An additional series of column experiments has been carried out to estimate longitudinal dispersivity, β_L. The experiments used sand columns of 4.97 cm in diameter and 29 cm in length, and a peristaltic pump maintained constant flow rates through the columns. Calcium chloride dehydrate concentrations (i.e. the same salt as used in the Werner et al. (2009) experiments) were determined using electrical conductivity (EC) and EC versus mass concentration relationships. The breakthrough of the salt tracer was fitted to the 1D analytical solution of Ogata and Banks (1961) and β_L values in the range 0.05 – 0.3 cm were obtained. This is in agreement with previous findings of Oswald and Kinzelbach (2004), Goswami and Clement (2007), and Konz et al. (2009), who reported similarly small β_L values. A value for β_L of 0.2 cm was adopted as the base case in all numerical simulations since it generally produced satisfactory predictions of the physical experiments. The transverse dispersivity, β_T, is commonly assumed to be 1/20 to 1/6 of β_L (Harleman and Rumer, 1963; Huang et al., 2003). Accordingly, a base β_T value was chosen as 0.01 cm. Trial and

error analysis indicated that β_T values within the range $\beta_L/20$ to $\beta_L/6$ produce similar results, although lower values were optimal relative to laboratory observations.

The modelling results were evaluated both qualitatively and quantitatively. Quantitative analysis of the modelling results involved several indicators of the flow and transport dynamics, including: salinity breakthrough curves from the pumping well, height of the interface apex, width of the salt plume, and drawdown at the side boundaries. Plume widths from the numerical model predictions were taken as the width of the 50% salinity contour (where 100% salinity coincides with the inflowing saltwater) at midway within the vertical extent of saltwater plumes. The temporal trends of these indicators were tracked during FEFLOW simulations to compare with the corresponding laboratory observations of Werner et al. (2009).

An attempt to compare model predictions with laboratory results was undertaken using image analysis. Saltwater was coloured with FWT Red (a form of Rhodamine WT dye produced by ENVCO, Australia) to allow visual observation of saltwater trends. Image analysis of the laboratory experimental photography was aimed at estimating dye concentration at each pixel in the image, by finding the optimal linear mixture model based on pure dye and pure background (i.e. no dye region in the sand tank). Unfortunately, the analysis was unable to accurately reconcile salinity differences due to excessive image non-homogeneities caused by imperfect lighting and variations in sand colour. Therefore, plume concentrations were interpreted through visual inspection only, i.e. qualitatively, as per Werner et al. (2009) who interpreted the mid-point of transition zones to infer plume shape (apex height and plume width at mid-height).

3.3 Results

3.3.1 Specified-head versus general-head boundary conditions

The main difference between SHB and GHB conditions is that GHB allows for the temporal development of drawdown in the sand tank, whereas SHB forces a constant water level (i.e. corresponding to the drawdown observed at the end of experiments) throughout the entire duration of experiments. Figure 3.3 illustrates the comparison of numerical model results using SHB and GHB conditions for Experiment 1. Similar results were obtained for other experiments but are not shown for brevity. The model with the SHB conditions applied only at the individual nodes overestimated the rise and width of the saltwater plume and the salinity of the pumping well. This is due to the lower water level (i.e. higher drawdown) and the associated higher saltwater influx at early times in the SHB case relative to the gradual evolution of drawdown and lower initial saltwater influx in the GHB case and in the laboratory experiments. However, the model with the SHB conditions applied continuously along the side boundaries underestimated the width of the saltwater plume and the salinity of the pumping well. This is due to the height of the saltwater at the boundary being fixed in this case, which inhibits salinity rise at the boundary and hence a plume of smaller width is produced.

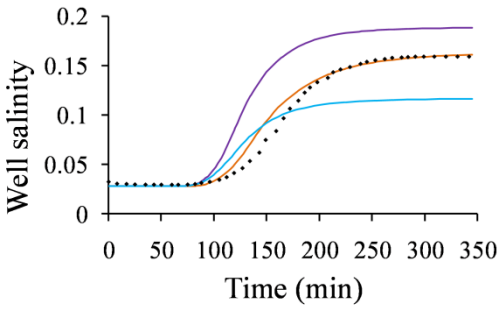

Figure 3.3. Numerical model results for well salinity (where a value of 1.0 represents saltwater) using SHB applied continuously along the side boundaries (solid blue line), SHB applied at the individual nodes (purple solid line) and GHB applied at individual nodes (orange solid line), compared to laboratory observations (black diamonds) for Experiment 1.

3.4 Qualitative observations

Experiment 1 laboratory images are compared to the simulated salinity contours in Figure 3.4. Model results were obtained using un-calibrated parameters (with the exception of some testing of the well representation as discussed previously). The freshwater-saltwater interface observed in the laboratory was dispersive at early times and non-dispersive at late times, and this appears to have been well captured by the numerical model. Some asymmetry in the plume shape was evident in the laboratory experiment, and was more noticeable in the latter stages of experiment (Figure 3.4d). It was possible to attain an improved match to the experimental plume asymmetry through calibration of M values for individual ports (simulation results not shown), thereby providing insight into possible variability in this aspect of the experimental set-up. Calibrated M values were: freshwater ports M = 0.24 m^2d^{-1}, right boundary saltwater port M = 0.20 m^2d^{-1}, and left boundary saltwater port M = 0.09 m^2d^{-1}, indicating that minor differences in inflow port performance probably occurred in laboratory experiments.

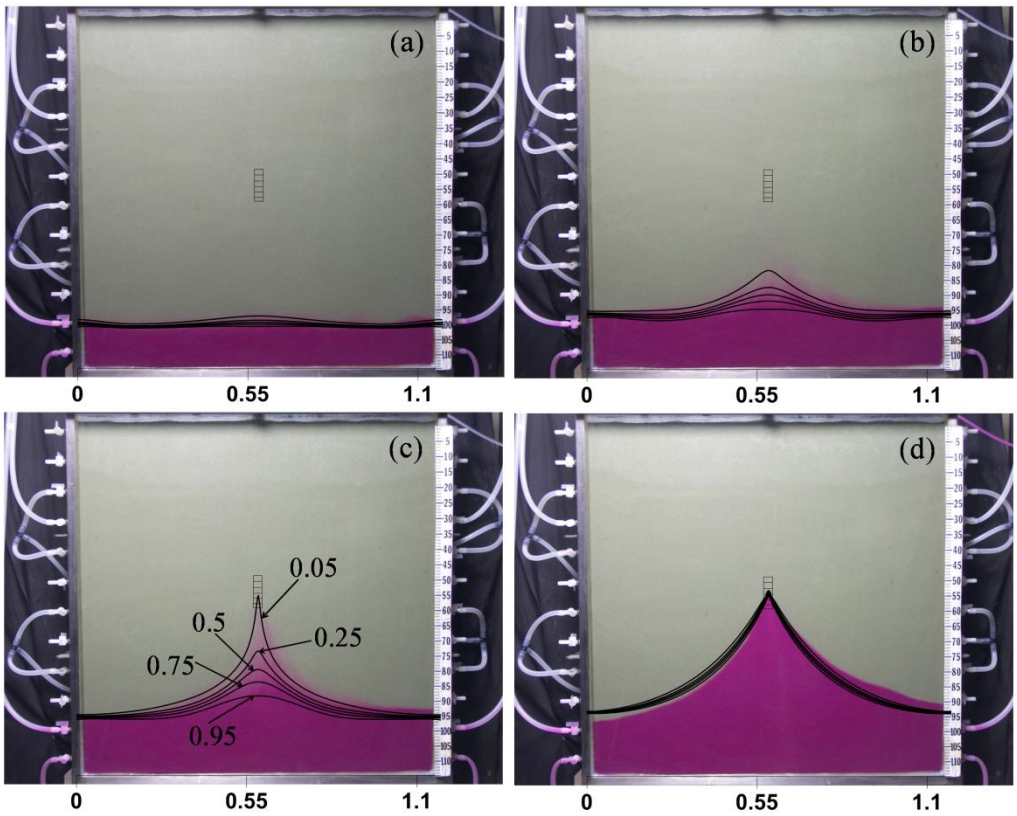

Figure 3.4. Plume images from Experiment 1 with comparison to simulated relative salinity contours: (a) 15 min, (b) 60 min, (c) 90 min, and (d) 345 min. In all figures, the scale is in metres and relative salinity contours of 0.05, 0.25, 0.5, 0.75 and 0.95 are shown (low salinity contours are located above high salinity contours in all experiments).

The wave-like rise of the interface (i.e. the early rise at the sides of the sand tank) at the start of the experiment was reproduced in the simulation (Figure 3.4a), and was therefore not simply an experimental aberration. Preliminary simulations using evenly distributed SHB conditions along the sand-tank sides (i.e., rather than through individual inflow ports) produced interface rise without the early-time wave-like trend (results not shown). The early-time wave-like rise of the interface was therefore likely due to the influence of localised circulations generated by point inflows at individual ports.

The numerical model produced a slightly dispersed interface in the latter stages of the experiment, whereas the interface appeared to have been sharp in the laboratory experiment at the same times (Figure 3.4d), albeit experimental results rely on visual inspection of photographs. Model testing of lower β_L and β_T values produced only small reductions in the interface width, and hence the

simulated interface width is near the lower bound of the model's capability to simulate a sharp interface.

Figure 3.5 illustrates the comparison of simulated salinity contours to laboratory images of salt plumes from Experiment 2. The simulated salinity contours are an excellent match with the experimental observations. The model captured the transition from dispersive to non-dispersive interface conditions that was apparent in the laboratory experiment. Some plume asymmetry was again evident in the laboratory results, although to a lesser degree relative to Experiment 1. As with Experiment 1, the model produced a slightly dispersed interface during the final stages of the experiment, whereas the laboratory experiment appeared to produce a sharp interface during latter stages.

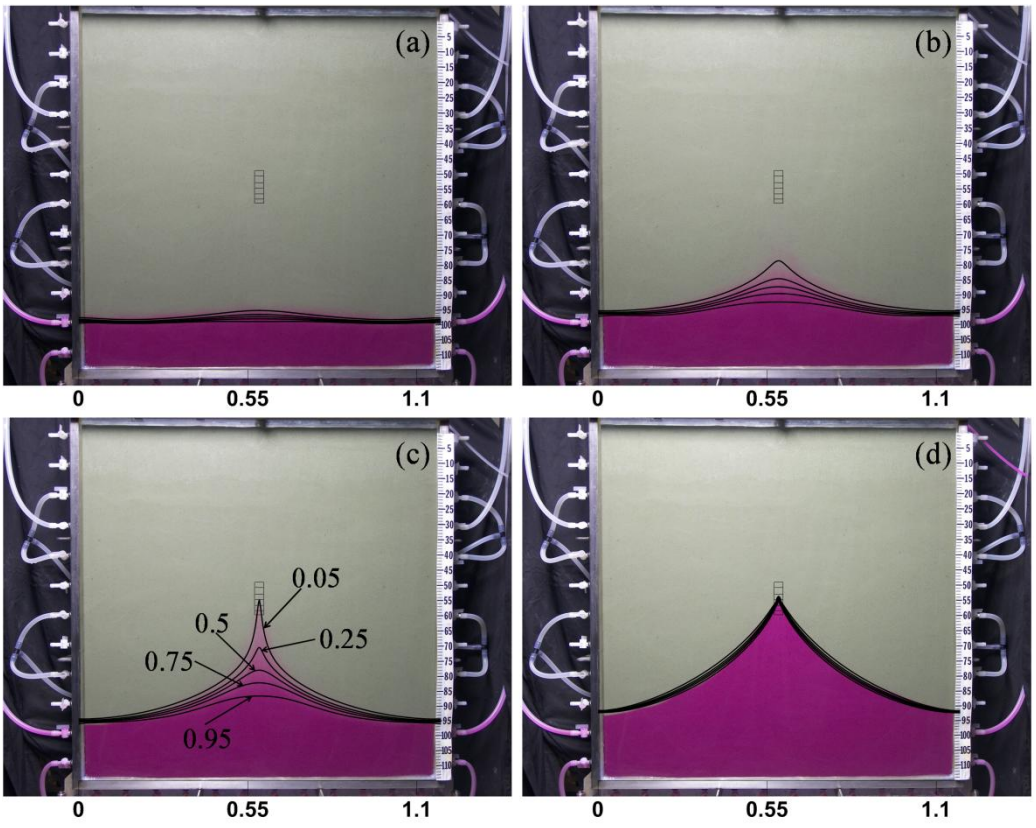

Figure 3.5. Plume images from Experiment 2 with comparison to simulated relative salinity contours; (a) 15 min, (b) 60 min, (c) 90 min and (d) 345 min.

Figure 3.6 shows the comparison of simulated salinity contours to laboratory salt plumes from Experiment 3. The lower pumping rate in Experiment 3 produced upconing in the form of a narrow, dispersed salt spike, both in the laboratory and

via the model. Experiment 3 upconing was clearly more dispersive than in the previous experiments. The simulated salinity contours again compare well with the experimental observations, demonstrating the ability of the numerical model to simulate more dispersive situations.

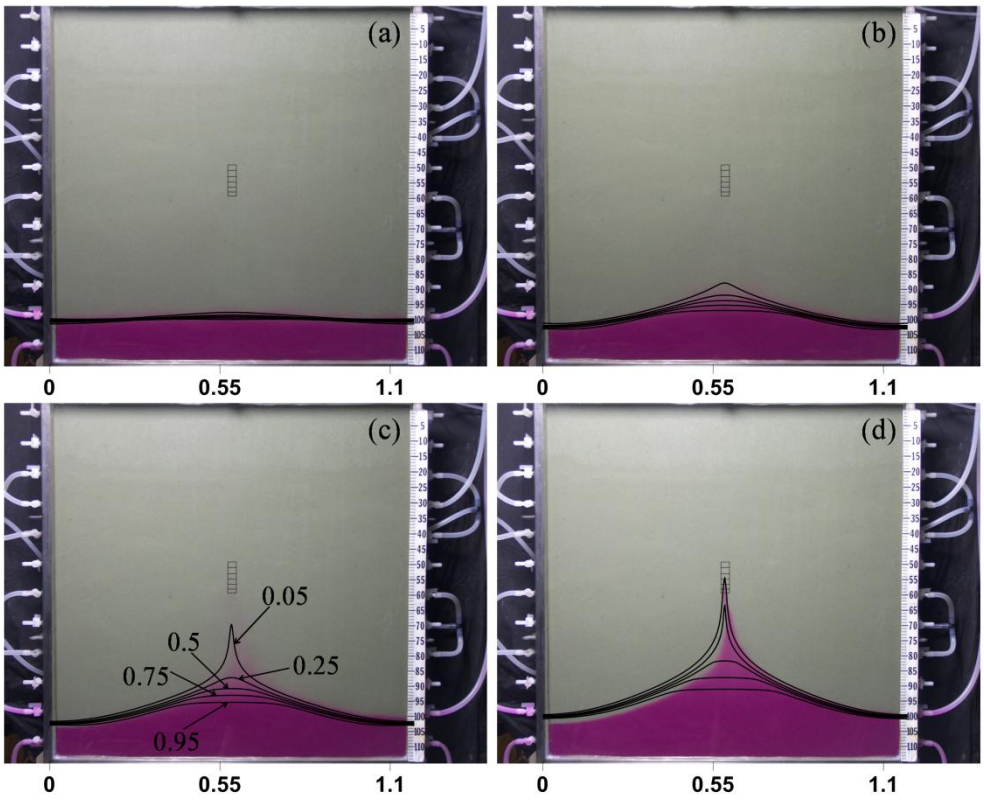

Figure 3.6. Plume images from Experiment 3 with comparison to simulated relative salinity contours; (a) 15 min, (b) 105 min, (c) 195 min and (d) 540 min.

Plume asymmetry was more obvious in Experiment 3 than in previous experiments, although again it was possible to match plume asymmetry through calibration of the *M* values for individual ports (calibrated model predictions not shown). Trial-and-error calibration produced the following boundary conductance values: freshwater ports M = 0.28 m^2d^{-1}, right boundary saltwater port M = 0.042 m^2d^{-1}, saltwater port left boundary M = 0.002 m^2d^{-1}, indicating, as for the Experiment 1, that differences in inflow port performance existed in laboratory experiments. The *M* values of individual ports varied across the experiments, perhaps partly attributable to non-linear *M*-*Q* relationships. Further assessment of experimental controls on the *M*-*Q* relationship is needed to ascertain physical causes of *M*-value variability between experiments.

Figure 3.7 illustrates the comparison of simulated salinity contours and laboratory images of salt plumes from Experiment 4. The simulated salinity contours compare well with the experimental observations for the early stages of the experiment. In the final stages of the experiment, the model failed to predict the "double-peak" upconing observed in the laboratory (i.e. upconing was double-peaked initially but became hollow crest-shaped during the latter stages of Experiment 4; see Figure 3.7d). The simulation captured the near-horizontal rise of the interface at early times (i.e. the 50% salinity contour remains almost horizontal), demonstrating that this was not a nuance of the experimental set-up. Towards the end of the experiment, the model produced a much more dispersed interface than observed in the laboratory, even though the mesh was refined (i.e. the number of nodes was doubled relative to the first three experiments). An additional simulation using a more refined mesh (i.e. up to 500,000 nodes) increased the time required for the simulation (i.e. by a factor of about ten) without narrowing the interface significantly (results not shown).

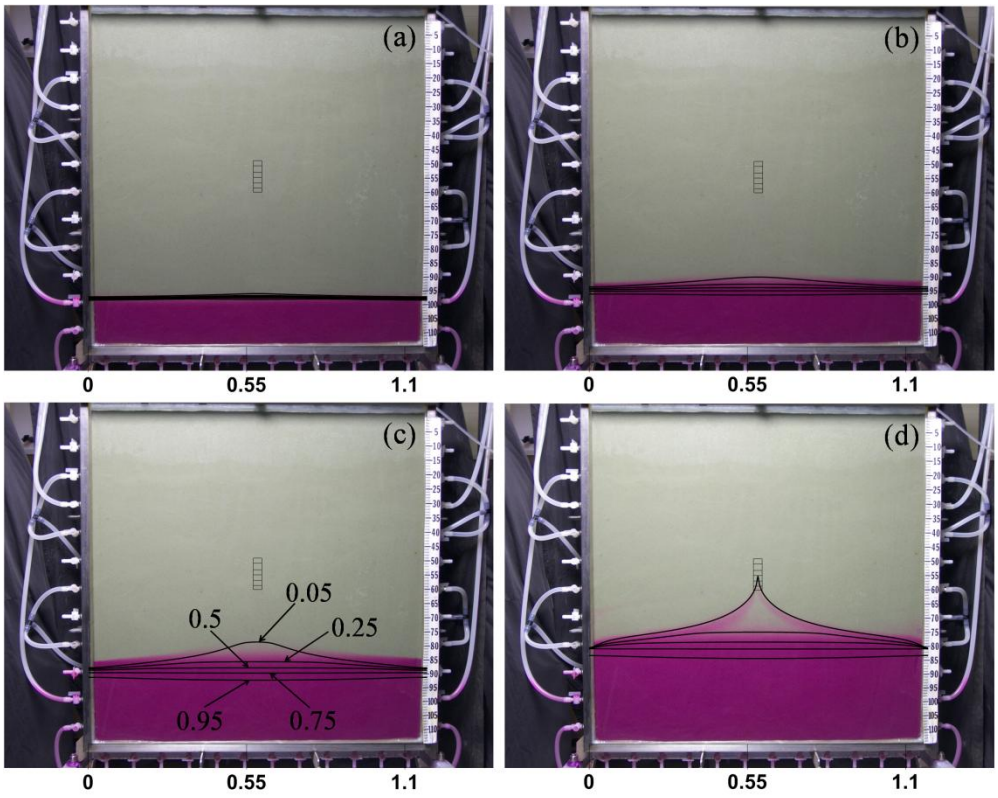

Figure 3.7. Plume images from Experiment 4 with comparison to simulated relative salinity contours; (a) 30 min, (b) 720 min, (c) 1800 min and (d) 2940 min.

3.5 Quantifying modelling results

Modelling results were quantitatively analysed in terms of the height and width (i.e. at mid-height) of the saltwater plume, drawdown at the side boundaries, and breakthrough curves for the pumping well. Comparisons with laboratory results and the Dagan and Bear (1968) analytical solution are given in the following section.

3.5.1 Height and width of the saltwater plume

Figure 3.8 illustrates the height of the saltwater plume with respect to time, for experimental (symbols), analytical (dashed line) and numerical modelling (solid line) approaches, and for all four Werner et al. (2009) experiments. The plume height was tracked only until the apex reached the well, which occurred around 120 min, 120 min, and 360 min for Experiment 1, 2 and 3, respectively, and did not occur in Experiment 4 (i.e. the 50% salinity contour did not reach the well). The height of upconing from numerical modelling was based on the predicted 50% salinity contour, which was presumed to coincide with the middle of the dispersion zone in visual interpretations of laboratory photographs. The highly dispersive nature of Experiment 3 made it difficult to estimate (by eye) the middle of the interface from laboratory experiments, and so numerical modelling predictions of the apex height using both 50% and 25% salinity contours were obtained (e.g. Figure 3.8c).

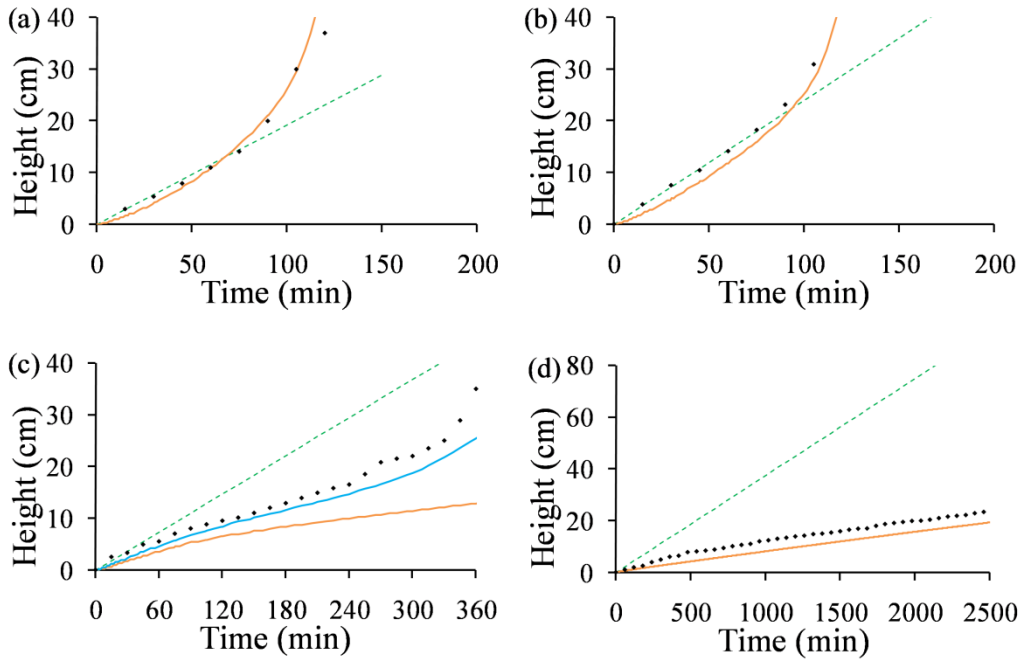

Figure 3.8. Comparison of plume apex height from the numerical model (solid orange line), laboratory experiments (black diamonds) and analytical solution (dashed green line) for (a) Experiment 1, (b) Experiment 2, (c) Experiment 3 and (d) Experiment 4. The height is based on the 50% salinity contour. In (c), the solid blue line represents the apex height using the 25% salinity contour.

Early-time ascent of the plume apex was reasonably well represented by both the analytical solution and the numerical model. The analytical solution departed from experimental trends after roughly 1-2 hours into experiments. The numerical model produced close-matching predictions for all times with the possible exception of Experiment 3, for which model predictions of the 50% contour position underestimated the laboratory interface rise. In Figure 3.8c (Experiment 3), the 25% salinity contour from the numerical modelling is closer to the plume height results interpreted from laboratory photos, relative to the 50% salinity contour. This indicates that visual inspection of laboratory photos was probably biased towards lower concentrations in selecting the mid-point of the dispersed interface (illustrated in Figure 3.6). As reported by Werner et al. (2009), the Dagan and Bear (1968) analytical solution is unable to adequately represent upconing under Experiment 3 conditions, most likely because of the dispersiveness of Experiment 3 (considering that the Dagan and Bear (1968) solution assumes a sharp interface). In this case, numerical modelling offers obvious advantages by capturing the dispersive processes of upconing,

confirming that the Experiment 3 results are valid despite the departure from the analytical solution.

Interestingly, the analytical solution slightly outperformed the numerical model in matching laboratory results at early times in Experiments 1 and 2 (Figure 3.8a and b). As mentioned above, there is some uncertainty in the interpretation of plume height from the Werner et al. (2009) laboratory results, and so the numerical model-laboratory experiment mismatch is probably within the margin of error incurred in interpreting experimental photos. The simulated interface rise of Experiment 4 slightly underestimated the interface rise observed in the laboratory, although the uncertainty in interpreting laboratory photos may account for the difference, given that Experiment 4 is highly dispersed relative to Experiments 1 and 2. As noted by Werner et al. (2009), the analytical solution significantly overestimated Experiment 4 laboratory observations of interface rise at almost all times. Therefore, numerical modelling again served as a useful basis by which to explore the laboratory upconing experiments, as evidenced by the reasonably good match between model and laboratory results given in Figure 3.8d.

Plume widths from laboratory experiments, analytical solution results and numerical modelling predictions are illustrated in Figure 3.9 for Experiments 1, 2 and 3. The width of the plume was difficult to interpret for Experiment 4 (since the interface mainly comprised a horizontal shape) and therefore is omitted from Figure 3.9.

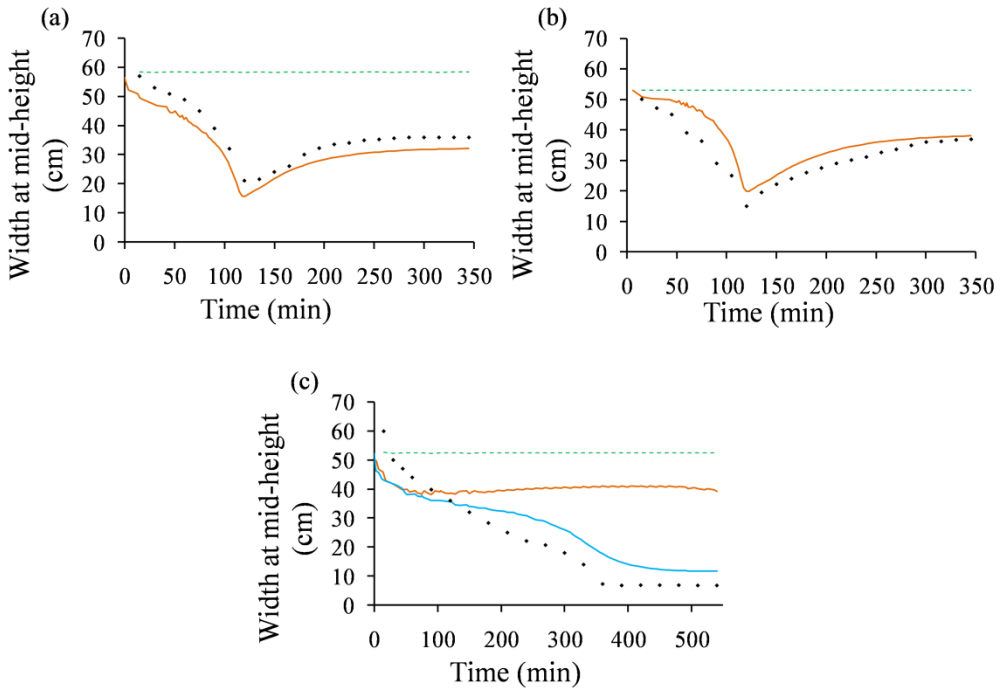

Figure 3.9. Comparison of plume width at 50% height from the numerical model (solid orange line), laboratory experiments (black diamonds) and analytical solution (dashed green line) for (a) Experiment 1, (b) Experiment 2 and (c) Experiment 3. The width is based on the 50% salinity contour. In (c), the solid blue line represents the plume width at 50% height using the 25% salinity contour.

Numerical model results and laboratory observations are a reasonably close match (Figure 3.9). The 25% salinity contour again needed to be used to obtain simulation predictions that corresponded to the Experiment 3 plume-widths interpretated from laboratory photographs. The likely reasons for this are explained above for the Experiment 3 apex height results. The model reproduced the nonlinear temporal trends in plume width that were observed in the laboratory, noting that the Dagan and Bear (1968) analytical solution produces a constant mid-height plume width (as indicated by Werner et al., 2009) that is higher than both the laboratory observations and the numerical model results.

Plume width minima are apparent in Experiments 1 and 2 (Figure 3.9a and b), and are well captured by the model results. The minima occur because of the narrow salt plume spikes forming below the well during the early stages of the experiment. However, once the salt reaches the well, the plume below the well starts widening, hence the increase in the plume width at later times.

3.5.2 Bore salinity

Figure 3.10 illustrates comparisons of saltwater breakthrough curves from both laboratory experiments and the numerical model. Reasonable matches were obtained for all four experiments. The numerical model slightly overestimated the experimental breakthrough curves for Experiments 1 and 2; this occurred during the intermediate period of the experiments. Various factors may have caused the mismatch including slightly higher dispersion in the model relative to the laboratory experiments, although the mismatch is considered relatively minor.

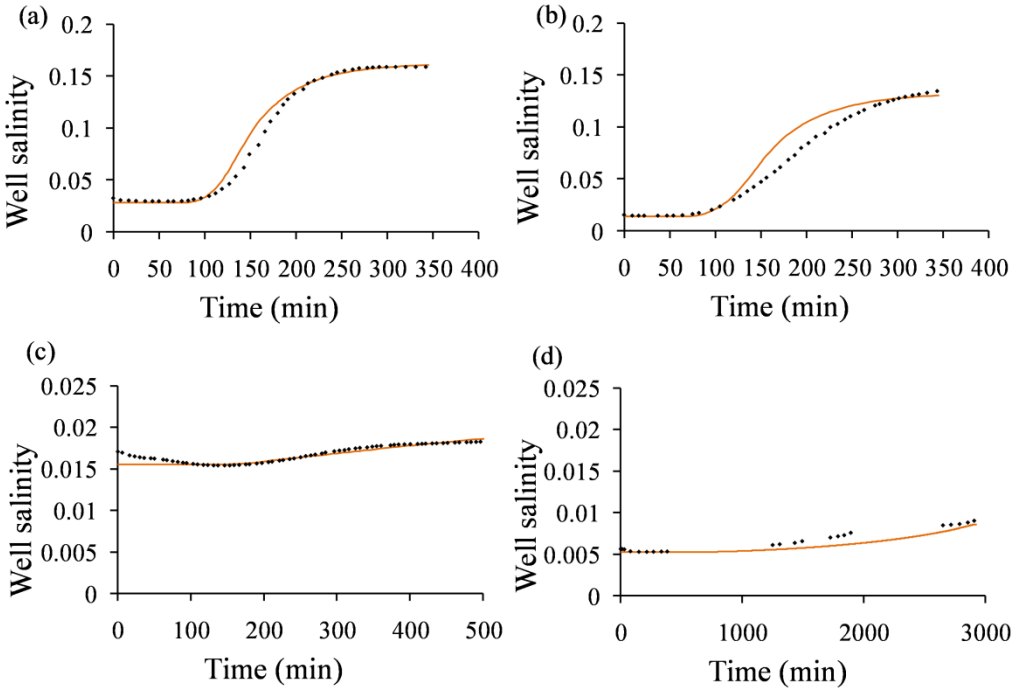

Figure 3.10. Comparison of breakthrough curve from the numerical model (solid orange line) and laboratory experiments (black diamonds) for (a) Experiment 1, (b) Experiment 2, (c) Experiment 3 and (d) Experiment 4. Salinity units are dimensionless and relative to the inflowing saltwater.

3.5.3 Drawdown at the side boundaries

Comparisons between numerical model results and laboratory observations of drawdown at the side boundaries are shown in Figure 3.11. The GHB conditions allowed the drawdown to evolve gradually, providing better predictions of

boundary head trends compared to the SHB conditions, as discussed previously (see Figure 3.3a). A close match was obtained for late-time drawdown, as expected because boundary conductance parameters were calculated from late-time laboratory observations. The match is weaker for transient drawdown behaviour, e.g. at early and intermediate times, during which the drawdown was initially under-estimated and then over-estimated during the middle phases of experiments. Model calibration would have improved the match between model and laboratory drawdowns, but the modelling analysis aimed to adopt experimentally obtained parameters and so there was no attempt to reduce any drawdown mismatch.

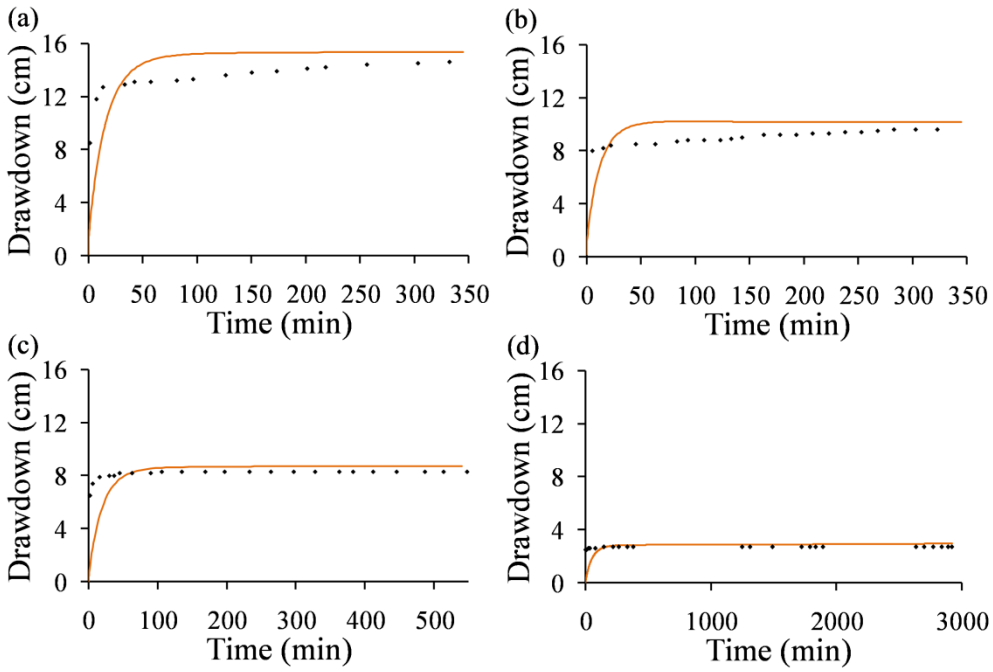

Figure 3.11. Comparison of drawdown at the side boundaries from the numerical model (solid orange line) and laboratory experiments (black diamonds) for (a) Experiment 1, (b) Experiment 2, (c) Experiment 3 and (d) Experiment 4.

Drawdown at the side boundaries seemed to be almost immediate in the sand tank (Figure 3.11). This may indicate that the inflows through the sand tank ports were low (relative to the model GHB boundary conditions) at the start of experiments, causing the watertable in the sand tank to drop faster under the influence of well pumping. A simulation with no flow boundary conditions applied to the sides of the model at the start of the experiment (i.e. for the first 5

min of the experiment) was tested to explore if a better representation of the drawdown at the side boundaries would be obtained. The model produced an almost immediate drawdown at the side boundaries as was observed in the experiment (results not shown). This indicates that the inflow across the boundaries was indeed lower (relative to the linear GHB equation) at the start of the experiment. A simple test of the fluid supply device (i.e. Mariotte bottle) flow versus head was performed to see how the flow responds to various head differences. The flow appears to be non-linear with respect to the change in head. For smaller head differences, the influx was disproportionally lower (and therefore resistance to flow was higher) than for larger head differences, leading to lower inflows across the sand tank side boundaries at the start of the laboratory experiments. Further experimental analysis is needed to devise non-linear relationships between boundary head and inflows for the Werner et al. (2009) experimental set-up, although in any case, the non-linear nature of the boundary inflows did not appear to adversely impact on saltwater upconing processes observed in the laboratory experiments.

3.6 Discussion

3.6.1 Diagnostic analyses of transient interface dispersivness

Both the laboratory experiments and numerical modelling demonstrated that the interface thickness changes as upconing progresses. The numerical modelling results were manipulated to provide quantification of interface thickness changes. Interface thickness (or "degree of dispersiveness") is defined here as the vertical distance between the apex of the 5% and 95% salinity contours. In Experiments 1, 2 and 3, the interface thickness was greatest when the 5% salinity contour first reached the bottom of the well, and then decreased rapidly to essentially a sharp interface as the 95% contour encountered the well bottom. Interface thickness analysis was not conducted for Experiment 4 (i.e. interface comprised a horizontal shape for the most of the duration of the experiment).

The transition from dispersive to non-dispersive saltwater upconing seems an intuitive result of longitudinal dispersion controlling early-time transport and the smaller transverse dispersion controlling late-time transport under conditions of

the interface being in contact with the well. That is, at the early stage of the upconing process, the flow near the initial interface is upwards and longitudinal dispersion dominates. This is pointed out also in the Holzbecher (1998) study. Once the salt plume is in contact with the well, the interface tends to become parallel to the flow directions, and hence the lower transverse dispersion controls the interface thickness, which subsequently reduces.

Density effects also influence the transition in interface dispersiveness. As the salt plume reaches the well and salinities rise in the region immediately below the well, buoyancy effects induced by the saltwater's higher density act to reduce upward groundwater velocities, and subsequently dispersion (which is proportional to velocity) reduces in this region. The temporal variations in the magnitude of velocity vectors, |v| (L/T), at three different points directly below the well, are illustrated for Experiment 4 in Figure 3.12. Vertical velocities increase during early stages of the simulation, reaching maximum values at around the time that the 50% isochlor rises to the elevation of the observation points (i.e. 15, 30 and 45 cm below the well; Figure 3.12). As the salinity below the well increases, the higher density of the salt plume induces a gravity effect that acts in opposition to the pumping well influence, and the vertical velocity reduces substantially in response to this. The effect was far less pronounced in the first two experiments, which involved higher pumping rates.

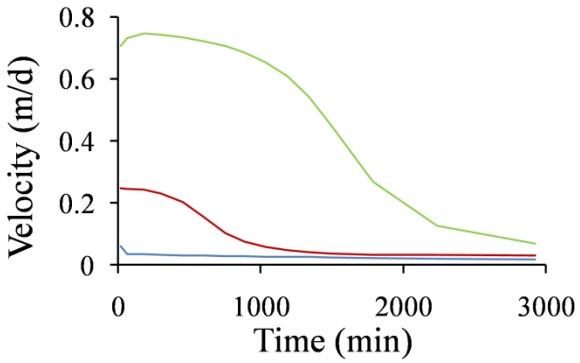

Figure 3.12. Experiment 4 magnitude of velocity vectors 15 cm (green solid line), 30 cm (red solid line) and 45 cm (blue solid line) directly beneath the well.

Early-time and late-time velocity distributions are shown for Experiments 1 and 4 in Figure 3.13. The results illustrate clear reductions in velocities within the

lower part of the domain in Experiment 4 (Figures 3.13c and 3.13d), due to the rise of the saltwater zone and the accompanying increase in the extent of mixed-convective flow processes (i.e. pumping-induced forced convection opposed by density-induced free convection ; Simmons et al. (2001)). The same effect is barely noticeable for Experiment 1 (Figures 3.13a and 3.13b). High-density water encroaches on the lowest freshwater inflow port in Experiment 4, and this has a major influence on the flow velocities in this vicinity, whereby flow vectors change direction through the course of the experiment. There is evidence of an outward component of flow within the interface (i.e. flow towards the side boundaries) that is likely the result of local-scale disturbances near the inflow port. This may contribute to the hollow shape of the upconing plume, notwithstanding the need to consider further such processes as adsorption. The local flow fields around inflow ports influence the area around the ports to an extent of about 10 cm, whereas the rest of the flow field appears free from boundary disturbances, indicating that the velocity perturbations of the inflow ports do not reach the well.

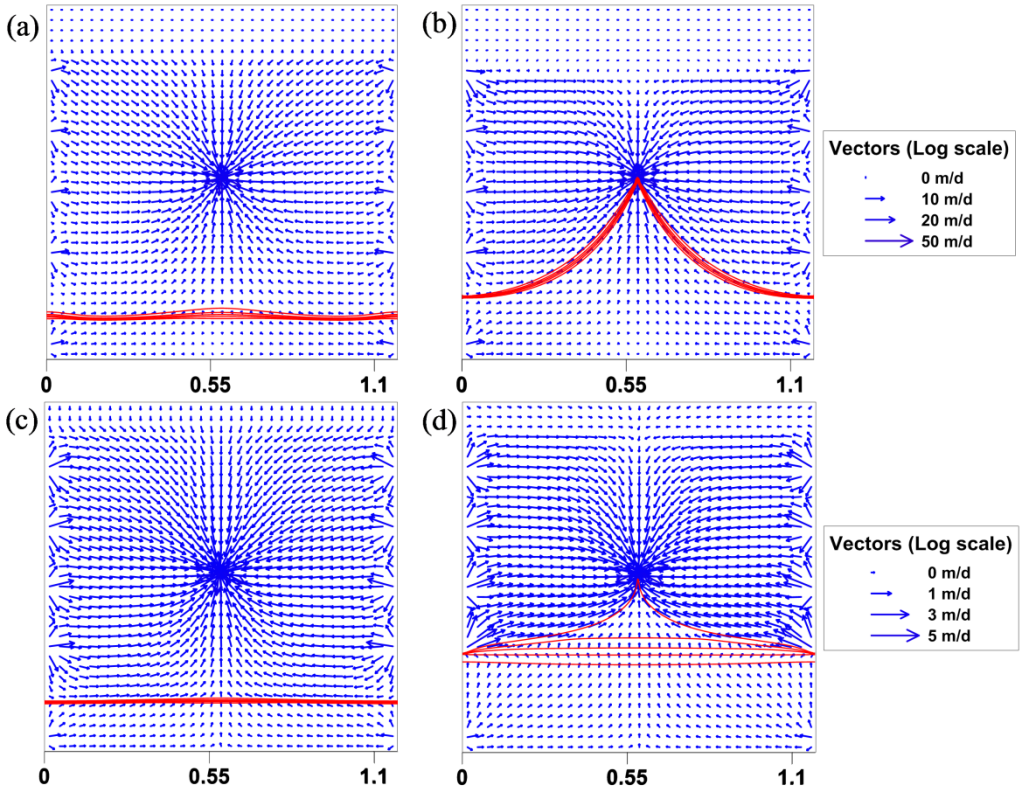

Figure 3.13. Experiment 1 and 4 velocity field distribution, plus simulated relative salinity contours: (a) Experiment 1 at 15 min, (b) Experiment 1 at 345 min, (c) Experiment 4 at 30 min, and (d) Experiment 4 at 2820 min. The scale is in metres. The top legend applies to Experiment 1 and bottom legend applies to Experiment 4.

The transition in dispersiveness was expected to have influenced the salinity breakthrough behaviour (which is arguably the most important measureable and impact of upconing). Salinity breakthrough was probably also influenced by the plume width, considering that the plume width probably has a bearing on the proportion of saltwater entering the well under conditions where saltwater encounters the well bottom. Further analyses sought to explore general relationships between the different measurables, such as plume width and well salinity, as drawn from the modelling results.

3.6.2 Wider sand-tank scenario

Simulations representing a wider sand tank were undertaken to provide insight into the effect of boundary conditions on the salt plume transience. The aim was not to reproduce the Werner et al. (2009) upconing observations in a wider sand-tank, but was simply to assess likely results from a corresponding upconing experiment undertaken using more distant side boundary conditions (Experiment 1 was used as the basis for the extended sand-tank simulation). The distance from the well to the side boundaries was increased from 0.589 m to 10.589 m. The model grid comprised 851,779 nodes and 848,776 elements producing long simulation run times, and hence the analysis was constrained to only a single additional scenario. The side boundary conditions in the extended-width model were adjusted by using simple Darcy Law calculations to estimate heads at the new side boundary positions and these produced consistent late-stage heads at the original sand-tank side boundary locations. The drawdown and interface rise were monitored through a vertical profile at the position of the original sand-tank side boundary.

The drawdown was observed to be more attenuated in the wider model compared to the original sand-tank domain (see Figure 3.14); an expected result

given the additional storage of the wider model. The delayed drawdown produced slower interface rise at the original sand-tank side boundary position. However, the plume rise beneath the well was more dispersed and subsequently rose faster, which caused an earlier breakthrough of the well salinity. This result indicates that the distance between the side boundaries and well influences the interface thickness, which is expected since the velocities along the interface increase (i.e. the flow interruptions at the original sand-tank side boundaries cease as the side boundaries are moved further away, which allows undisturbed flow across these locations) and therefore dispersion increases. While there is clearly a boundary influence on upconing processes observed in the Werner et al. (2009) laboratory experiments, this does not detract from the usefulness of these laboratory observations as reasonable depictions of saltwater upconing albeit under constrained conditions.

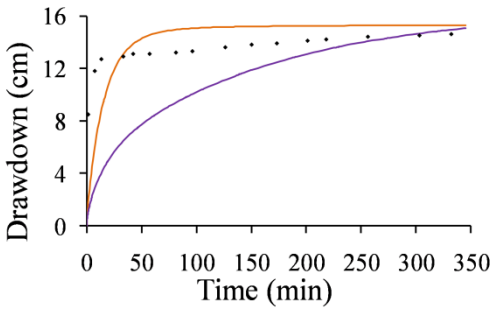

Figure 3.14. Experiment 1 comparison of drawdown at the side boundaries from the laboratory observations (black diamonds), original numerical model (solid orange line), and wider sand-tank simulation (solid purple line).

3.6.3 Plume width influence on well salinities

The results obtained from high-pumping experiments (i.e. Experiments 1 and 2) indicate that salinity breakthrough curves were controlled by both the transition in the interface thickness and the width of the salt plume. This is in agreement with Diersch et al. (1984) who suggested that the transitive phase of the breakthrough is governed by dispersion. In Experiments 1 and 2, the well salinity started to rise at about the same time as the 5% salinity contour reached the well bottom. When the 50% salinity contour reached the well, the interface width was at its minimum and the well salinity was rising rapidly. The well salinity continued to increase after the interface thickness reduced to near zero

(i.e. sharp-interface conditions), demonstrating the important role of plume width on the well salinity breakthrough in the high-pumping experiments. It might be possible to infer the plume width from the well salinity under conditions of a sharp interface being in contact with the well, although this requires further analysis to evaluate the conditions under which such correlations may exist.

As mentioned above, plume-width minima are apparent in the results from Experiments 1 and 2 (Figure 3.9). In these cases, plume-width minima occur at roughly the same time that high salinity (approximately 50% isochlor) reaches the bottom of the well. Increases in the plume width (i.e. once the plume encountered the well bottom) were the result of the rise in the saltwater plume at the sand tank side boundaries. A comparison between numerical model predictions of plume width and the freshwater-saltwater interface thickness showed a generally inverse relationship – i.e. the plume width reduced as the interface thickness (dispersion zone) increased, and the plume width increased as the interface dispersion zone decreased (Figure 3.15). There is a timing offset between interface thickness maximum and plume width minimum, which arises since the interface thickness maximum occurs at about the time when the 5% salinity contour reaches the well, and the plume width minimum conincides approximately with the time when the 50% contour reaches the well. Larger distances between the well and the interface would be necessary to explore plume width-interface thickness relationships in a more generalised manner (i.e. the transition of the interface thickness happened rather quickly since the well and the interface were within relatively close proximity).

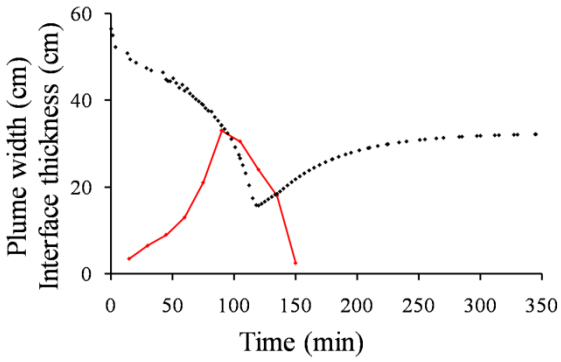

Figure 3.15. Comparison between model predictions of plume width (black diamonds) and the freshwater-saltwater interface thickness (red solid line) for Experiment 1.

3.6.4 Mismatch between numerical modelling and laboratory experiments

Mismatches in the various measurables between the numerical model and laboratory experiments were expected to show functional relationships, and provide insight into possible reasons for model-laboratory experiment discrepancies. However, the mismatch in the breakthrough curves is difficult to relate to mismatches in other measurables. For example, slight over-estimation of salinity breakthrough by the model occurs in Experiments 1 and 2 at a time when the height of the plume is under-estimated. The mixture of over- and under-prediction of salt plume width further confounds the interpretation of mismatch in Experiments 1 and 2. Given that each laboratory experiment was undertaken only once due to time constraints, it is problematic to quantify experimental error, which we surmise is the primary source of model-laboratory experiment mismatch. Future laboratory experimentation should attempt to measure in-situ groundwater salinities to reduce the dependency on laboratory photos for interpreting salt plume distributions.

The weakest match between laboratory observations and numerical model predictions of salt plume distributions occurred in Experiment 4, in which the ‘double-peak’ upconing observed in the laboratory was not reproduced by the model. One plausible source of mismatch may be the occurrence of adsorption, in particular of the Rhodamine tracer. Schincariol and Schwartz (1990) used Rhodamine in density-dependent sand-tank experiments without taking into account adsorption effects. However, Sutton et al. (2001) suggest that adsorption

may have a significant influence on Rhodamine transport. Literature values of Rhodamine adsorption parameters (isotherms) are widely varied (e.g. Sabatini and Alaustin, 1991), and further laboratory experimentation is needed to obtain representative adsorption parameters for the Werner et al. (2009) experimental conditions, e.g. accounting for the combination of the porous medium, groundwater flow rates and Rhodamine concentrations used in Experiment 4. Sabatini and Alaustin (1991) suggest that adsorption is higher at lower pore velocities, and therefore the effects of adsorption are likely to be most pronounced in Experiment 4, in which the rate of pumping was lowest. Exploration of the possible effects of Rhodamine adsorption warrants an additional laboratory experiment to evaluate whether the double-peak observations from Experiment 4 are reproducible under alternative experimental conditions.

3.7 Conclusions

Numerical modelling of the Werner et al. (2009) saltwater upconing laboratory experiments has been undertaken in order to explore the numerical reproducibility of the experimentally observed transient rise in saltwater plumes under pumping bores. In general, good agreement of the experimental observations and numerical simulations was observed with minimal calibration. The consistency between the numerical model results and laboratory observations for three of the experiments indicates that the first three Werner et al. (2009) laboratory observations are reproducible. This implies two things; that the density-dependent flow and transport simulator FEFLOW is able to predict the saltwater upconing processes of the experiments, including the transition from dispersive to non-dispersive plumes and the drawdown associated with upconing, and that the laboratory observations produced by Werner et al. (2009) are reliable depictions of upconing processes, albeit in two-dimensions. A weaker match between numerical model results and observations from a fourth experiment was obtained, and further laboratory and numerical modelling work is needed to assess whether adsorption effects may have caused a delay in the vertical transport of the colour tracer.

An assessment of the width and dispersiveness of the plume indicates that the well salinity breakthrough in the high-pumping laboratory experiments was controlled primarily by the width of the plume and not the degree of dispersiveness. This implies that it may be possible to infer plume width from bore salinity (and vice-versa) under certain conditions.

This study also demonstrates the importance of the boundary conditions adopted in the Werner et al. (2009) laboratory experiments. In simulating their experimental configuration, a head-dependent flux representation of the inflow ports better represented the system (i.e. provided a better match of breakthrough curves and salinity contours) than constant-head boundaries. The head-dependent flux boundary required evaluation of the boundary conductance (i.e. resistance to flow) at the sand-tank inflow ports. Conductance values were calculated from the laboratory measurements and were subsequently used in the simulations to provide a good match with the experimental results for Experiments 1, 2 and 3, demonstrating the applicability of this boundary inflow representation. However, variation in boundary inflow conductance between experiments was observed, the causes of which remain unclear; though each successive experiment showed lower conductance, perhaps indicating compaction and/or clogging effects.

The modelling presented in this study is the first attempt at matching a numerical simulator with direct visualisations of saltwater upconing and builds on similar studies by Johanssen et al. (2002) and Oswald and Kinzelbach (2004) who numerically modelled geophysical interpretations of upconing in a three-dimensional sand-box. Numerical results were also compared to Dagan and Bear's (1968) sharp-interface analytical solution of saltwater upconing. In general terms, Dagan and Bear's (1968) sharp-interface solution compared reasonably well with the laboratory observations for early-time behaviour in terms of interface rise. In the middle stages of upconing experiments, the analytical solution over-predicted the interface rise of lower-pumping experiments (i.e. Experiments 3 and 4). Plume width trends obtained from both laboratory experiments and numerical modelling were not obtained through the analytical solution.

Chapter 4

Tracer adsorption in sand-tank experiments of saltwater upconing

This chapter is based on the following paper:

Jakovovic D., Post V.E.A., Werner A.D., Männicke O., Hutson J.L., Simons C.T., 2012. Tracer adsorption in sand-tank experiments of saltwater up-coning. Journal of Hydrology 414-415: 476-481.

Abstract

This study aims to substantiate otherwise unresolved double-peaked plumes produced in recent saltwater upconing experiments (see Jakovovic et al. (2011), *Numerical modelling of saltwater upconing: Comparison with experimental laboratory observations*, Journal of Hydrology 402, 261-273) through additional laboratory testing and numerical modelling. Laboratory experimentation successfully reproduced the double-peaked plume demonstrating that this phenomenon was not an experimental nuance in previous experiments. Numerical modelling by Jakovovic et al. (2011) was extended by considering adsorption effects, which were needed to explain the observed upconing double peaks of both previous and current laboratory experiments. A linear adsorption isotherm was applied in predicting dye tracer (Rhodamine WT) behaviour in the sand-tank experiments using adsorption parameters obtained experimentally. The same adsorption parameters were tested on all laboratory experiments and it was found that adsorption had insignificant effect on experiments with high pumping rates. However, low pumping rates produced pronounced spatial velocity variations within the dense salt plume beneath the pumping well, with velocities within the plume increasing from the centre of the plume towards the interface. The dye tracer was retarded relative to the salt and was transported

preferentially along the higher-velocity paths (i.e. along the edges of the salt plume) towards the well forming double-peaked upconing patterns. This illustrates the sensitive adsorptive nature of Rhodamine WT and that care should be taken when it is used in similar sand-tank experiments. Observations from this study offer insight into the separation of chemicals in natural systems due to different adsorption characteristics and under conditions of density-dependent flow.

4.1 Introduction

Recently, Werner et al. (2009) performed a series of saltwater upconing experiments in which they used Rhodamine WT as a visual tracer. One of their experiments (referred to as Experiment 4) produced a double-peaked plume beneath the pumping well, which could not be reproduced by the subsequent non-reactive numerical modelling of the laboratory experiments by Jakovovic et al. (2011). Jakovovic et al. (2011) suggested further analysis and hypothesised that the adsorption of Rhodamine WT may have been the cause of this effect.

The literature on Rhodamine WT adsorption is somewhat conflicting; some studies consider it as a conservative tracer (e.g. Schincariol and Schwartz, 1990; Pang et al., 1998) and some consider it as a non-conservative tracer (e.g. Ghanem et al., 1999; Close et al., 2008). Studies that have investigated sorption characteristics of Rhodamine WT (e.g. Shiau et al., 1993; Sutton et al., 2001; Vasudevan et al., 2001) concluded that the extent of sorption is affected by different factors, which include its aqueous concentration, the ionic strength of the solution and sorption characteristics of the porous medium. In addition to these, the distribution coefficient, K_d (cm^3/g), which represents the ratio of sorbed to solute concentrations, has been found to vary between column experiments depending on the water flow velocity and column dimensions (EPA, 1999).

Rhodamine WT has been employed as a dye tracer in several laboratory sand-tank studies (e.g. Schincariol and Schwartz, 1990; Geith and Schwartz, 1998; Precht and Huettel, 2003; Close et al., 2008). In their experimental investigation of variable-density flow and mixing, Schincariol and Schwartz (1990) used Rhodamine WT as a visual aid, and treated it as a conservative tracer, since Schincariol (1989) demonstrated that the tracer was suitable to use for visualisation purposes for a similar experiment. Similarly, Precht and Huettel (2003) used Rhodamine WT in their laboratory wave tank as a conservative tracer to investigate and quantify fluid exchange between a sandy bed and an overlying water column. However, Close et al. (2008) who investigated spatial variations in aquifer properties in a sand-tank experiment, recognized the non-

conservative nature of Rhodamine WT and noted sorption of the tracer onto the aquifer medium. They reported a retardation factor, $R = 1 + (\rho_b/\varepsilon)K_d$, ranging between 1.15 and 1.80, where ρ_b is the bulk density (g/cm^3) and ε is porosity (dimensionless).

In this study, a laboratory experiment, which will be referred to as Experiment 5, was carried out to determine whether the double-peak upconing that occurred beneath the pumping well in Experiment 4 was a reproducible feature. The numerical models by Jakovovic et al. (2011) were extended to incorporate adsorption effects. The aim was to test the hypothesis that the hollow crest upconing observed in Experiment 4 is not an accurate representation of the salt movement, but is due to the adsorption of Rhodamine WT.

4.2 Laboratory experimentation

The laboratory methods applied in the current study consisted of column experiments to obtain the adsorption parameters of the porous medium (medium sand, 30-CFS grade, Sloan Sands, Dry Creek, South Australia) and a sand-tank experiment to investigate adsorption effects of Rhodamine WT in a saltwater upconing setting. The mineralogy of the porous medium was the same as that used by Werner et al. (2009), but the grain size distribution differed slightly, and therefore new properties needed to be obtained for Experiment 5. The properties of the sand were determined using the same methods as used by Werner et al. (2009). The grain-size distribution curve gave a representative grain size (d_{50}) of 0.39 mm and a uniformity coefficient (d_{60}/d_{10}) of 1.96. The porosity (ε) was determined to be 0.35, the bulk density (ρ_b) was 1.76 g/cm^3 and hydraulic conductivity (K) was 0.057 cm/s. The dye tracer used in the sand-tank experiment and tested in column studies was Red FWT (a form of Rhodamine WT dye produced by ENVCO, Australia). The same dye tracer was used by Werner et al. (2009) in their sand-tank experiments, as was the calcium chloride dehydrate ($CaCl_2{\cdot}2H_2O$) that was used as a conservative dissolved solute in the column studies and in Experiment 5.

4.2.1 Column experiments

A total of three column experiments were conducted with varying tracer concentrations and flow rates (Table 4.1). The experiments were conducted using acrylic columns 4.95 cm in diameter and 30 cm in length. Constant flow rates throughout the experiments were maintained using a peristaltic pump (Masterflex®, L/S). Discrete outflow samples were collected for electrical conductivity (EC) and Rhodamine WT concentration analysis. The EC was measured using an electrical conductivity meter (Cond 315i, WTW). Rhodamine WT concentrations were analysed with a spectrophotometer (Cary® 50 UV – Vis spectrophotometer, Varian, Inc.). High and low concentrations of both Rhodamine WT and $CaCl_2 \cdot 2H_2O$ were tested to evaluate sorption variation with different solute concentrations. The breakthrough curves were fitted by the Ogata and Banks (1961) equation that includes retardation due to linear sorption, and were numerically reproduced using FEFLOW (Diersch, 2005).

Table 4.1. Parameters of column experiments.

Experiment	**Tracer concentration (mg/l)**		**Flow rate (cm^3/min)**
	Rhodamine WT	$CaCl_2 \cdot H_2O$	
Column 1	10	140000	7.7
Column 2	10	140000	20.6
Column 3	500	2000	11

4.2.2 Additional laboratory upconing experiment

The experimental apparatus for Experiment 5 was the same as that used by Werner et al. (2009) unless stated otherwise, and the reader is referred to that reference for a detailed description of experimental methods. In contrast to Werner et al. (2009), the pumping well was modified to have a shorter slotted interval of 0.025 m, and was installed to a shallower depth of 0.3 m from the top of the sand tank. The larger distance between the well bottom and the initial freshwater-saltwater interface was chosen to allow the flow to occur over a

larger distance, thereby providing more opportunity for the effects of adsorption. Table 4.2 lists the parameters used in Experiment 5. The density difference between saltwater and freshwater is smaller compared to Experiment 4 in order to explore conditions with a density difference similar to seawater-fresh groundwater. Also, the pumping rate used in Experiment 5 was lower than that used in Experiment 4 to maximise the likelihood of double peaks occurring, which were found to occur only for the lowest pumping rate (i.e. Experiment 4) by Werner et al. (2009).

Table 4.2. Experiment 5 parameters.

Pumping rate, Q (m^3/s)	3.34×10^{-7}
Saltwater density, ρ_s (kg/m^3)	1025
Freshwater density, ρ_f (kg/m^3)	998
Initial freshwater thickness, a (m)	0.99
Initial saltwater thickness, D (m)	0.11
Bore to initial interface distance, d (m)	0.69

The same monitoring as in Werner et al. (2009) was performed throughout Experiment 5, including bore water EC, bore pumping rate, hydraulic heads and time-lapse photography of the sand tank. In addition, samples were collected through the ports at the back of the sand-tank to compare the spatial distributions of salinity (measured as EC) and Rhodamine WT concentrations. For minimal disturbance of the flow field, 1 mL samples were taken and these were diluted 25-fold with demineralised water prior to testing.

4.3 Numerical modelling

Numerical modelling was used to re-simulate the Werner at al. (2009) experiments with the inclusion of adsorption effects in order to evaluate whether Rhodamine WT adsorption led to incorrect visualization of the salt distribution in the sand-tank experiments. Experiment 5 was simulated both with and without adsorption to evaluate its influence on plume migration. The numerical modelling was carried out using FEFLOW (Diersch, 2005). The main

modification to the previously produced models by Jakovovic et al. (2011) was the incorporation of multi-species transport instead of single-species transport. This allowed the transport of salt and Rhodamine WT to be modelled independently (i.e. as two non-interacting species). Rhodamine WT was modelled as a reactive species undergoing adsorption using the linear sorption isotherm, whereas salt was considered as a conservative species. The linear sorption model was adopted since this model best represented the breakthrough curves of the column experiments. Also, previous studies (Sabatini and Austin, 1991; Everts and Kanwar, 1994; Vasudevan et al., 2001) indicate that low-concentration Rhodamine WT adsorption is well represented by a linear isotherm. Experiment 5 was modelled using Table 2 parameters and otherwise the same flow and transport parameters as adopted by Jakovovic et al. (2011).

4.4 Results

Figure 4.1 shows the breakthrough curves of Rhodamine WT and EC from the Column 1 experiments, compared with the Ogata and Banks (1961) equation and the numerical simulations. The results are shown for Column 1 only, as the other experiments produced similar findings. The lag in the Rhodamine WT breakthrough curve relative to that of EC demonstrates an adsorption effect. Both the Ogata and Banks (1961) and FEFLOW solutions were fitted to the measured Rhodamine WT breakthrough curves by adjusting the retardation factor R, which gave a reasonable representation of the experimental data (Figure 3.1). The distribution coefficient K_d for Rhodamine WT ranged between 0.04 and 0.07 cm^3/g between the three column experiments, with an average of K_d = 0.06 cm^3/g, which corresponds to R = 1.3. This average value was used in the numerical simulations of the sand-tank experiments. The literature values for K_d obtained from column studies of Rhodamine WT adsorption range from 0.04 to 15.7 cm^3/g (Sabatini and Austin, 1991; Shiau et al., 1993; Sutton et al., 2001; Close et al., 2008). The K_d value obtained in this study is therefore close to the lower end of the range reported in the literature.

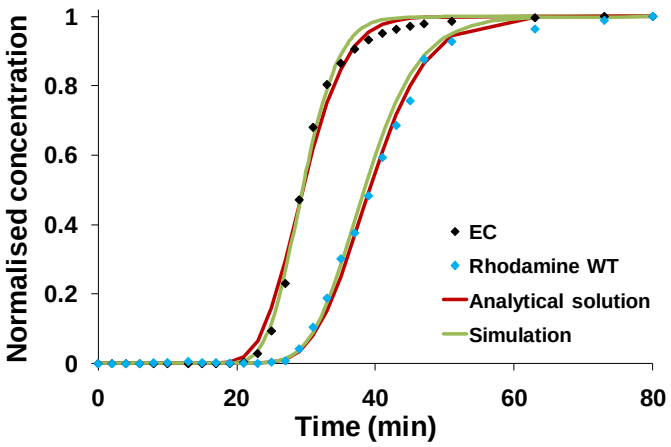

Figure 4.1. Normalised breakthrough curves of EC (black diamonds) and Rhodamine WT (blue diamonds) for the Column 1 experiment. For both $CaCl_2 \cdot 2H_2O$ and Rhodamine WT, the red solid line represents results obtained by the Ogata and Banks (1961) equation and the green solid line represents FEFLOW simulation results. Concentrations were normalised with respect to the injectant concentrations.

The numerical model results for Experiment 4 are shown in Figure 4.2 overlayed on laboratory photographs. They show that the distribution of Rhodamine WT differs significantly from that of the dissolved salt in the latter stages of Experiment 4. Only the late time results are shown since the early-stage distributions of dissolved salt and Rhodamine WT are similar, and the double-peak pattern of Rhodamine WT is more pronounced towards the end of the experiment. The double peaks represent only the low normalised Rhodamine WT concentrations, but nevertheless, they form a marked feature of the experiment. Including adsorption in the simulations of the remaining three experiments from Werner et al. (2009) did not affect the shape of the concentration contours for Rhodamine WT, and no double peak occurred (i.e. Rhodamine WT and salt distributions were essentially the same).

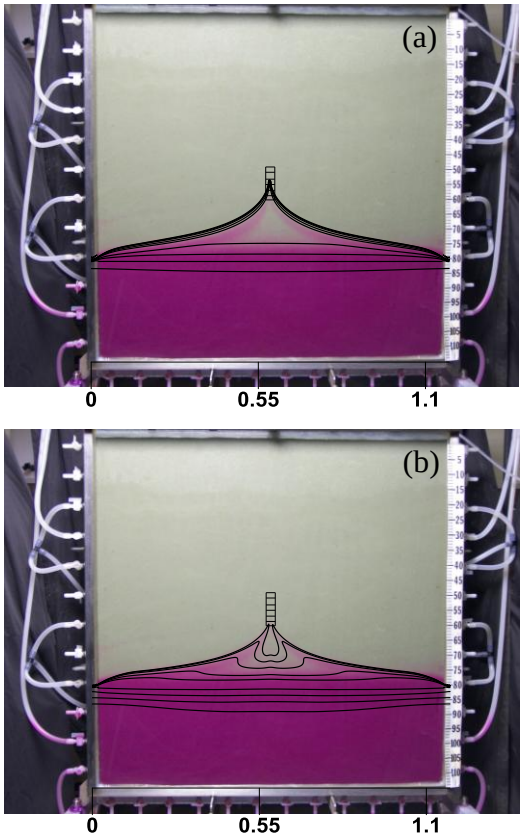

Figure 4.2. Plume images from Experiment 4 with comparison to simulation results in terms of: (a) normalised salinity contours and (b) normalised Rhodamine WT concentration contours at 2940 min from the start of the experiment. Normalised salinity and Rhodamine WT concentration contours of 0.008, 0.009, 0.0125, 0.025, 0.05, 0.25, 0.5, 0.75 and 0.95 are shown from top to bottom. In all figures, the scale is in metres. Concentrations were normalised with respect to injectant concentrations.

Figure 4.3 shows a time-series of both Rhodamine WT and salt modelling results overlaid on laboratory photographs for Experiment 5. The double-peak upconing was visible in this new laboratory experiment indicating that the phenomenon observed by Werner et al. (2009) is reproducible under different experimental conditions. Water samples taken from the back of the sand tank, in the areas below the well, showed that Rhodamine WT lagged behind the saltwater by about 12 hours, which we attribute to the effects of adsorption. The numerical model also captures the double-peak behaviour of the Rhodamine WT. As in Experiment 4, the double-peak pattern is most pronounced for the lowest concentrations (i.e. normalised concentrations of 0.05 and below).

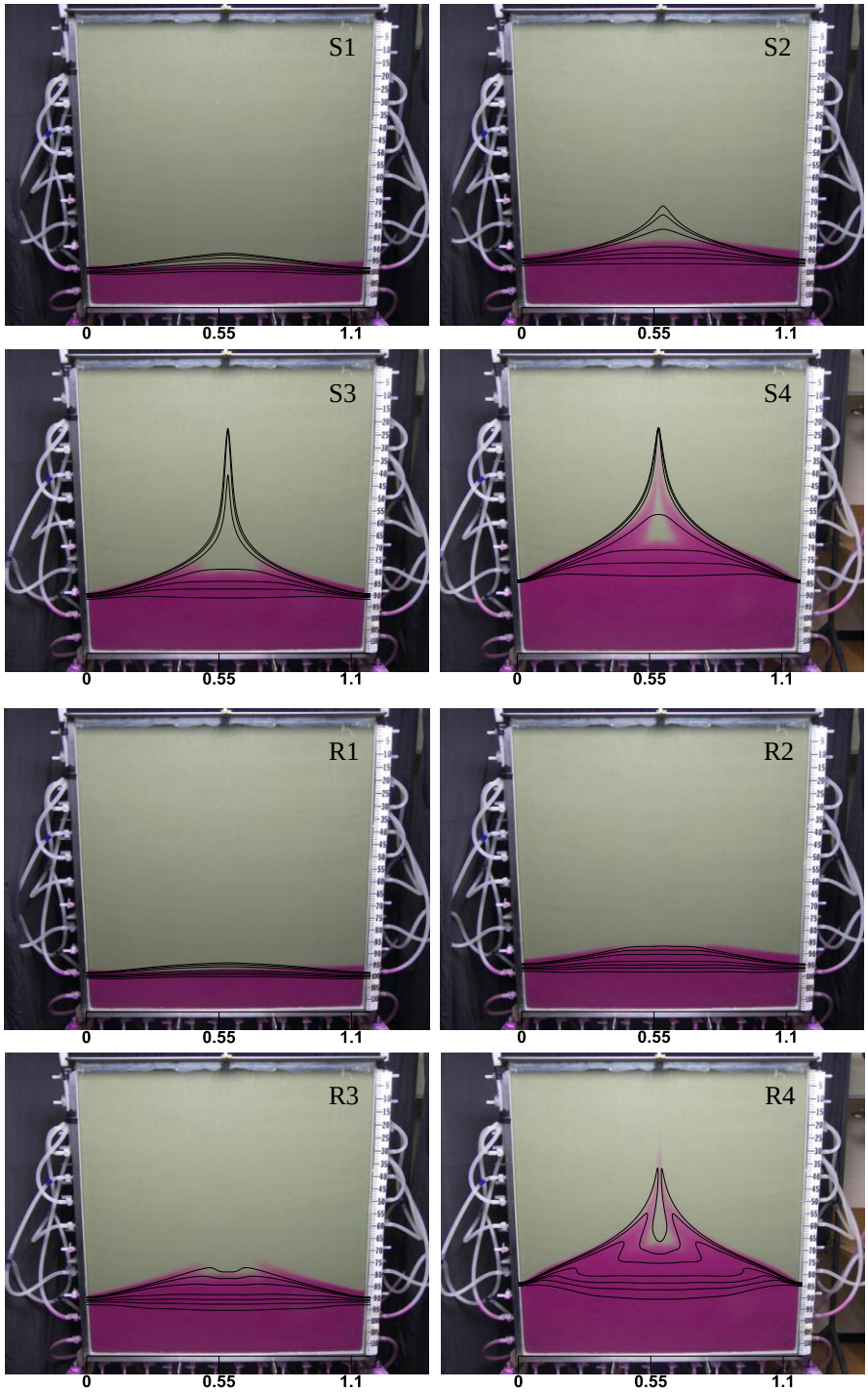

Figure 4.3. Experiment 5 results: plume images compared to salinity (S1 to S4) and Rhodamine WT distributions (R1 to R4) at four different times: 675 min (S1 and R1), 1830 min (S2 and R2), 3585 min (S3 and R3), and 7080 min (S4 and R4). Normalised salinity and Rhodamine WT concentration contours of 0.02, 0.025, 0.05, 0.25, 0.5, 0.75 and 0.95 are shown from top to bottom. Concentrations were normalised with respect to injectant concentrations.

4.5 Discussion

Experiment 4 had the lowest pumping rate and the highest density difference of the four Werner et al. (2009) experiments. This combination caused pronounced spatial variations in velocity, with the lowest velocities in the centre of the plume below the well and highest velocities on the outer edges of the plume, as discussed by Jakovovic et al. (2011). The slightly lower pumping rate and lower density difference of Experiment 5 resulted in a comparable spatial velocity pattern in the salt plume beneath the well. Figure 4.4 shows early-time velocity distributions together with the normalised salinity and Rhodamine WT concentration contours for Experiments 1 and 5. A comparison of the two experiments demonstrates the difference in velocity contrasts across the salt plume, created by differences in buoyancy and advection between the two cases. The results show that the double-peaked upconing of Rhodamine WT is induced by a combination of the lag effect of adsorption and the density effects of the dissolved salt. That is, salt plume density effects modify the flow field ahead of the Rhodamine WT plume due to the retardation of Rhodamine WT, which encounters a stronger velocity contrast in Experiment 5 compared to Experiment 1 (see Figure 4.4). Where Rhodamine WT reaches regions of faster flow (i.e. along the edges of the salt plume), it is transported along the higher-velocity paths towards the well. The dye in the central plume region, i.e. directly beneath the well, moves upward slower and this combination of effects creates the double-peaked images of Figures 4.2 and 4.3. In contrast, the velocity difference between the centre and the edges of the salt plume is hardly noticeable for experiments with high pumping rates (e.g. Experiment 1; Figure 4.4), and consequently the double-peak plume behaviour is not observed.

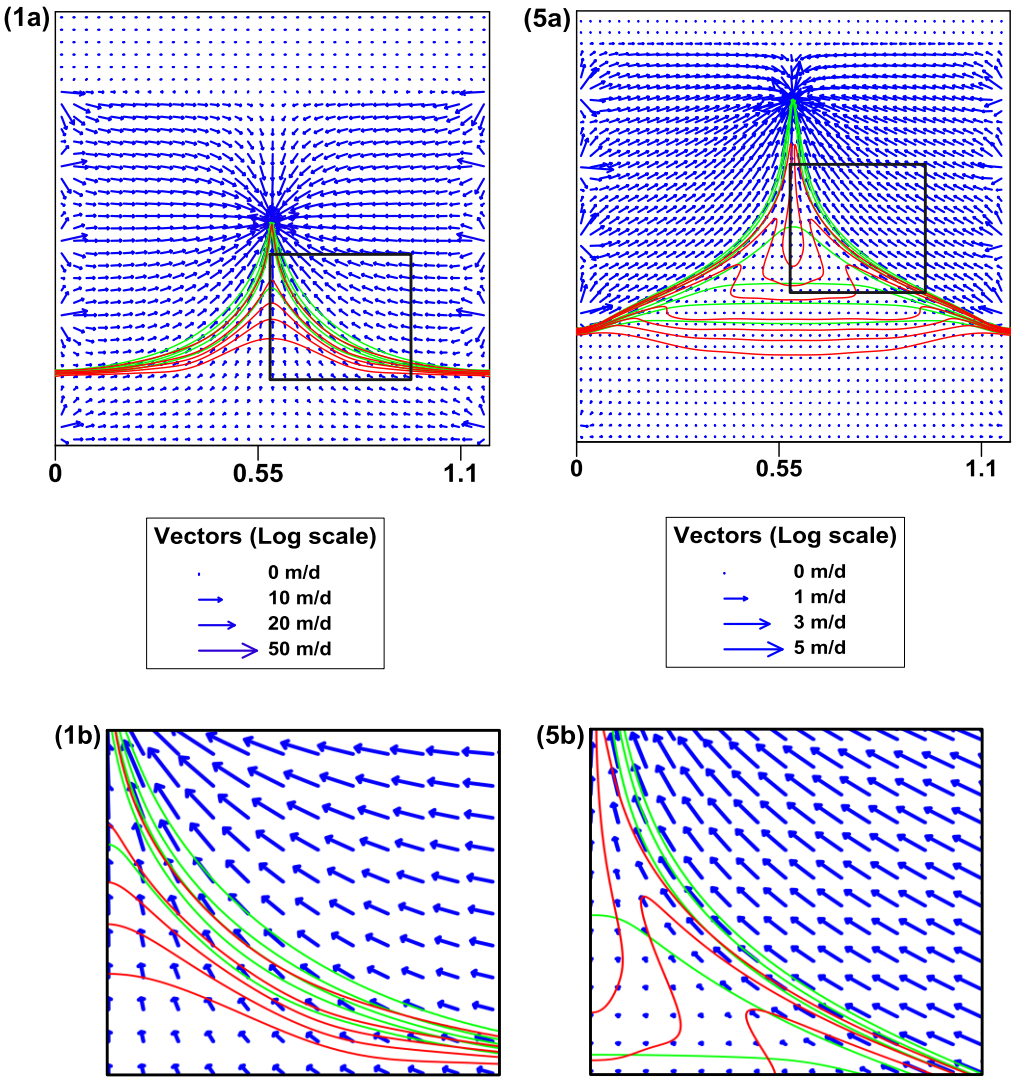

Figure 4.4. Experiment 1 and 5 simulation results: velocity (arrows), salinity (green lines) and Rhodamine WT (red lines) distributions at two different times: (1a) Experiment 1 at 150 min and (5a) Experiment 5 at 7080 min. (1b) and (5b) are close-ups of the black rectangle regions in (1a) and (5a), respectively. For Experiment 1, normalised salinity and Rhodamine WT concentration contours of 0.05, 0.25, 0.5, 0.75 and 0.95 are shown from top to bottom, respectively. For Experiment 5, normalised salinity and Rhodamine WT concentration contours of 0.02, 0.025, 0.05, 0.25, 0.5, 0.75 and 0.95 are shown from top to bottom, respectively. Concentrations were normalised with respect to injectant concentrations.

Plume development differences between conservative constituents (e.g. salt) and visual tracers have been observed in other numerical evaluations of groundwater flow and transport in variable-density environments (e.g. Hughes et al., 2005). The differences observed in Hughes et al. (2005) were for a simulation of a Hele-Shaw cell experiment and were attributed to differences in the molecular

diffusion rates of sodium chloride and a dye tracer. The current study attributes the plume development differences between salt (e.g. conservative constituent) and Rhodamine WT (e.g. visual tracer) to tracer adsorption and indicates that these differences may be common in similar experimental studies.

The relatively low K_d value found in this study shows that for even small retardation effects, the interpretation of the salt plumes from dye tracer observations may be significantly mistaken. While the effect was obvious in the sand-tank experiments undertaken in this study, these effects might be unnoticed in experiments involving heterogeneity, or in those with complex flow patterns (i.e. free convection experiments). Our results show that sorption is an important consideration when using Rhodamine WT as a visual aid in sand-tank experiments, especially under slow flow, density-dependent conditions. Furthermore, the observations made here offer some insight into chemical separation in natural systems that are characterised by slow-moving groundwater, density effects and multiple species of varying chemical/adsorptive properties, although the separation of chemicals in natural settings is likely to be more complicated.

4.6 Conclusion

Laboratory experimentation and numerical modelling were carried out to extend the studies by Werner et al. (2009) and Jakovovic et al. (2011) by investigating double-peak upconing that remained unresolved in their studies. Double-peak upconing was reproduced in sand-tank experimentation demonstrating that this phenomenon was not an experimental nuance in the original experiment. The feature could also be simulated by a numerical model which incorporated adsorption effects. It is inferred from this that the double peak below the pumping well was caused by adsorption of the Rhodamine WT tracer, which was used in the laboratory experiments to enable visualisation of plume movements.

An average linear adsorption isotherm obtained from Rhodamine WT and salt column experiments was used in the numerical model to successfully reproduce double-peak upconing observations by Werner et al. (2009) and from the current

sand-tank experiment. The same isotherm was tested on the other three Werner et al. (2009) experiments which were run under different experimental conditions (i.e. different combinations of flow rates and salt concentrations), and adsorption effects were found to be insignificant. In the experiments that displayed double-peak behaviour, pronounced spatial velocity variations within the dense salt plume beneath the pumping well formed. Flow rates within the plume increase from the centre towards the edges of the plume. The retardation of the dye tracer caused it to arrive after the salt had modified the flow field through density effects. It was then transported at low concentrations along the faster flow paths at the edges of the salt plume, causing the observed double-peaked upconing.

Although the representation of the adsorption processes by a linear isotherm is arguably a simplification, the appropriateness of a linear sorption model for this study may be justified for the following reasons: a linear sorption model using the same sorption parameters appears to work well for numerical simulations of Experiments 4 and 5, and the variation in K_d values obtained from the column experiments is relatively small (especially when compared to the range of literature values provided earlier). Further to this, it is clear that adsorption of Rhodamine WT can account for the double-peak upconing that occurred in the sand-tank experiment. These results illustrate the sensitive adsorption nature of Rhodamine WT and that care should be taken when it is used in sand-tank experiments for visualisation purposes. The separation of chemicals due to adsorption and under the influence of density effects observed in this study serve as a simple depiction of the possible chemical separation effects in natural mixed convection systems, which are subjected to geochemical reactions, such as cation exchange and mineral precipitation.

Chapter 5

Discussion on: "Experimental observations of saltwater upconing"

This chapter is based on the following paper:

Werner A.D., Jakovovic D., Barry D.A., Simmons C.T., Zhang H., 2012. Discussion on: "Experimental observations of saltwater up-coning" by Werner A.D., Jakovovic D., Simons C.T., 2009. Journal of Hydrology 373, 230-241. Journal of Hydrology 458-459, 118-120.

Recently, Zhang et al. (2012) highlighted that analytical solutions for steady critical withdrawal can be used to characterise the saltwater upconing experiments of Werner et al. (2009). In summary, Zhang et al. (2012) made the following points: (1) a critical pumping rate for the Werner et al. (2009) experimental set-up can be determined and, based on this, the experiments can be characterised as subcritical, critical or supercritical pumping cases, (2) the shapes of the plumes in the four experiments of Werner et al. (2009) accord with the criticality classification of Zhang et al. (2012), (3) Werner et al.'s (2009) Experiment 3 is better predicted by the formulation of Zhang et al. (1997) than by Dagan and Bear's (1968) analytical approximation, and (4) the plume widths reported by Werner et al. (2009) are not for the full-plume widths. Since the appearance of Werner et al. (2009), and subsequent to the submission of Zhang et al. (2012), further work has appeared, viz. Jakovovic et al. (2011, 2012), which report numerical modelling of the Werner et al. (2009) experiments and additional laboratory testing. These offer new information on the Werner et al. (2009) experiments (i.e., that was not available to Zhang et al. (2012) at the time of their comment), and offer important insights into many of the points raised by Zhang et al. (2012). Thus, here we take the opportunity to re-evaluate the four remarks of Zhang et al. (2012).

In brief, Jakovovic et al. (2011) simulated the Werner et al. (2009) laboratory experiments to assess the numerical reproducibility of the experimentally observed transient rise in saltwater plumes under pumping bores. Jakovovic et al. (2012) undertook additional laboratory testing and numerical modelling to explore further the double-peaked upconing of one of the Werner et al. (2009) experiments that was not reproducible from previous modelling attempts.

First, it is worthwhile reiterating briefly the upconing criticality concepts raised by Zhang et al. (2012), who focussed their attention on steady conditions. Previous studies that mention upconing criticality consider one or both of the following definitions: (1) the critical pumping rate is that for which the underlying salt water will just reach the well (e.g., Zhang et al., 1997), and (2) the critical height of upconing relates to the position of the plume apex at which the shape of upconing changes from convex to concave (Bear, 1979). In the past, the critical pumping rate has typically been analysed and described considering that the freshwater–saltwater interface is sharp. In that case, changes in the shape of upconing only occur in the transition from subcritical to critical pumping. In other words, subcritical pumping is consistent with a steady convex fresh/saltwater interface. As the (steady) pumping rate is increased, the interface abruptly becomes concave, corresponding to saltwater breakthrough to the pumping well. An important question remains: To what extent is the sharp interface assumption of Zhang et al. (2012) – which is the point of departure of their analysis – affected by the gradual transition from saltwater to freshwater?

Second, we mention that the analytical results of Zhang et al. (1997) were based on the assumptions: (1) an aquifer that extended without bound laterally, (2) that the freshwater–saltwater interface was fixed at two points equidistant from the pumping well and (3) that the phreatic surface was fixed and horizontal. Any laboratory experiment will involve conditions for which these assumptions are approximations. Zhang et al. (2012) already noted that the experimental conditions of Werner et al. (2009) differ from the theoretical basis of the theory of Zhang et al. (1997), so we do not reconsider that issue here.

Werner et al. (2009) highlighted that criticality definitions by Bear and Dagan (1964), Bear (1979) and Bower et al. (1999) do not appear to apply to their

laboratory observations, in terms of both plume stability and plume shape. The flux-based definition of criticality developed by Zhang et al. (1997), and applied by Zhang et al. (2012) to the experiments of Werner et al. (2009), matched reasonably well the laboratory results, in terms of late-stage plume apex heights and plume shapes. In addition to the assumptions listed above, we note that, necessarily, Zhang et al. (2012) assumed steady conditions existed in the experiments. Independent of this, the unresolved issue of dispersive upconing is perhaps of most interest. Groundwater of significant salinity enters the pumping well in Experiment 4 of Werner et al. (2009), despite that Zhang et al.'s (2012) criticality analysis indicates subcritical conditions due to the low pumping rate and high freshwater– saltwater density difference. A similar result (salinity-impacted wells despite stable upconing conditions) was observed by Reilly and Goodman (1987). We remark also that Experiment 5 of Jakovovic et al. (2012) can also be characterised as a subcritical case according to the theory of Zhang et al. (1997). However, the plume reached the pumping well in this experiment, causing significant salinity in the extracted water.

The shape of upconing plumes also requires discussion, especially given that the transient numerical modelling of Jakovovic et al. (2011, 2012) offers further insight into plume shapes and the associated convex-to-concave transitions. Generally, the dispersive simulation results of Jakovovic et al. (2011, 2012) show that for all laboratory experiments (i.e., Experiments 1–4 of Werner et al., 2009, and Experiment 5 by Jakovovic et al., 2012), the shape of salinity contours changed from convex at early stages to concave later in the experiments. The definition of upconing shapes (i.e., convex or concave) depends on whether the interface is viewed from above or below. Werner et al. (2009) and Zhang et al. (2012) adopt the former perspective and we adopt the same here, although it should be noted that on one occasion, Werner et al. (2009) mistakenly referred to an interface transition from concave to convex in their description of Experiment 1. Consistent with the gradual salinity transition across the freshwater–saltwater interface, the numerical simulation results of Jakovovic et al. (2011) show that, simultaneously, low concentration salinity contours can have a concave shape (indicating supercritical upconing; Zhang et al., 2012), while high salinity contours have the convex shape associated with subcritical conditions. As such,

upconing criticality is concentration-dependent, as opposed to sharp-interface criticality (assumed by Zhang et al., 2012). Further research is needed to identify better the salinities associated with critical states of upconing, following the initial work of Reilly and Goodman (1987) that compares dispersive and sharp-interface representations of upconing. Reilly and Goodman (1987) found that the 50% salinity contour was a reasonable approximation of the predicted position of a sharp interface in their investigation. The suggestion by Zhang et al. (2012) that Experiment 4 has a convex shape (based on the laboratory photographs of Werner et al. (2009)) is valid if the double peaks that formed in the latter stages of the experiment are neglected. However, Jakovovic et al. (2012) demonstrated that adsorption caused the dye tracer to lag the salinity plumes, especially in Experiment 4 (and Experiment 5 of Jakovovic et al., 2012), and hence saltwater plumes were in fact more concave than the shapes produced by the dye tracer. The results of the adsorption analyses by Jakovovic et al. (2012) thereby introduce new information regarding the laboratory experiments, and therefore the applicability of the Zhang et al. (1997) criticality definitions to the Werner et al. (2009) experiments needs to be addressed in accordance with this.

New conclusions can be drawn from the combined results of Zhang et al. (2012), Werner et al. (2009) and Jakovovic et al. (2011, 2012). All of the laboratory experiments and numerical simulations of Werner et al. (2009) or Jakovovic et al. (2011, 2012) obtained concave-shaped upconing plumes, despite some of these being designated as subcritical using the sharp-interface theory of Zhang et al. (1997). The concavity in plume shape was only obtained for the low salt concentrations in some cases. This is consistent with the theory of Zhang et al. (1997), which includes the density difference in its prediction of critical flux. Nonetheless, it may be the case that sharp-interface interpretations of criticality that rely on the development of steady-state conditions do not adequately characterise the laboratory experiments of Werner et al. (2009) and Jakovovic et al. (2012). We undertook further numerical simulation to test this notion, using an extended version of Experiment 5 of Jakovovic et al. (2012), involving a 10-d period of pumping (i.e., twice as long as the original experiment). Figure 5.1 presents the salinity distribution after 10 d, at which time the 50% salinity contour is clearly concave and in contact with the well, causing a significant

influx of saline groundwater. Clearly, steady-state, subcritical conditions are not obtained. There is evidence in Figure 5.1 that the side inflow ports start to impact on the plume shape near the side boundaries at 10 d, and hence the results are representative of the experimental conditions.

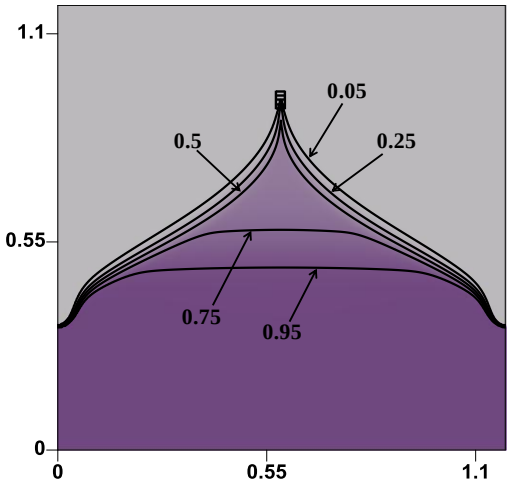

Figure 5.1. Simulated relative salinity contours for a 10-d extended version of Experiment 5 from Jakovovic et al. (2012).

The modelling for Figure 5.1, and the original laboratory experiments and numerical modelling by Werner et al. (2009) and Jakovovic et al. (2011, 2012), were unable to generate stable (subcritical) plumes, despite that two of the cases are classified as subcritical using the theory of Zhang et al. (1997). Therefore, it is likely that experimental nuances of the laboratory sand-tank that was used by Werner et al. (2009) and Jakovovic et al. (2011, 2012) preclude steady-state upconing, and therefore, the steady criticality definitions of Zhang et al. (1997) do not strictly apply to the laboratory experiments. Numerical testing of upconing under idealised field-scale conditions is warranted to test further the applicability of the Zhang et al. (1997) criticality definitions under real-world situations. Such an analysis of field-scale upconing should evaluate whether the dispersive nature of upconing processes can preclude the formation of stable plumes, as was observed in the laboratory experiments described above, considering a range of field situations.

Zhang et al. (2012) present a prediction of the Experiment 3 interface position. The results of Zhang et al. (2012) compare more closely to the Jakovovic et al.

(2011) numerical results for Experiment 3, relative to the Dagan and Bear (1968) prediction. This is expected, given that the perturbation approximation of Dagan and Bear (1968) is valid only for the early stages of the experiments. However, we recall that the Experiment 3 plume position given by Zhang et al. (2012) is for a steady-state condition, rather than a transient snapshot. We suggest that Experiment 3 was yet to reach steady state, and that this likely contributed to the differences in the comparison between Zhang et al.'s (1997) prediction and the laboratory results. Experiments 1 and 2 of Werner et al. (2009) were closer to a steady-state situation, while Experiment 4 (and Experiment 5 from Jakovovic et al., 2012) was still rising at the termination of the experiment.

We reconfirm that in Table 4 of Werner et al. (2009), full-plume widths at the plume half-depth (i.e., at halfway between the plume apex and the initial interface position) were reported and not half-plume widths as Zhang et al. (2012) suggest. This is supported by Jakovovic et al. (2011) numerical simulation results of the full-plume widths that were a reasonable match to the experimental plume widths reported by Werner et al. (2009). The simulated 50% salinity contours were considered the closest match to plume widths obtained from laboratory photography of Experiments 1 and 2, whereas the simulated 25% salinity contour was a closer match to the plume widths obtained from laboratory photographs of Experiment 3. Further research is needed to better quantify the salinities associated with plume widths obtained from laboratory photography.

The numerical simulations of Jakovovic et al. (2011, 2012) reproduced reasonably well the laboratory observations of Werner et al. (2009) and Jakovovic et al. (2012), thereby demonstrating advantages of numerical modelling, which led to important insights into upconing processes and experimental nuances (e.g., adsorption of the dye tracer) that would have not been characterised properly from physical experiments and sharp-interface analyses alone. The characterisation of criticality should be reassessed, by considering a concentration-dependent criticality condition, whereby pumping precludes the interaction of a specific salinity contour with the well. Three-dimensional modelling of this problem is needed, especially for application to the field. This would, we suggest, lead to better understanding of saltwater intrusion

to wells under the (pseudo-)radial flow conditions that are expected in the field, as opposed to the two-dimensional laboratory experiments discussed here.

Chapter 6

Saltwater upconing zone of influence: Characterization using axisymmetric and three-dimensional models

6.1 Introduction

Saltwater upconing is the rise in the freshwater-saltwater interface that occurs beneath pumping wells where fresh groundwater is underlain by saltwater. The salinization of wells due to saltwater upconing is a widespread issue in coastal aquifers (Saeed et al., 2002; Werner et al., 2013). Previous studies of saltwater upconing focus on theoretical analyses (Dagan and Bear, 1968; Rubin and Pinder, 1977; Zhang et al., 1997), laboratory experimentation (Oswald and Kinzelbach, 2004; Werner et al., 2009) and numerical modelling (Diersch, 1984; Reilly and Goodman, 1987; Zhou et al., 2005; Jakovovic et al., 2011). Field studies of saltwater upconing are rare. The aspects of upconing that are the focus of previous investigations include the salinity response of pumping wells, the rise of the interface below the well, and the influence of dispersion on upconing processes. The regional-scale, lateral extent of salinity impacts due to saltwater upconing has received considerably less attention. In this chapter, the saltwater upconing zone of influence (SUZI), defined as the zone around a well within which significant interface rise occurs, is examined.

While the SUZI has not been characterised previously in the literature, the hydraulic zone of influence of a pumping bore, i.e. the region around a well within which a cone of depression develops, is well defined and routinely used in water management (Dragoni, 1998). The hydraulic zone of influence is usually delineated by the distance from the well to a specific pumping-induced drawdown. For example, Osiensky et al. (2000) suggest using a drawdown of 0.05 m for this purpose. The hydraulic zone of influence is commonly obtained using the Theis equation for transient flow problems, or from the Thiem equation

for systems where steady-state conditions are an adequate approximation (Chu, 1994; Kasenow, 2000).

While the zone of influence of a pumping well can be clearly defined in terms of hydraulics (e.g. drawdown), the same intuition does not exist for saltwater rise attributable to pumping in a coastal aquifer (i.e. the SUZI). In the absence of previous guidance on defining the SUZI, we adopt an interface rise of 2 m to delineate SUZI extent, given that this is commensurate with a 0.05 m drawdown based on the Ghyben-Herzberg (GH) approximation (Ghyben, 1888; Herzberg, 1901), as follows. The well-known GH relationship, which assumes a sharp transition zone between freshwater and saltwater and steady-state conditions, is commonly used in coastal aquifer studies to obtain a first approximation of the freshwater-seawater interface (e.g. Moore et al., 1992; Guo and Jiao, 2007). The GH depth of the interface, z [L], can be estimated by $z = \delta h_f$, where h_f is the freshwater head above mean sea level (MSL) [L], and δ is the density ratio given by $\rho_f/(\rho_s-\rho_f)$, where ρ_f and ρ_s are the freshwater and seawater densities [ML^{-3}], respectively. δ is commonly taken as 40. We apply the GH approximation, to convert the hydraulic zone of influence drawdown limit of 0.05 m to the SUZI limit of 2 m.

An important aspect of delineating the SUZI, considering the dispersive interfaces that occur in nature, is to identify the salinity (and rise thereof) that represents upconing extent. While it might seem intuitive to adopt the 50% seawater salinity (e.g. 17,500 mg/L), which is commonly used for comparison with sharp-interface analyses, wells become unusable at much lower salinities (e.g. 2000 mg/L; Sherif and Singh, 2002), and hence the vertical rise of lower salinity groundwater also needs to be considered in assessing the SUZI.

The GH approximation was adopted by Strack (1976), who applied the method of potentials to produce analytical solutions for steady-state interface problems, including those of coastal aquifers in which pumping wells operate. Previous studies of pumping impacts on the interface position have applied GH-based approaches, including the Strack (1976) solutions, to investigate critical pumping rates (i.e. maximum permissible discharge without the interface encountering the well), and the steady-state position of the freshwater-seawater interface (e.g.

Cheng et al., 2000; Mantoglou, 2003). However, these studies did not characterise the SUZI, but rather, the main focus was on pumping optimization in saltwater-intruded coastal aquifers. Although the GH approximation is known to lack accuracy in the region of significant vertical flow (i.e. near a partially penetrating well; Rushton, 2004), we anticipate that the GH relationship allows for a preliminary estimate of SUZI. The accuracy of the GH approximation for this application needs to be assessed, given that upconing in coastal settings involves dispersive processes, transient effects and lateral flow impacts, and hence GH-based approaches may be overly simplified and fail to capture important processes in some cases.

Numerical modelling studies of saltwater upconing, aimed at exploring upconing processes in a generalised fashion, have been conducted mainly by considering axisymmetric flow conditions (i.e. Diersch et al., 1984; Wirojanagud and Charbeneau, 1985; Reilly and Goodman, 1987; Holzbecher, 1998; Zhou et al., 2005). Axisymmetric analyses assume that the initial freshwater-saltwater interface is horizontal and that the flow towards the well is radially symmetric (e.g. Langevin, 2008). These assumptions are violated in typical coastal aquifer situations, which involve a seawater wedge and lateral flow towards the coast. Hence, three-dimensional flow and transport processes need to be resolved in evaluating the SUZI in coastal aquifer settings (Langevin, 2008), albeit axisymmetric models may provide a rough approximation of the SUZI if superposition principles apply. The applicability of axisymmetric simulation to evaluate regional-scale upconing impacts requires further investigation.

The current analysis applies both axisymmetric and three-dimensional (3D) models of density-dependent flow and transport to assess the SUZI under a range of conditions. The mathematical simplicity of axisymmetric models allows for an assessment of a multitude of parameter combinations in characterising the SUZI. 3D models are used to examine a selection of coastal aquifer settings, and these are compared to idealised axisymmetric models to investigate the role of lateral groundwater flow and the associated sloping interface on the SUZI, and to evaluate whether axisymmetric models provide a reasonable estimate of the SUZI (i.e. whereby superposition is applied to overlay saltwater rise, from an axisymmetric analysis, over an undisturbed coastal aquifer situation).

Following the laboratory experiments of Pennink (1915), we expect lateral groundwater flow to create complex flow patterns around wells where upconing has been induced. Pennink (1915) used two-dimensional sand-tank models to show that lateral flow causes a downstream shift in the saline water below the well. The saltwater interception of the well then occurs from the ocean side, i.e. rather than from beneath the well as expected in the absence of lateral flow. Olsthoorn (2010) reproduced this situation numerically. He concluded that lateral flow would extend the saltwater-impacted region around the well along the flow direction and cause a higher salinization of the aquifer on the downstream side of the well than on the upstream side, although the extent to which this might occur was not explored. Bear et al. (2001) and Bear and Cheng (2010) numerically modelled a coastal pumping well and also noted asymmetry in saltwater upconing caused by the seaward flow. Further analysis is required to understand and quantify the role of lateral flow in modifying the SUZI.

Despite that lateral flow impacts upconing geometry, De Louw et al. (2013) in their study of natural saltwater upconing caused by boils suggested that lateral flow did not significantly influence the salinities of the boils. The system they modelled represented an aquifer with a point sink positioned above an initially horizontal transition zone and lateral groundwater flow entering the system at a distance of 1500 m from the boil. They found that lateral flow divided the aquifer into a local boil system and an underlying regional flow system, separated by a dividing streamline. This resulted in the boil water coming from shallow depths (i.e. from above the dividing streamline). They suggested that in coastal aquifers where lateral flow is present, leaving the lateral flow component out of saltwater upconing studies could be considered as a worst-case scenario. An analysis of the influence of lateral flow on SUZI would add to the study of De Louw et al. (2013) by offering improved understanding on the spatial extent of upconing plumes and associated well salinities.

The objective of this chapter is to characterize the SUZI under a range of hypothetical aquifer settings, using parameter ranges based on values from previous publications. We evaluate the applicability of the GH approximation, including in cases where sloping interfaces occur and where solute dispersion is significant. Both axisymmetric and three-dimensional simulations will be used to

develop enhanced intuition on both the SUZI extent in coastal aquifers and the processes influencing the SUZI.

6.2 Methodology

The numerical modelling was carried out using FEFLOW (Diersch, 2005), which is a finite-element code that simulates density-dependent flow and solute transport processes. Two types of models were developed: 1) axisymmetric models to analyse the SUZI under radially symmetric flow conditions, and 2) three-dimensional (3D) models to evaluate the SUZI incorporating inclined interfaces and lateral flow towards the coast. The various problem configurations are illustrated in Figure 6.1. The axisymmetric model was more computationally efficient, and allowed for a grid resolution analysis to be undertaken. Axisymmetric and 3D results were compared to validate the 3D models, which necessarily used relatively coarse grid spacings. The rectangular 3D model is rectangular and therefore slightly larger than the corresponding axisymmetric model. However, this was expected to have only a small effect on the comparison given that the boundaries are positioned at a distance from the well where upconing is anticipated to be small.

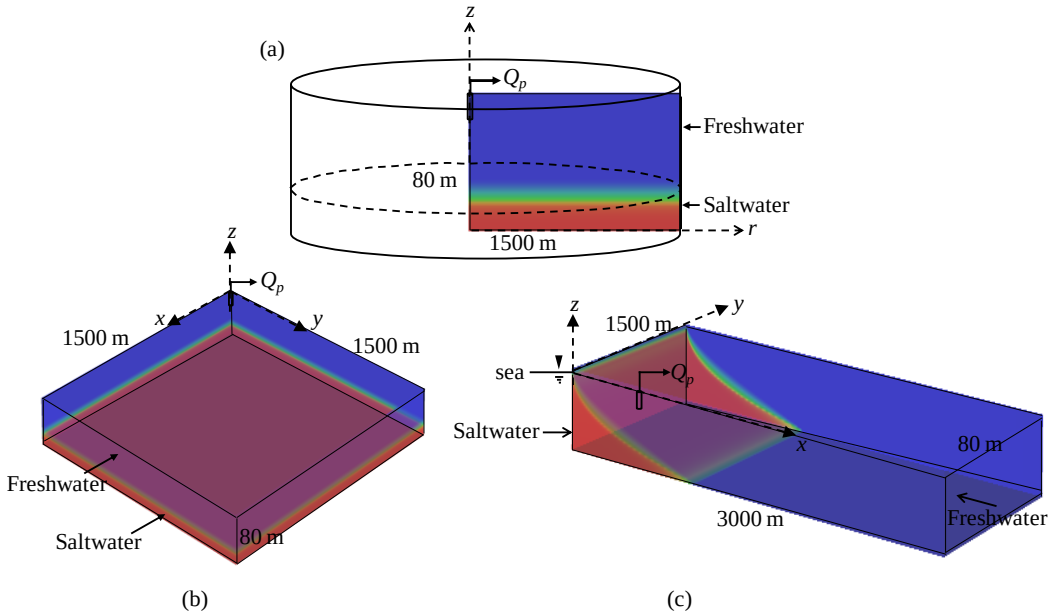

Figure 6.1. General set-up of axisymmetric and 3D models: (a) Axisymmetric representation of a well pumping above a horizontal freshwater-saltwater interface, (b) 3D model corresponding to the axisymmetric model (i.e. a quarter of the system is simulated), and (c) 3D model of a coastal system with an inclined freshwater-saltwater interface. Colour distributions represent the pre-pumping salinity distributions.

The axisymmetric model (Figure 6.1a) is similar to the set-up of Zhou et al. (2005), representing a homogeneous, anisotropic confined aquifer. The external radial boundary is located at r = 1500 m and the depth z = 80 m. A partially penetrating well is placed at r = 0 m and comprises a 10 m long well screen centred at 5 m below the top of the aquifer. The domain discretization is such that the cell sizes increase horizontally away from the well, with a minimum cell width of 0.5 m at the well boundary, increasing to a constant spacing of 20 m for $r \geq 240$ m. A uniform discretization of 2 m is adopted in the vertical direction. The model represents an aquifer with freshwater within the upper 60 m and saltwater throughout the lower 20 m, prior to pumping (i.e. the salinity stratification is initially uniform throughout). The freshwater-saltwater interface is initially sharp. The top and bottom boundaries of the aquifer are impervious (i.e. no-flow boundaries), producing confined-aquifer conditions. Apart from the screened portion, the inner radial boundary at r = 0 m is also a no-flow boundary. Recharge to the aquifer occurs at the external radial boundary, where specified-head boundary conditions represent a hydrostatic pressure distribution

taking into account the vertical distribution of water density (Diersch, 2005). The upper and lower portions of this boundary are specified as constant freshwater ($c = 0$) and saltwater ($c = 1$) relative concentrations, respectively.

The 3D model corresponding to the axisymmetric model has a rectangular prism geometry that represents a quarter of the flow domain (Figure 6.1b), to reduce calculation times. The domain discretization is the same as in the axisymmetric model. That is, the same cell size expansion occurs from the well towards external boundaries in the horizontal direction. The pre-pumping salinity stratification is again uniform throughout, and the initial interface is horizontal. The same boundary conditions are applied as in the axisymmetric case, except in this case the boundaries are rectangular (e.g., the longest distance from the well to a fixed-head boundary is 2121 m) and not located at a radial distance (1500 m) from the well.

The 3D model was modified to represent a body of seawater on one side and freshwater inflow on the opposite side (Figure 6.1c), i.e. a typical coastal aquifer setting. The rectangular prism geometry represents half of the flow domain (i.e. the domain is cut into half along the well symmetry axis to reduce calculation times). The conceptualisation is that of pumping wells located at 3 km intervals parallel to the coast. Hence symmetry boundaries, perpendicular to the shoreline, occur through the pumping well and at 1500 m from the pumping well in the *y* direction (see Figure 6.1c). The model is 3000 m long in the *x* direction, 1500 m wide in the *y* direction and 80 m thick. The discretization around the well is similar to the axisymmetric models (i.e. a minimum cell size of 0.5 m). However, the maximum cell size is larger, reaching 250 m at the inland boundary. The cells located between the well and the coast needed to be refined to avoid numerical oscillations, and these have a maximum cell size of 4 m. Similarly, as for the axisymmetric model, a vertical discretization of 2 m was applied throughout the domain. The 3D model's level of discretization was obtained after considerable trial-and-error, and was a trade-off between run-times and numerical accuracy. For example, the 3D model simulations take up to 30 days on an Intel® Core™ i7 2600 CPU. A grid-discretization analysis was performed using the axisymmetric base-case model to evaluate the adequacy of the spatial discretization, in lieu of attempting to produce finer-resolution 3D

models. The grid was refined twice so that three different levels of grid dicretization were tested: 4840, 19,360 and 77,440 elements. The steady-state head and salinity distributions were in close agreement for the different levels of discretization, and therefore, the grid with the least number of elements was used because it allowed for the shortest run-times.

For the 3D inclined interface cases, the inland boundary is represented by specified head and concentration (freshwater) conditions. At the coastal boundary, the pressure distribution is hydrostatic and seawater concentrations are applied. The lower portion of this boundary (i.e. lower 60 %) is assigned a constant saltwater concentration and the remainder is assumed to have zero solute concentration gradients normal to this boundary (i.e. this allows solute mass fluxes (outflow) by advection only through this part of the boundary). Similar coastal boundary conditions were imposed by Bear et al. (2001), who also modelled a 3D seawater intrusion problem. Initially, the aquifer contains only freshwater. A transient simulation is used to determine the steady-state extent of seawater in the aquifer under conditions of no pumping. A pumping well is then introduced above the inclined interface, and the simulation continues until a new steady-state condition is obtained.

The model parameters for a suite of axisymmetric and 3D numerical experiments are listed in Table 6.1. A base case was developed using parameters from Bear et al. (2001) and Zhou et al. (2005). The base case represents an anisotropic confined aquifer of 80 m depth, a well positioned 50 m above 20 m of saltwater, and pumping at 500 m^3/day. For the 3D inclined interface base case, the inland head is 3 m higher than the ocean, giving rise to 1600 m^3/d of freshwater flow towards the sea in the absence of pumping. Sensitivity analyses are conducted by varying the pumping rate, Q_p [L^3T^{-1}], distance between the bottom of the well and initial interface, d [L], well distance from the coast, x_w [L], and lateral freshwater discharge, q_0 [LM^{-1}], as indicated in Table 6.1.

Table 6.1. Model parameters for axisymmetric and 3D inclined interface cases. Base case values are shown in bold. Alternative values are those used for testing q_0, Q_p, x_w and d.

Parameter	Symbol	Value	Unit
Aquifer thickness	D	**80**	m
Distance between well and interface	d	40, **50**, 60	m
Well distance from the coast	x_w	393, **573**, 793	m
Porosity	n	**0.2**	-
Horizontal hydraulic conductivity	K_x, K_y	**20**	m d^{-1}
Vertical hydraulic conductivity	K_z	**8**	m d^{-1}
Lateral freshwater discharge	q_0	0.008, **0.013**, 0.023	m d^{-1}
Pumping rate	Q_p	250, **500**, 1000	m^3 d^{-1}
Density of freshwater	ρ_f	**1000**	kg m^{-3}
Density of saltwater	ρ_s	**1025**	kg m^{-3}
Longitudinal dispersivity	α_L	**2.5**	m
Transverse dispersivity	α_T	**0.25**	m
Molecular diffusivity	D	**10^{-9}**	m^2 s^{-1}

The focus of results from GH analyses is the lateral extent of the SUZI (i.e. near-well upconing is not considered). To obtain a first-order estimate of the SUZI in a radial flow system, we modify Thiem's (1906) equation for radial, confined flow towards a well to account for interface flow, using the GH approximation to specify the head-interface position relationship. The resulting sharp-interface, steady-state estimates, based on equation 6.1 (referred to hereafter as the GH-1D approach), are compared to the dispersive axisymmetric model predictions to obtain and compare SUZI estimates from the two approaches.

$$\phi = \frac{[H_S(\delta+1)-D]+\sqrt{[H_S(\delta+1)-D]^2+4\left(\frac{\delta}{2}\right)\{\left(\frac{\delta}{2}\right)\phi_R^2-[H_S(\delta+1)-B]\phi_R+\frac{Q_P}{2\pi K}ln\frac{r}{R}}}{\delta} \qquad (6.1)$$

In equation 6.1, ϕ is the head (m), ϕ_R is the head at the radial boundary (m), R is the radial distance to the boundary (m) and H_s is the elevation of the sea level (m). The remaining variables are as defined earlier.

Strack's (1976) solution for confined, regional interface problems involving pumping wells (equation 6.2) is used to obtain an estimate of the SUZI in a coastal setting, for comparison with the SUZI predictions obtained by the 3D dispersive model for the inclined interface cases.

$$\frac{1}{2\delta} Kz^2 = q_0 Dx + \frac{Q_p}{4\pi} \ln\left[\frac{(x - x_w)^2 + y^2}{(x + x_w)^2 + y^2}\right] \tag{6.2}$$

Variables in equation 6.2 are as described earlier. Strack's (1976) solution is based on the GH and Dupuit approximations, and as such neglects vertical flows and assumes static seawater conditions. We refer to equation 6.2 as GH-2D in what follows. The interface is expected to be landward in both the GH-1D and GH-2D analyses, relative to dispersive approaches (Pool and Carrera, 2011).

Rather than choosing a single salinity contour to define the SUZI, the lateral extents of the 10% and 50% relative salinity contours rise were examined. As such, we consider the maximum SUZI extent to be the lateral extent of a 2 m interface rise in the 10% relative salinity contour. Well salinity trends are also evaluated, given their importance in coastal aquifer management.

6.3 Results and Discussion

A comparison between the GH-1D approach and the dispersive model results is shown in Figure 6.2 for the axisymmetric base case. The GH-1D results fall between the 35% and 50% (relative to seawater) salinity contours obtained from the numerical model. The GH-1D method fails to reproduce the dispersive model results in the region near the well, as expected given that vertical flows are most prominent in this area. Further away from the well, the GH-1D results are a reasonable representation of the numerical results. For example, the GH-1D interface is well matched to the 35% relative salinity contour at distances larger than 250 m from the well.

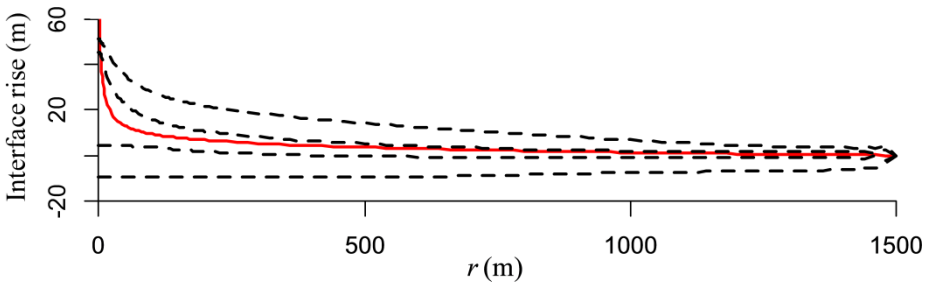

Figure 6.2. Comparison of the GH-1D approach (equation 6.1) (red solid line) with the dispersive numerical model results (black dashed line) of the steady-state interface position (given as interface rise above the starting sharp-interface location) for the axisymmetric base case. Relative salinity contours from the numerical modelling results of 10%, 35%, 50% and 90% are shown from top to bottom, respectively.

Figure 6.3 shows the base case comparison, in terms of the salinity distribution below the well and the salinity breakthrough curve, between the axisymmetric and the full 3D numerical simulations. The salinity distribution below the well (Figure 3b) seems to be virtually the same for both simulations, as expected. However, a minor discrepancy in the breakthrough curves at later times is evident. Namely, the full 3D simulation breakthrough plateaus slightly earlier than the axisymmetric simulation breakthrough curve. This difference is attributed to the larger domain simulated in the full 3D model. Overall, the comparison validates the use of the coarse grid of the 3D models.

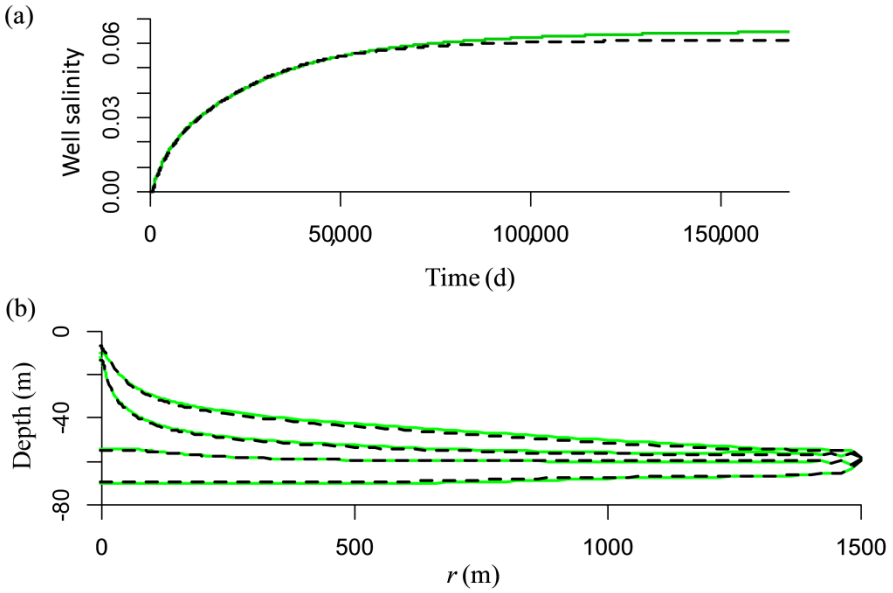

Figure 6.3. Comparison of the axisymmetric (solid green line) and 3D (black dashed line) simulation results for the steady-state base case: (a) breakthrough curve and (b) relative salinity distribution. In (b), relative salinity contours of 10%, 35%, 50% and 90% are shown from top to bottom, respectively.

Figure 6.4 compares the numerical model predictions of the steady-state salinity contours to the GH-2D estimate of the interface rise for the base case of the 3D inclined interface model. As in the axisymmetric base case, the GH-2D results are closer to the numerically simulated salinity contours further from the well, as expected. The 50% relative salinity contour is matched quite well as close as 100 m away from the well.

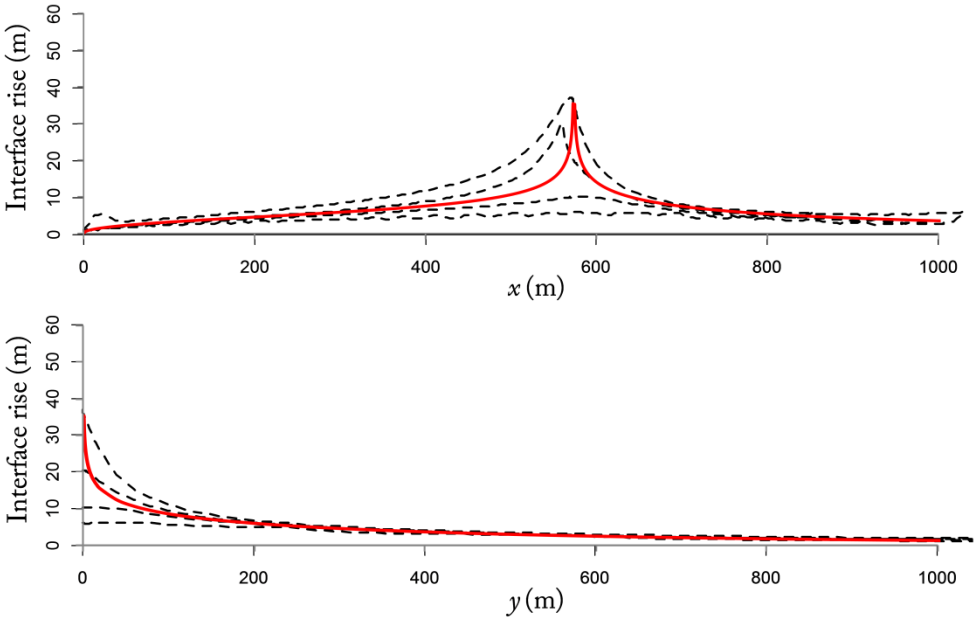

Figure 6.4. The 3D inclined interface base case comparison of the steady-state numerically simulated (black dashed line) and the GH-2D approach (red solid line) prediction of the interface rise for the relative salinity contours of 10%, 35%, 50% and 90%; (a) in the direction perpendicular to the coast, and (b) in the direction parallel to the coast.

The lateral SUZI shape and extent for the 3D inclined interface base case, overlayed with the GH-1D approach prediction, are shown in Figure 6.5. The SUZI predicted by the GH-1D approach is of a circular form, as expected. Figure 6.5 also highlights the asymmetrical shape of the SUZI in the 3D inclined interface case, i.e. the SUZI is largest in the direction parallel to the coast. This occurs because the specified head boundary condition at the ocean limits the drawdown near the coast. Also, the inland extent of seawater in the aquifer further limits the propagation of the SUZI perpendicular to the coast, thereby compressing the SUZI in this direction. Figure 6.5 also illustrates the larger SUZI extent in terms of the 10% relative salinity contour compared to the 50% relative salinity contour, which highlights the importance of considering dispersion in the analysis of SUZI. The areas covered by the 10% and 50% relative salinity contours are 0.94 km^2 and 0.57 km^2, respectively.

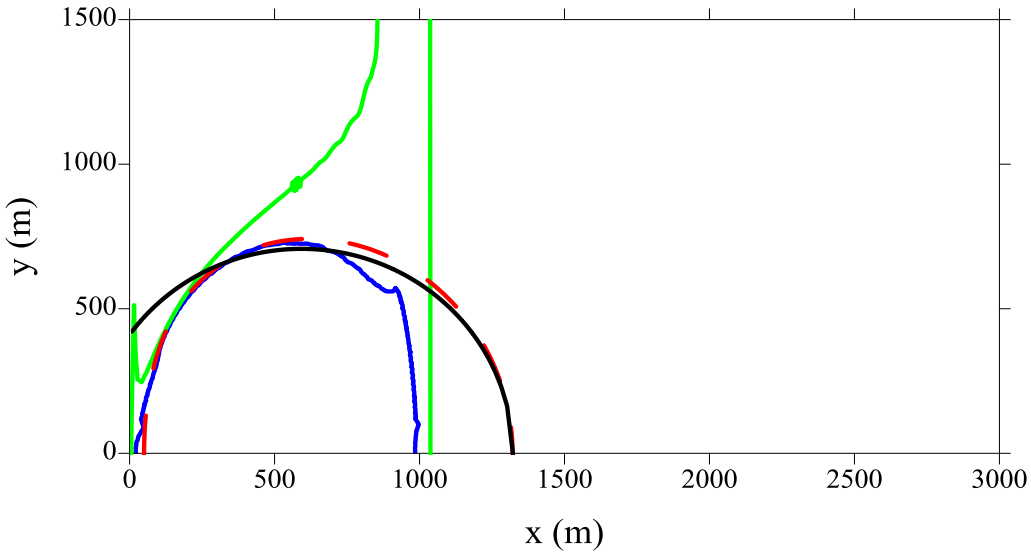

Figure 6.5. Top view of the lateral extent of the 2 m interface rise predicted by the GH-2D approach (equation 2) (dashed red line), GH-1D approach (equation 1) (solid black line) and the rise of the 10% (solid green line) and 50% (solid blue line) numerically simulated relative salinity contours for the 3D inclined interface base case.

Figure 6.5 results also show that the GH-1D and GH-2D predictions of the 2 m interface rise are landward compared to the numerically simulated 10% and 50% relative salinity contours. The over-estimation of impacts using the GH-1D and GH-2D approach is consistent with previous studies (e.g. Pool and Carrera, 2011). However, the GH-2D estimate of the 2 m interface rise compares well with the 50% relative salinity contour on the seaward side of the well, whereas the GH-1D approach over-estimates the SUZI between the well and the coast. This is intuitive because of the radially symmetric conditions in the GH-1D approach. A slight elongation of the SUZI obtained by the GH-2D approach is observed parallel to the coast (Figure 6.5). Again, this occurs because of the specified heads at the ocean which, limit the drawdown near the coast.

Figure 6.6 illustrates the difference in the maximum SUZI extent estimated for the axisymmetric base case and 3D inclined interface base case, for different pumping cases tested. It is apparent that the maximum SUZI extent (i.e. in terms of the 10% relative salinity contour) is larger for the axisymmetric base case than for the 3D inclined interface base case. This difference is attributed to the coastal head effects (i.e. for the 3D inclined interface case the drawdown is limited near the coast) and to the limits in upconing imposed by the seawater

wedge toe beyond which the aquifer does not have salt in it to rise. Figure 6.6 also shows that larger SUZI extents are obtained for higher pumping rates, as expected.

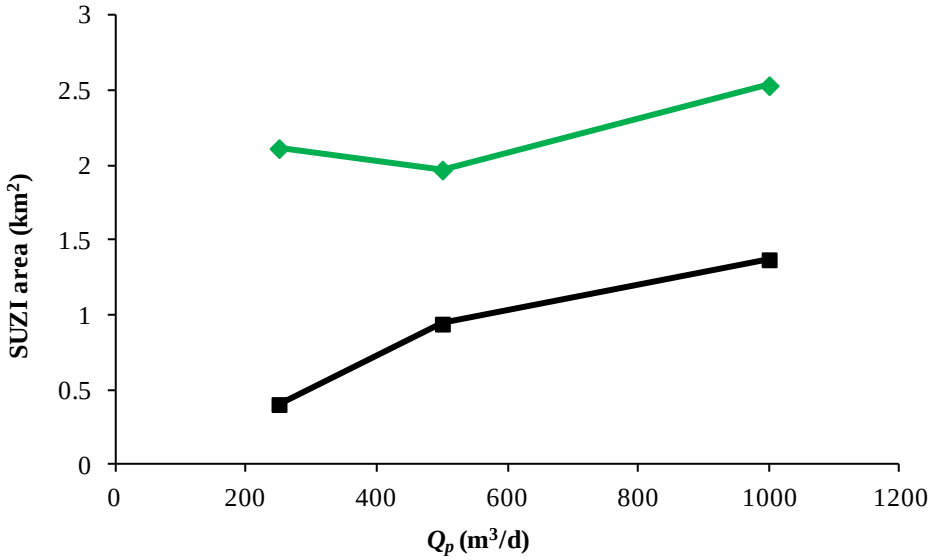

Figure 6.6. Comparison of the SUZI extent in terms of 10% relative salinity contour for the axisymmetric base case (green) and 3D inclined interface base case (black).

Figure 6.7 illustrates the SUZI extent observed for the 3D inclined interface cases in which different q_0 and x_w were tested. Note that as the lateral freshwater discharge was changed in the 3D inclined interface cases, the x_w position was also changed, in order to keep the distance between the bottom of the well and the initial interface the same. Figure 6.7a shows that the SUZI extent decreased with the increase in q_0 (and the accompanying seaward shift in x_w to maintain the same well-to-interface depth). To further explore the effect of changing q_0, the GH-2D approach was used to evaluate the relationship between SUZI extent and q_0 without the influence of x_w changes, as shown in Figure 6.8. The SUZI extent-q_0 relationship is again a downward trend, although without x_w changes (and dispersion effects), the slope is reduced. This result shows the importance of considering lateral flow in saltwater upconing analysis, which cannot be tested in axisymmetric models. Figure 6.7b shows that the SUZI extent increased with increase in x_w. As the well is shifted landward from the coast, the larger distance

to the fixed head boundary allows more extensive drawdown to develop, and hence, the SUZI increases.

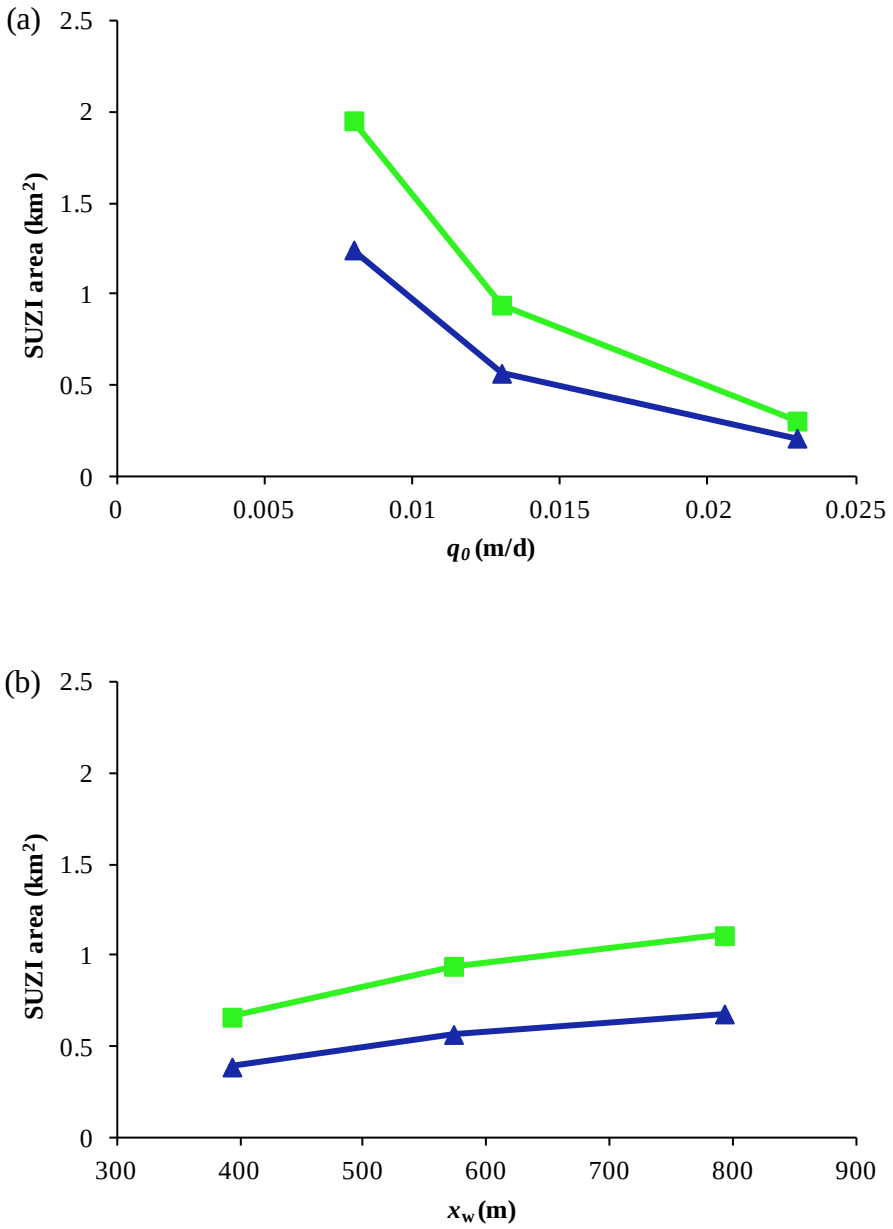

Figure 6.7. SUZI extent in terms of the 10% (green) and 50% (blue) relative salinity contours for the 3D inclined interface cases: (a) q_0 changes, (b) x_w changes.

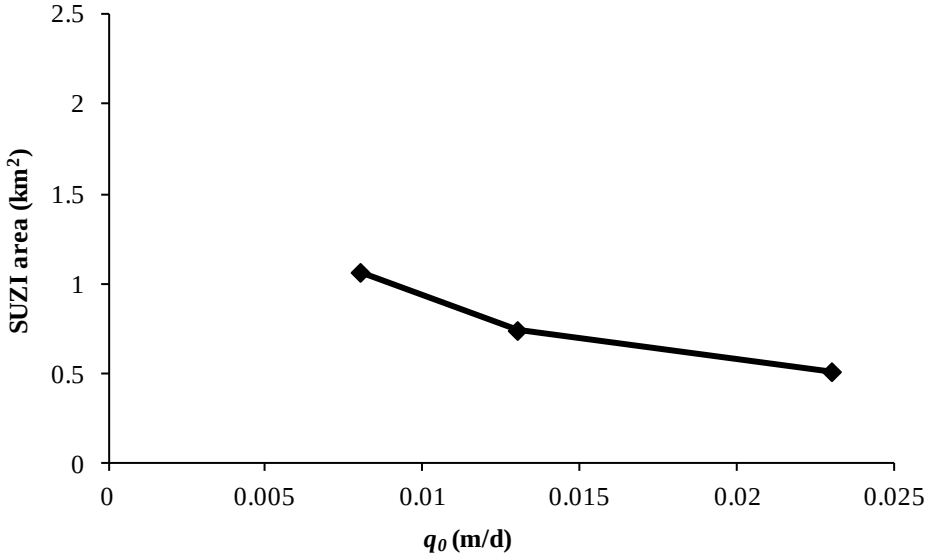

Figure 6.8. SUZI extent predicted by the GH-2D approach for the 3D inclined interface cases with different lateral flows towards the sea.

Table 6.2 summarises the maximum well salinities for the evaluated range of 3D inclined interface cases. The results in Table 2 show a number of intuitive trends. For example, as anticipated, the highest well salinity occurs for the case with the highest pumping rate (Case 5; Table 6.2). Similarly, the lowest well salinity occurs for the case with the lowest pumping rate (Case 3; Table 6.2). Cases 1, 4 (the base case) and 7 show that the maximum well salinity decreases with increasing lateral flow. This result is consistent with the decrease in SUZI as q_0 increases, as was already shown (Figure 6.8). Cases 2, 4 and 6 show that the highest salinity in the well occurs for the well placed closest to the coast. This has the opposite trend to the SUZI (i.e. the SUZI increased as the well was moved further away from the coast; Figure 6.7b). The decrease in the well salinity with the increase of x_w occurs because the distance between the initial interface and well bottom increases as x_w increases. This indicates that lower well salinities do not imply smaller SUZI.

Table 6.2. Summary of the maximum well salinities for the 3D inclined interface cases.

Case	q_0 (m/d)	d (m)	x_w (m)	Q_p (m^3/d)	Maximum well salinity (%)
1	0.008	50	853	500	5.60
2	0.013	60	793	500	1.60
3	0.013	50	573	250	1.54
4*	0.013	50	573	500	3.95
5	0.013	50	573	1000	9.10
6	0.013	40	393	500	7.61
7	0.023	50	353	500	1.63

*Base case

Similar well salinity trends were observed for the axisymmetric simulations (i.e. the well salinities increased with the increasing pumping rate and decreasing distance between the bottom of the well and initial interface). However, the maximum well salinities were observed to be consistently larger in the axisymmetric setting (i.e. when considering the same parameters except without a lateral flow towards the sea). For example, the maximum well salinity for the 3D inclined interface base case was found to be 3.95% (relative to seawater), whereas for the axisymmetric base case it was found to be 6.21%. Lower well salinities for the 3D inclined interface cases are attributed to the lateral flow towards the sea, which is expected to reduce well salinities, as observed previously by De Louw et al. (2013).

6.4 Conclusions

In this chapter the saltwater upconing zone of influence (SUZI) is defined and explored. The SUZI is taken as the zone around the well within which significant interface rise occurs. Presently, there is no intuition on the extent of impact in terms of saltwater rise attributed to pumping and current study investigates this through simulating radially symmetric flow conditions as well as the 3D modelling of a coastal setting involving an inclined regional freshwater-seawater interface and lateral flow towards the sea. It is anticipated

that the Ghyben-Herzberg relationship based approach can be used as the first approximation of the SUZI.

The results revealed that the SUZI shape in the radially symmetric cases is of a circular form, as expected. For the 3D inclined interface cases the SUZI shape was found to be of an asymmetrical shape, i.e. the SUZI is largest in the direction parallel to the coast. This occurs because of the drawdown limit near the coast, as well as because of the limits imposed by the seawater wedge toe beyond which the aquifer does not have saltwater in it to rise.

From the cases considered in this study, it was found that the radially symmetric (i.e. not accounting for the lateral flow) numerical simulations estimate the maximum SUZI extent as well as the well salinities to be larger than for the 3D inclined interface setting. The difference in the pumped water salinity is attributed to the lateral flow effects, which cannot be captured with the axisymmetric model, as observed previously by De Louw et al. (2013). The SUZI extent for the radially symmetric conditions and 3D inclined interface settings differs because of the specified head boundary conditions at the ocean, which limit the drawdown near the coast, which in turn limits the SUZI. Also, the inland extent of seawater in the aquifer limits the propagation of the SUZI perpendicular to the coast.

The results showed that the sharp-interface approximation of SUZI over-predicts the numerically simulated 50% relative salinity contour, for both axisymmetric and inclined interface cases. This result is consistent with the study of Pool and Carrera (2011). The results also show that the SUZI extent in terms of the 10% relative salinity contour is considerably larger than in terms of the 50% relative salinity contour. This highlights the importance of considering dispersive effects in SUZI analysis.

The lateral flow towards the sea influences the formation of saltwater upconing and hence the SUZI, and therefore the salinity of the extracted groundwater as well. The results reveal that the SUZI and maximum well salinity decreased as the lateral flow towards the coast increased. This highlights the importance of considering the 3D modelling, which captures the lateral flow effects, when studying saltwater upconing. The SUZI extent and well salinity had opposing

trends for the cases in which the well was moved further away from the coast. That is, as the well was moved further away from the coast, the SUZI extent increased but the well salinity decreased. This indicates that lower well salinities do not imply smaller SUZI extent.

This study can be extended by taking into account transient effects and in particular intermittent pumping, which would most likely significantly affect the SUZI shape and extent. It can be deduced that once the well would stop pumping, the diluted saltwater beneath the well would be taken seawards with the lateral flow, which would increase the SUZI extent. The degree to which SUZI, as well as salinities in the well would be affected would again depend on the relative strengths of the pumping rate and lateral flow.

Chapter 7

Conclusions

Saltwater upconing is a process that occurs when salty groundwater that sits beneath fresh groundwater rises towards a pumping well. In this study, the mechanisms of saltwater upconing are assessed to improve the current body of knowledge of the associated density-dependent flow and transport mechanisms. Laboratory experiments and numerical modelling analyses of saltwater upconing processes were undertaken to produce the first published images of saltwater upconing for a range of mixed convective cases, to test whether analytical solutions are a reasonable representation of laboratory upconing, to evaluate the dispersive processes associated with saltwater upconing, to examine the transport processes observed under controlled laboratory conditions, and to explore the saltwater upconing zone of influence.

The first stage of this thesis describes the investigation of saltwater upconing imagery and experimental data to produce a well-characterised account of laboratory measurements of saltwater upconing, thereby extending the work of Dagan and Bear (1968) and Oswald (1998). This part of the study provided the first published time-series observations of saltwater upconing under controlled laboratory experimental conditions. Patterns of upconing were in agreement with the analytical solution of Dagan and Bear (1968) up to a certain density-pumping condition, but beyond that there was a departure from theoretical sharp-interface upconing behaviour in terms of rates and upconing shapes.

The most rapid and significant upconing occurred under high pumping and low density difference. The influence of density was shown to be minor relative to combined influence of the rate of pumping and the distance from the bore to the initial interface. Dispersive transport processes dominated during phases of near-well upconing, causing gradual increases in pumped water salinity, although plumes became non-dispersive after the interface made contact with the bore. A departure of classical upconing shape was obtained for the situation of highest

saltwater density and lowest pumping, in which a double-peak shape upconing occurred.

Following the analysis of the saltwater upconing laboratory experiments, numerical modelling of the experiments was undertaken in order to explore the numerical reproducibility of the experimentally observed transient rise in saltwater plumes under a pumping bore. In general, good agreement of the experimental observations and numerical simulations was observed with minimal calibration. The consistency between the numerical model results and laboratory observations of the experiments indicates that the laboratory observations are reproducible. This implies two things: that the density-dependent flow and transport simulator FEFLOW is able to predict the saltwater upconing processes of the experiments, including the transition from dispersive to non-dispersive plumes and the drawdown associated with pumping, and that the laboratory observations carried out are reliable depictions of upconing processes, albeit in two-dimensions. A weaker match between numerical model results and the highest saltwater density and lowest pumping experiment (in which double-peak upconing was observed) was obtained.

An assessment of the width and dispersiveness of the plume indicates that the well salinity breakthrough in the high-pumping laboratory experiments was controlled primarily by the width of the plume and not the degree of dispersiveness. This implies that it may be possible to infer plume width from bore salinity (and vice-versa) under certain conditions. The modelling presented in this study is the first attempt at matching a numerical simulator with direct visualisations of saltwater upconing and builds on similar studies by Johanssen et al. (2002) and Oswald and Kinzelbach (2004) who numerically modelled geophysical interpretations of upconing in a three-dimensional sand-box.

Additional laboratory experimentation and numerical modelling were carried out to investigate double-peak upconing that remained unresolved. Double-peak upconing was firstly reproduced in new sand-tank experimentation, demonstrating that this phenomenon was not an experimental nuance in the original experiment. The feature could also be simulated by a numerical model which incorporated adsorption effects. It is inferred from this that the double

peak below the pumping well was caused by adsorption of the Rhodamine WT tracer, which was used in the laboratory experiments to enable visualisation of plume movements. These results illustrate the sensitive adsorption nature of Rhodamine WT and that care should be taken when it is used in sand-tank experiments for visualisation purposes, especially under slow flow conditions.

Laboratory experiments and numerical modelling undertaken in this study were unable to generate stable plumes, despite that two of the cases are classified as subcritical using the theory of Zhang et al. (1997). It is likely that the steady criticality definitions of Zhang et al. (1997) do not strictly apply to the laboratory experiments. Numerical testing of upconing under idealised field-scale conditions is warranted to test further the applicability of the Zhang et al. (1997) criticality definitions under real-world situations. Such an analysis of field-scale upconing should evaluate whether the dispersive nature of upconing processes can preclude the formation of stable plumes, as was observed in the laboratory experiments described here, considering a range of field situations.

The final component of the study extended the laboratory-scale investigation to scales that apply to real-world settings. The aim was to define and characterize the "saltwater upconing zone of influence" (SUZI), which is the zone around the well within which significant interface rise occurs. Both radial and three-dimensional numerical modelling of saltwater upconing at the field scale were undertaken considering dispersive effects. Also, first approximations of the SUZI were obtained using the sharp-interface approximation; i.e. the Ghyben-Herzberg relationship. The results indicate that the sharp-interface approximations of SUZI, for both radial and three-dimensional cases, are larger compared to the numerical model predictions, in terms of the 50% salinity, as expected. It was also found that the lateral flow towards the coast significantly influences both the SUZI and the salinity of the extracted groundwater. This part of the study demonstrated that the three-dimensional modelling that includes inclined interfaces and lateral flow towards the coast is essential in studying SUZI in typical coastal areas. That is, radial modelling, which does not capture the lateral flow effects, over-estimates the SUZI extent as well as the pumped water salinity.

References

Abarca E., Clement T.P., 2009. A novel approach for characterising the mixing zone of a saltwater wedge. Geophysical Research Letters 36, L06402, doi: 10.1029/2008GL036995.

Aharmouch A., Larabi A., 2001. Numerical modelling of saltwater interface upcoming in coastal aquifers. First International Conference on Saltwater Intrusion and Coastal Aquifers Monitoring, Modelling and Management. Essaouira, Morocco, April 23-25.

Aliewi A.S., Mackay R., Jayyousi A., Nasereddin K., Mushtaha A., Yaqubi A., 2001. Numerical simulation of the movement of saltwater under skimming and scavenger pumping in the Pleistocene aquifer of Gaza and Jericho areas, Palestine. Transport in Porous Media 43, 195-212.

Bear J., 1979. Hydraulics of groundwater. McGraw-Hill Book Company, New York, USA, 569pp.

Bear J., Cheng A.H.-D., 2010. Modeling Groundwater Flow and Contaminant Transport, Springer, Dordrecht Heidelberg London New York, 834pp.

Bear J., Dagan G., 1964. Some exact solutions of interface problems by means of the hodograph method. Journal of Geophysical Research 69 (8), 1563-1572.

Bear J., Zhou Q., Bensabat J., 2001. Three dimensional simulation of seawater intrusion in heterogeneous aquifers, with application to the coastal aquifer of Israel. First International Conference on Saltwater Intrusion and Coastal Aquifers – Monitoring, Modelling and Management. April 23-25, Essaouira, Morocco.

Bower J.W., Motz L.H., Durden D.W., 1999. Analytical solution for determining the critical condition of saltwater upconing in a leaky artesian aquifer. Journal of Hydrology 221, 43-54.

Chandler R.L., McWhorter D.B., 1975. Upconing of the saltwater-freshwater interface beneath a pumping well. Ground Water 13 (4), 354-359.

Cheng A.H.D., Halhal D., Naji A., Ouazar D., 2000. Pumping optimization in saltwater-intruded coastal aquifers. Water Resources Research 36 (8), 2155-2165.

Chu S.T., 1994. Transient radius of influence model. Journal of Irrigation and Drainage Engineering 120 (5), 964-967.

Close M., Bright J., Wang F., Pang L., Manning M., 2008. Key features of artificial aquifers for use in modelling contaminant transport. Ground Water 46 (6), 814-828.

Custodio E., Bruggeman G.A., 1987. Groundwater problems in coastal areas. Studies and Reports in Hydrology, UNESCO, International Hydrological Programme, Paris, 596pp.

Dagan G., Bear J., 1968. Solving the problem of local interface upconing in a coastal aquifer by the method of small perturbations. Journal of Hydraulic Research 6 (1), 15-44.

De Louw P.G.B., Vandenbohede A., Werner A.D., Oude Essink G.H.P., 2013. Natural saltwater upconing by preferential groundwater discharge through boils. Journal of Hydrology 490, 74-87.

Diersch H-J.G., 2005. FEFLOW: Finite element subsurface flow and transport simulation system. Reference manual, User's manual and White Papers Vol. 1, 2, 3, 4, WASY GmbH Institute for Water Resources Planning and Systems Research, Berlin, Germany.

Diersch H-J.G., Kolditz O., 2002. Variable-density flow and transport in porous media: approaches and challenges. Advances in Water Resources 25, 899-944.

Diersch H-J.G., Prochnow D., Thiele M., 1984. Finite-element analysis of dispersion-affected saltwater upconing below a pumping well. Applied Mathematical Modelling 8, 305-312.

Di Fazio A., Vurro M., 1994. Experimental tests using rhodamine WT as tracer. Advances in Water Resources 17, 375-378.

Dragoni W., 1998. Some considerations regarding the radius of influence of a pumping well. Hydrogéologie 3, 21-25.

EPA (U.S. Environmental Protection Agency), 1999. Understanding variation in partition coefficient, K_d, values. EPA/402/R-99/004A, Office of Radiation and Indoor Air, Office of Solid Waste and Emergency Response, Washington, D.C.

Everts C.J., Kanwar R.S., 1994. Evolution of Rhodamine WT as an adsorbed tracer in an agricultural soil. Journal of Hydrology 153, 53-70.

FAO, 1997. Seawater Intrusion in Coastal Aquifers. Guidelines for Study, Monitoring and Control. Food and Agriculture Organization of the United States, Water Reports No. 11, Rome, Italy, 152pp.

Geith H.M., Schwartz F.W., 1998. Electrical and visual monitoring of small scale three-dimensional experiments. Journal of Contaminant Hydrology 34, 191-205.

Ghanem A., Smith J., Elzey M., Soerens T.S., Miah M.A., Thoma G., 1999. Locating NAPLs in groundwater using partitioning fluorescent dyes. Journal of Arkansas Academy of Science 53, 55-60.

Ghyben B.W., 1888. Nota in verband met de vurgenomen putboring nabij Amsterdam. Tijdschrift van het Koninklijk Institut van ingeniers, The Huage, 8-22.

Goswami R., Clement P., 2007. Laboratory-scale investigation of saltwater intrusion dynamics. Water Resources Research 43, W04418. doi:10.1029/2006WR005151.

Guo H., Jiao J.J., 2007. Impact of coastal land reclamation on ground water level and the sea water interface. Ground Water 45 (3), 362-367.

Harbaugh A.W., Banta E.R., Hill M.C., McDonald M.G., 2000. MODFLOW-2000, the U.S. Geological Survey modular ground-water model. User

guide to modularization concepts and the Ground-Water Flow Process: U.S. Geological Survey Open-File Report 00-92, 121pp.

Harleman D.R.F., Rumer R.R., 1963. Longitudinal and lateral dispersión in an isotropic porous medium. Journal of Fluid Mechanics 16 (3), 385-394.

Haubold R.G., 1975. Approximation for steady interface beneath a well pumping fresh water overlying salt water. Ground Water 13 (3), 254-259.

Herzberg A., 1901. Die wasserversorgung einiger Nordseebader. Journal Gabeleuchtung und Wasserversorgung 44, 815-819, 824-844.

Holzbecher E., 1998. Modelling density-driven flow in porous media. Springer-Verlag Berlin Heidelberg, Germany, 286pp.

Hocking G.C., Zhang H., 2009. Coning during withdrawal from two fluids of different density in a porous medium. Journal of Engineering Mathematics doi: 10.1007/s10665-009-9267-1.

Huang W.E., Oswald S.E., Lerner D.N., Smith C.C., Zheng C., 2003. Dissolved oxygen imaging in a porous medium to investigate biodegradation in a plume with limited electron acceptor supply. Environmental Sciences and Technology 37 (9), 1905-1911.

Hughes J.D., Sanford W.E., Vacher H.L., 2005. Numerical simulation of double-diffusive finger convection. Water Resources Research 41, W01019. doi: 10.1029/2003WR002777.

Jakovovic D., Post V.E.A., Werner A.D., Männicke O., Hutson J.L., Simmons C.T., 2012. Tracer adsorption in sand-tank experiments of saltwater up-coning. Journal of Hydrology 414, 476-481.

Jakovovic D., Werner A.D., Simmons C.T., 2011. Numerical modelling of saltwater up-coning: Comparison with experimental laboratory observations. Journal of Hydrology 402, 261-273.

Johannsen K., Kinzelbach W., Oswald S.E., Wittum G., 2002. The saltpool benchmark problem – numerical simulation of saltwater upconing in a porous medium. Advances in Water Resources 25, 335-348.

Kasenow M.C., 2000. Applied groundwater hydrology and well hydraulics, 2nd Ed. Water Resources Publications, LLC, Colorado, USA, 837pp.

Konz M., Ackerer P., Younes A., Huggenberger P., Zechner E., 2009. Two-dimensional stable-layered laboratory-scale experiments for testing density-coupled flow models. Water Resources Research 45, W02404, doi: 10.1029/2008WR007118.

Langevin C.D., 2008. Modelling axisymmetric flow and transport. Ground Water 46 (4), 579-590.

Lin C.H., Tsay T.K., Hsu N.S., 1999. Saltwater upconing due to freshwater pumping. Proceedings of the National Science Council, ROC(A) 23 (2), 248-258.

Lu C., Kitanidis P.K., Luo J., 2009. Effects of kinetic mass transfer and transient flow conditions on widening mixing zones in coastal aquifers. Water Resources Research 45, W12402, doi:10.1029/2008WR007643.

Mantoglou A., 2003. Pumping management of coastal aquifers using analytical models of saltwater intrusion. Water Resources Research 39 (12), 1335, http://dx.doi.org/10.1029/2002WR00189.

Massmann G., Simmons C.T., Love A., Ward J., James-Smith J., 2006. On variable density surface water-groundwater interaction: a theoretical analysis of mixed convection in a stably-stratified fresh surface water-saline groundwater discharge zone. Journal of Hydrology 329, 390-402.

Moore Y.H., Stoessell R.K., Easley D.H., 1992. Fresh-water/sea-water relationship within a ground-water flow system, Northeastern Coast of the Yucatan Peninsula. Ground Water 30 (3), 343-350.

Motz L.H., 1992. Salt-water upconing in an aquifer overlain by a leaky confining bed. Ground Water 3 (2), 192-198.

Narayan K.A., Charlesworth P.B., Bristow K.L., 2006. Investigation of groundwater salinity in the Ardmillan Road Area, North Burdekin Delta Water Board. CSIRO Land and Water Science Report, July 2006.

Ogata, A., Banks, R.B., 1961. A solution of the differential equation of longitudinal dispersion in porous media. US Geological Survey Professional Paper 411-A.

Olsthoorn T.N., 2010, Upconing-related downstream long-term salinisation and head phenomena in the Amsterdam Water Supply Dunes. 21st Saltwater Intrusion Meeting (SWIM21), June 16-21, Ponta Delaga, Azores, Portugal.

Osiensky J.L., Williams R.E., Williams B., Johnson G., 2000. Evaluation of drawdown curves derived from multiple well aquifer tests in heterogeneous environments. Mine Water and the Environment. International Mine Water Association 19 (1), 30-55.

Oswald S.E., 1998. Density-driven flow in porous media: three-dimensional experiments and modelling. Ph.D. Thesis, Institute of Hydromechanics and Water Resources Management, ETH Zurich, Switzerland.

Oswald S.E., Kinzelbach W., 2004. Three-dimensional physical benchmark experiments to test variable-density flow models. Journal of Hydrology 290, 22-42.

Pang L., Close M., Noonan M., 1998. Rhodamine WT and Bacillus subtilis transport through an alluvial gravel aquifer. Ground Water 36 (1), 112-122.

Paster A., Dagan G., 2008. Mixing at the interface between two fluids in aquifer well upconing steady flow. Water Resources Research 44, W05408, doi: 10.1029/2007WR006510.

Pennink J.M.K., 1915. Grondwater stroombanen. Stadsdrukkerij, Amsterdam, The Netherlands, 151pp.

Pool M., Carrera J., 2011. A correction factor to account for mixing in Ghyben-Herzberg and critical pumping rate approximations of seawater intrusion in coastal aquifers. Water Resources Research 47, W05506, http://dx.doi.org/10.1029/2010WR010256.

Precht E., Huettel M., 2003. Advective pore water exchange driven by surface gravity waves and its ecological implications. Limnology and Oceanography 48 (4), 1674-1684.

Reilly T.E., Goodman A.S., 1987. Analysis of saltwater up coning beneath a pumping well. Journal of Hydrology 89, 169-204.

Rubin H., Pinder G.F., 1977. Approximate analysis of upconing. Advances in Water Resources 1 (2), 97-101.

Rushton K.R., 2004. Groundwater hydrology: conceptual and computational models. John Wiley and Sons, Hoboken, 430pp.

Sabatini D.A., Alaustin T., 1991. Characteristics of rhodamine WT and fluorescein as adsorbing groundwater tracers. Ground Water 29 (3), 341-349.

Saeed M.M., Bruen M., Asghar M.N., 2002. A review of modelling approaches to simulate saline-upconing under skimming wells. Nordic Hydrology 33, 165-188.

Schincariol R.A., 1989. Migration of dense aqueous phase liquids in homogeneous and heterogeneous porous media. M.S. Thesis, Department of Geology, University of Alberta, Edmonton.

Schincariol R.A., Schwartz F.W., 1990. An experimental investigation of variable density flow and mixing in homogeneous and heterogeneous media. Water Resources Research 26 (10), 2317-2329.

Schmorak S., Mercado A., 1969. Upconing of fresh water-sea water interface below pumping wells, field study. Water Resources Research 5 (6), 1290-1311.

Sherif M.M., Singh V.P., 2002. Effect of groundwater pumping on seawater intrusion in coastal aquifers. Journal of Agriculture Sciences 7 (2), 61-67.

Shiau B.J., Sabatini D.A., Harwell J.H., 1993. Influence of rhodamine WT properties on sorption and transport in subsurface media. Ground Water 31 (6), 913-920.

Strack O.D.L., 1976. A single-potential solution for regional interface problems in coastal aquifers. Water Resources Research 12 (6), 1165-1174.

Sutton D.J., Kabala Z.J., Francisco A., Vasudevan D., 2001. Limitations and potential of commercially available rhodamine WT as a groundwater tracer. Water Resources Research 37 (6), 1641-1656.

Thiem G., 1906. Hidrologische Methoden. J.M. Gebhardt, Leipzig, Germany, 56pp.

van Genuchten M.Th., 1980. A closed-form equation for predicting the hydraulic conductivity of unsaturated soils. Soil Science Society of America Journal 44, 892-898.

Vasudevan D., Fimmen R.L., Francisco A.B., 2001. Tracer-grade Rhodamine WT: structure of constituent isomers and their sorption behaviour. Environmental Science and Technology 35 (20), 4089-4096.

Webb M.D., Howard K.W.F., 2011. Modelling the transient response of saline intrusion to rising sea-levels. Ground Water 49 (4), 560-569.

Werner A.D., Bakker M., Post V.E.A., Vandenbohede A., Lu C., Ataie-Ashtiani B., Simmons C.T., Barry D.A., 2013. Seawater intrusion processes, investigation and management: Recent advances and future challenges. Advances in Water Resources 51, 3-26.

Werner A.D., Gallagher M.R., 2006. Characterisation of seawater intrusion in the Pioneer Valley, Australia, using hydrochemistry and three-dimensional numerical modelling. Hydrogeology Journal 14, 1452-1469.

Werner A.D., Jakovovic D., Simmons C.T., 2009. Experimental observations of saltwater up-coning. Journal of Hydrology 373, 230-241.

Wirojanagud P., Charbeneau R.J., 1985. Saltwater upconing in unconfined aquifers. Journal of Hydraulic Engineering 111 (3), 417-434.

Wraith J.M., Or D., 1998. Nonlinear parameter estimation using spreadsheet software. Journal of Natural Resources and Life Sciences Education 27, 13-19.

Zhang H., Barry D.A., Hocking G.C., 2012. Comment on "Experimental observations of saltwater up-coning". Journal of Hydrology 422-423, 81-83.

Zhang H., Hocking G.C., Barry D.A., 1997. An analytical solution for critical withdrawal of layered fluid through a line sink in a porous medium. Journal of Australian Mathematical Society, Series B 39 (2), 271-279.

Zhang Q., Volker R.E., Lockington D.A., 2004. Numerical investigation of seawater intrusion at Gooburrum, Bundaberg, Queensland, Australia. Hydrogeology Journal 12, 674-687.

Zhou Q., Bear J., Bensabat J., 2004. Saltwater upconing and decay beneath a well pumping above an interface zone. Transport in Porous Media 61, 337-363.